lower than those for 5-AVA, at a concentration of 10⁻³ mM. Previously, 5-AVA was shown to stimulate larval attachment in H. rufescens at 1 mM (Morse Hooker, Duncan et al. 1979), and attachment without metamorphosis in H. virginea at 1 mM. Commercially available 5-AVA at 10^{-3} mM has been shown to induce 43% of H. discus discus and H. discus hannai larvae to metamorphosis at 43%. Subsequently, 5-AVA has been isolated from the alga H. samoense (Suenaga et al. 2004), but not tested for settlement potential. We have found 5-AVA to be better than GABA. Previously, Kaspar and Mountfort (1995) demonstrated that GABA receptors have an absolute need for the primary carboxyl group, with minor substitutions at the γ position, but with no major deviation in chain length. Hence, compounds with GABA-like settlement-inducing properties are dependent on receptor requirements. Therefore, we hypothesize that GABA and 5-AVA may have induced more settlement numbers due to a structural feature of a selective external receptor or a receptor within ciliated larvae, as GABA seems to be a true inducer and 5-AVA as well, as it is structurally analogous (Morse Hooker, Duncan et al. 1979).

L-glutamic acid, the precursor of GABA, was also used in our study and was effective in inducing larval settlement. Although Morse et al. (1979) reported that GA induced *H. rufescens* to settle in low numbers (12%), later investigations showed that this chemical was a potent larval settlement inducer and induced 33% larvae of H. discus hannai to settle after 24 h (Kang et al. 2003). When GA was used in conjunction with benthic diatoms, the numbers of settled larvae increased to 82% (Kang et al. 2003). Our data are consistent with their results regarding GA ability to induce settlement in H. asinina. We also tested another form of glutamate, MSG, which is inexpensive when compared with the other three chemicals. MSG showed settlement-inducing responses similar to L-glutamate, but a much higher dose is required, where MSG at 25 mM was effective (50%) in settling larva. Moreover, MSG appeared to be the least toxic. Due to its easy availability in local markets, including efficiency, when compared with expenditure (\$US $2.6 \,\mathrm{kg}^{-1}$) for the other chemicals, GABA (\$US 654), 5-AVA (\$US 9880) and GA (\$US 158) (prices sourced from Sigma-Aldrich and local markets 2006), therefore, it may be of more practical use for lower-funded facilities and farmers. Publication of the results of this study provides much-needed information for aquaculture of abalone, which are important economically. The yield of larvae in abalone farms could

be increased by using any one of these inducers, especially MSG, which is a cheap alternative to the other expensive chemical inducers.

Acknowledgments

We thank the Thailand Research Fund (Senior Research Scholar Fellowship to Prof. Prasert Sobhon) and the Commission on Higher Education Thailand (PhD scholarship to Praphaporn Stewart) and Mahidol University for research support.

References

Akashige S., Seki T., Kan-no H. & Nomura T. (1981) Effects of γ-aminobutyric acid and certain neurotransmitters on the settlement and the metamorphosis of the larvae of *Haliotis discus hannai* Ino (Gastropoda). *Bulletin Tohoku Regional Fisheries Research Laboratory* **43**, 37–45.

Anguiano B.C., Seary B.R., Lizarraga P. & Marcial L. (1998) Pathogenic effects of *Vibrio alginolyctus* on larvae and postlarvae of the red abalone *Haliotis rufescens*. *Diseases of Aquatic Organism* **33**, 119–122.

Bryan P.J. & Qian P. (1998) Induction of larval attachment and metamorphosis in the abalone *Haliotis diversicolor* (Reeve). *Journal of Experimental Marine Biology and Ecol*oay 223, 39–51.

Dobretsov S.V. & Qian P. (2003) Pharmacological induction of larval settlement and metamorphosis in the blue mussel *Mytilus edulis* L. *Biofouling* **19**, 57–63.

Gacía-Lavandeira M., Silva A., Abad M., Pazos A.J., Sánchez J.L. & Parallé L. (2005) Effects of GABA and epinephrine on the settlement and metamorphosis of the larvae of four species of bivalve molluscs. *Journal of Experimental Marine Biology and Ecology* 316, 149–156.

Gallardo W.G. & Buen S.M.A. (2003) Evaluation of mucus, Navicula, and mixed diatoms as larval settlement inducers for the tropical abalone Haliotis asinina. Aquaculture 221, 357–364.

Gapasin R.S.J. & Polohan B.B. (2004) Induction of larval settlement and metamorphosis in the donkey-ear abalone, *Haliotis asinina* Linnaeus, by chemical cues. *Hydrobiologia* **519**, 9–17.

Gapasin R.S.J. & Polohan B.B. (2005) Response of the tropical abalone, *Haliotis asinina*, larvae on combinations of attachment cues. *Hydrobiologia* **548**, 301–306.

Huang C., Liu P. & Lee K. (2001) Withering syndrome of the small abalone, Haliotis diversicolor supertexta, is caused by Vibrio parahaemolyticus and associated with thermal induction. Zeitschrift Fur Naturforschuny C – A Journal of Bioscience 56, 898–901.

Kang K.H., Kim B., Kim J.M. & Kim Y.H. (2003) Effects of amino acids on larval settlement and metamorphosis in

- Haliotis discus hannai. Korean Journal of Malacology 19, 95-106
- Kaspar H.F. & Mountfort D.O. (1995) Microbial production and degradation of γ-aminobutyric acid (GABA) in the abalone larval settlement habitat. *FEMS Microbiology Ecology* **17**, 205–212.
- Laimek P., Clark S., Stewart M., Pfeffer F., Wanichanon C., Hanna P. & Sobhon P. (2008) The presence of GABA in gastropod mucus and its role in inducing larval settlement. *Journal of Experimental Marine Biology and Ecology* 354, 182–191.
- Morse D.E., Hooker N., Duncan H. & Jensen L. (1979) γ-aminobutyric acid, a neurotransmitter, induces planktonic abalone larvae to settle and begin metamorphosis. *Science* 204, 407–410.
- Morse D.E., Hooker N., Jensen L. & Duncan H. (1979) Induction of larval settling and metamorphosis by γ -aminobutyric acid and its congeners from crustose red algae. II. Applications to cultivation, seed-production and bioassays; principle causes of mortality and interference. *Proceedings World Marine Society* **10**, 81–91.
- Morse D.E., Hooker N. & Duncan H. (1980) GABA induces metamorphosis in *Haliotis*, V: stereochemical specificity. *Brain Research Bulletin* 5, 381–387.
- Morse A.N.C. & Morse D.E. (1984a) GABA-mimetic molecules from *Porphyra* (Rhodophyte) induce metamorphosis of *Haliotis* (Gastropoda) larvae. *Hydrobiologia* 116, 155–158.
- Morse A.N.C. & Morse D.E. (1984b) Recruitment and metamorphosis of *Haliotis* larvae induced by molecules uniquely available at the surfaces of crustose red algae. *Journal of Experimental Marine Biology and Ecology* 75, 191–215.
- Morse A.N.C., Froyd C.A. & Morse D.E. (1984) Molecules from cyanobacteria and red algae that induce larval settlement and metamorphosis in the mollusc *Haliotis rufescens*. *Marine Biology* **81**, 293–298.
- Morse D.E. (1990) Recent progress in larval settlement and metamorphosis: closing the gap between molecular biology and ecology. Bulletin Marine Science 46, 465–483.
- Morse D.E. (1992) Molecular mechanisms controlling metamorphosis and recruitment in abalone larvae. In: *Abalone of the World. Biology, Fisheries and Culture, Fishing* (ed. by S.A. Shepherd, M. Tegner & S.A. Guzman), pp. 107–119. News Books, Oxford, USA.
- Moss G.A. (1999) Factors affecting settlement and early postsettlement survival of the New Zealand abalone Haliotis

- australis. New Zealand Journal of Marine and Freshwater Research 33, 271–278.
- Nicolas J.L., Basuyaux O., Mazurie J. & Thebault A. (2002) Vibrio carchariae, a pathogen of the abalone Haliotis tuberculata. Diseases of Aquatic organisms 50, 35–43.
- Roberts R. (2001) A review of settlement cues for larval abalone (Haliotis spp.). Journal of Shellfish Research 20, 571–586
- Roberts R.D. & Nicholson C.M. (1997) Variable response from abalone larvae (*Haliotis iris*, H. virginea) to a range of settlement cues. Molluscan Research 18, 131–141.
- Rumrill S.S. & Cameron R.A. (1983) Effects of gamma-aminobutyric acid on the settlement of larvae of the black chiton Katharina tunicata. Marine Biology 72, 243–247.
- Searcy-Bernal R. & Anguiano-Beltran C. (1998) Optimizing the concentration of gamma-aminobutyric acid (GABA) for inducing larval metamorphosis in red abalone, *Haliotis rufescens* (Mollusca: Gastropod). *Journal of World Aquaculture Society* **29**, 463–470.
- Searcy-Bernal R., Salas-Garza A.E., Flores-Aguilar R.A. & Hinojosa-Rivera P.R (1992) Simultaneous comparison of methods for settlement and metamorphosis induction in the red abalone (*Haliotis rufescens*). Aquaculture 105, 241–250.
- Seki T. & Kan-no H. (1981) Induced settlement of the Japanese abalone *Haliotis discus hannai*, veliger by the mucous trails of the juvenile and adult abalones. *Bulletin Tohoku*. *Regional Fishery Research Laboratory* **43**, 29–36.
- Singhagraiwan T. & Sasaki M. (1991) Breeding and early development of the donkey's ear abalone, Haliotis asinina Linne. Thailand Marine Fisheries Research Bulletin 2, 83–94.
- Singhagraiwan T. & Doi M. (1993) Seed Production and Culture of a Tropical Abalone, Haliotis asinine Linné, 1st edn. EMDEC. Rayong. Thailand.
- Suenaga K., Hori H., Ishida H., Nukaya H., Roberts R.D. & Tsuji K. (2004) Inducing substance for abalone larval metamorphosis from the crustose coralline alga *Hydrolithon* samoense. Fisheries Science 70, 342–344.
- Takahashi K. & Koganezawa A. (1988) Mass culture of *Ulvella lens* as a feed for abalone *Haliotis discus hannai*. NOAA Technical Report NMFS **70**, 29–36.
- Yang Y. & Wu B. (1995) Induction of larval settlement and metamorphosis of *Haliotis discus hannai* Ino (Gastropoda, Mollusca). Chinese Journal of Oceanology and Limnology 13, 71–77

ORIGINAL ARTICLE

Morphological and Biochemical Alterations of Abalone **Testicular Germ Cells and Spawned Sperm** and their Fertilizing Ability

Worawit Suphamungmee · Wattana Weerachatyanukul · Tanes Poomtong · Peter Hanna · Prasert Sobhon

Received: 17 July 2007 / Accepted: 15 March 2008 / Published online: 1 May 2008 © Springer Science + Business Media, LLC 2008

Abstract In this study, we aimed to detect morphological and biochemical changes in developing germ cells (Gc), testicular sperm (Tsp), and spawned sperm (Ssp) using capacitation-associated characteristics. Gradual changes in the profiles of two membrane proteins, namely NaCl- and detergent-extractable proteins, were observed as compared Gc with Tsp and Tsp with Ssp. These membrane modifications were accomplished mostly through the introduction of new protein sets, both peripheral and integral, into Tsp and Ssp membranes. Activation of serine proteases, particularly in Ssp detergent-extracted proteins with the molecular masses of 38-130 kDa was evident and marked a major difference between Ssp and Tsp. An increase in the level of tyrosine phosphorylation of the proteins ranging from 15 to 20 kDa was noted in Tsp and remained constant in Ssp. Specifically, these three capacitation-associated characteristics could be detected in Ssp, possessing full fertilizing capacity. The lack of an activated proteolytic activity in Tsp resulted in a delayed fertilization, but not affected fertilizing ability. We believe that these characteristics should be advantageous in predicting abalone sperm fertilizing capability, particularly in cases when isolated germ cells or purified Tsp are used in place of spawned sperm in abalone aquaculture.

W. Suphamungmee · W. Weerachatyanukul (⋈) · P. Hanna · P. Sobhon

Rama 6 Road,

e-mail: scwwy@mahidol.ac.th

T. Poomtong The Coastal Aquaculture Research and Development Center,

Department of Fisheries, Klongwan, Prachuabkirikhun 77000, Thailand

Department of Anatomy, Faculty of Science, Mahidol University, Bangkok 10400, Thailand

Keywords Abalone · Sperm · Capacitation · Phosphorylation · Acrosomal enzymes

Introduction

In marine invertebrates, sperm readily possess fertilizing capability upon their release into seawater to fertilize eggs externally in natural habitats. Success of gamete interaction appears to be limited by a rapid dispersion of the released gametes upon spawning (Giese and Kanatani 1987; Levitan et al. 1991). Therefore, synchronization or "broadcast" release of the gametes significantly enhances a chance of contact between sperm and eggs (Dusenbury 2000). In addition, factors such as period of time over which the gametes are released, the number of gamete released, and the proper ratio between sperm and eggs determine the success of fertilization (Yund 2000; Meidel and Yund 2001). In abalones, the low yield of fertilization rate encountered in their aquaculture is frequently due to the non-simultaneous spawning of male and female animals (Encena II et al. 1998; Grubert et al. 2005). Therefore in practice, testicular cell isolates are sometimes used in place of spawned sperm to fertilize the freshly spawned eggs, which results in some degree of success but also with highly variable outcomes. This inconsistency may be partly due to the variable amount of mature testicular sperm and contamination from testicular extracts.

Many molecular events required for enhancing sperm fertilizing capability are associated with the process known as "sperm capacitation" (Bedford 1983; Yanagimachi 1994). Although extensive accounts on sperm capacitation have been mostly reported in mammals, the evidence of capacitation-like process in some crustaceans, such as



shrimp (Sicyonia ingentis and Penaeus monodon) and crabs (Pseudocarcinus gigas), has also been reported (Lindsay and Clark 1992; Gardner and Williams 2002; Alfaro et al. 2003; Vanichviriyakit et al. 2004). Most biochemical alterations during capacitation take place at sperm plasma membranes which involve extensive modifications of sperm membranes through the adsorption of proteins from the fluid environment where sperm reside or the removal of preexisting membrane proteins (Yanagimachi 1994; Vanichviriyakit et al. 2004). In addition, a pronounced increase in the level of protein tyrosine phosphorylation closely associated with sperm capacitation has been extensively evident in mammals (Visconti and Kopf 1998; Naz and Rajesh 2004) and to some extent in invertebrates (Vanichviriyakit et al. 2004). Additionally, it has also been reported in penaeoid shrimp that sperm serine proteases, in particular trypsin-like enzymes, known to be crucial for acrosome reaction (Rios and Barros 1997; Griffin and Clark 1990), are activated upon transfer of spermatophoric sperm into female storing sac (thelycum), the site where sperm of the closed-thelycal shrimp acquire their fertilizing ability (Lindsay and Clark 1992; our unpublished results). In this study, we monitored the distinctive morphological and biochemical changes that occurred in developing germ cells, testicular sperm, and spawned sperm using capacitationassociated characteristics which may be used to predict sperm fertilizing ability, thus enhancing the successful fertilization rates in abalone aquaculture.

Materials and Methods

Preparations of Germ Cells and Sperm

Sexually mature males (>24 months old with 250–280 g in body weight) were maintained in concrete tanks at the Coastal Aquaculture Research and Development Center, Prachuabkirikhun province, Thailand. To collect testicular germ cells, fully mature testes with a creamy yellowish appearance were carefully dissected free from hepatopancreas in filtered seawater (FSW). The tissues were washed extensively with FSW, minced into small pieces, and subjected to gentle agitation (room temperature, 30 min) to release testicular germ cells. The cell suspension was centrifuged (600×g, 4°C, 10 min), and the pellet was resuspended in FSW. Separation of testicular sperm from other germ cells was performed by a discontinuous Percoll gradient centrifugation. Briefly, 2 ml of testicular cell suspension was layered on top of an 8-ml Percoll gradient (20-80%) in FSW and centrifuged $(1,000\times g, 4^{\circ}C, 30 \text{ min})$. Two population of cells, one sedimented at the interphase between 40% and 60% Percoll (composed mainly developing germ cells—Gc) and the other pelleted at the bottom of the tubes (enriched in testicular sperm—Tsp, see "Results"), were carefully collected and processed for a Hoechst 33258 nuclear staining according to the manufacturer's protocol (Molecular Probes, Eugene, OR, USA). Cell identification and counting were performed under light and fluorescence microscopes. For physiological tests, the isolated cells were washed $(600 \times g, 4^{\circ}C, 5 \text{ min})$ with FSW, and the pellet was resuspended with FSW to a final concentration of 10^{7} sperm/ml. Spawned sperm were freshly collected from seawater surrounding the male broodstocks during spawning (referred to as "Ssp"). They were washed and resuspended as mentioned above and immediately used in the following experiments.

Scanning and Transmission Electron Microscopy

Samples of Tsp and Ssp were immediately fixed with 2.5% glutaraldehyde in 0.1 M cacodylate buffer, pH 7.8 (4°C, 4 h). After washing, samples were post-fixed with 1% osmium tetroxide in the same buffer (4°C, 1 h). Subsequently, samples were washed twice and dehydrated with a series of increasing concentrations of ethanol. For scanning electron microscopy (SEM), samples were further subjected to critical point drying in liquid CO2 and sputter-coated with palladium. Finally, they were observed under a Hitachi S-2000 SEM at 20 kV. For transmission electron microscopy (TEM), the dehydrated samples were transferred to acetone, infiltrated in the mixture of acetone/resin, and embedded in Araldite 502 resin (Electron Microscopy Sciences, Fort Washington, PA, USA). Thin sections (70 nm thick) were cut and placed on 300-mesh copper grids, stained sequentially with uranyl acetate and lead citrate, and then observed under a Tecnai T20 TEM at 80 kV. The dimension (width × length) of the sperm head were measured from at least 25 sperm to obtain mean±SD, and the data were analyzed statistically by a Student's t test.

Extraction of Cell Surface Proteins

Isolated Gc, Tsp, and Ssp were washed twice with prechilled phosphate-buffered saline (PBS) and centrifuged $(600 \times g, 4^{\circ}\text{C}, 5 \text{ min})$ to eliminate loosely bound molecules from the cell surface. The pellet was then resuspended and incubated (4°C, 30 min) with 1 M NaCl in PBS with gentle shaking. After centrifugation, the supernatant (referred to as "NaCl extract") was collected and re-centrifuged $(12,000 \times g, 4^{\circ}\text{C}, 10 \text{ min})$ to eliminate any small particulates. Protein concentration was measured by Bradford's protein assay (Bradford 1976) using a Sigma Bradford's protein assay reagent (Sigma, Saint Louis, MO, USA).

To isolate integral membrane proteins, a detergent partitioning protocol was followed (Bordier 1981). Briefly, Triton X-114 in PBS at a final concentration of 1% was



added to the pellets remaining from NaCl treatment. This cell suspension was briefly sonicated (100-W output, 15-s intervals, three times) and allowed to stand on ice (15 min) with occasional agitations. The cellular fragments were then pelleted (12,000×g, 4°C, 10 min), and the resulting supernatants were left at room temperature until cloudiness in the suspension was observed. Thereafter, this suspension was then laid on a sucrose cushion containing 6% sucrose and 0.06% Triton X-114, and the phase separation was facilitated by centrifugation (500×g, room temperature, 3 min). The bottom detergent phase was collected, and the phase separation on sucrose cushion was repeated to clean the detergent soluble materials (assigned as "detergent extract"). To remove detergent from the extracted membrane proteins, an ice-cold delipidation mixture consisting of tri-*n*-butylphosphate:acetone:methanol (1:12:1, v/v/v) was used in an incubation (4°C, 4–5 h) with the detergent extracts at a final proportion of 14:1 (Mastro and Hall 1999). The precipitated proteins were pelleted (2,000×g, 4°C, 10 min), washed twice with cold acidified acetone (100:1, acetone/1 N HCl, v/v), and finally resuspended in 10 mM Tris-buffered saline (TBS). Protein concentration was determined by a detergent compatible Lowry's protein assay using bovine serum albumin (BSA) as the standard (Lowry et al. 1951).

SDS-PAGE and Immunoblotting

Sperm proteins (~10 µg) including whole cell lysates, NaCl- and detergent-extracted fractions obtained from Gc, Tsp, and Ssp were denatured in sample buffer and electrophoretically resolved in 12.5% sodium dodecyl sulfate-polyacrylamide gel electrophoresis (SDS-PAGE) under a reducing condition (Laemmli 1970). Molecular weight standards were co-electrophoresed as protein markers. The protein profile in one set of gel was visualized by silver staining. Resolved proteins in the duplicated gel were electro-transferred onto a 0.45-µm nitrocellulose membrane (Amersham Biosciences, Buckinghamshire, UK). These transferred protein were treated with 5% skimmed milk in TBS containing 0.1% Tween-20 (TBS-T) to block non-specific binding and further exposed (1 h, room temperature) to an anti-tyrosine phosphate monoclonal antibody (clone P-Tyr 102, Cell Signaling, Beverly, MA, USA) at a dilution of 1:20,000 followed by a horse radish peroxidase (HRP) conjugated rabbit anti-mouse IgG (Zymed Laboratory, San Francisco, CA, USA) at a dilution of 1:3,000. The immunoreactivity was visualized with an enhanced chemiluminescence detection kit (ECL, Amersham Biosciences). Specificity of the anti-tyrosine phosphate antibody was determined by an inclusion of an excess amount (20-fold) of tyrosine phosphate conjugated with BSA (Sigma) into the antibody suspension before proceeding for antibody staining as described above.

Zymography

The isolated protein samples from Gc, Tsp, and Ssp were separated by 10% SDS-PAGE containing 0.3% gelatin under a non-reducing condition. Purified porcine pancreatic trypsin (500 ng) was also co-electrophoresed as a positive control. After protein separation, the sample was treated with 3% Triton X-100 and further incubated in the reaction buffer containing 100 mM NaCl and 10 mM Tris-HCl, pH 7.4 (37°C, overnight). Visualization of the proteolytically active band (as a clear band against dark background) was performed by staining the gel with 0.125% Coomassie brilliant blue R-250 and then de-staining with 70% ethanol containing 10% acetic acid. Alternatively, the resolved proteins in the duplicate gel were pretreated with 1 mM phenylmethylsulphonyl fluoride (PMSF) or 0.5 mM soybean trypsin inhibitor before developing enzymatic reaction in the reaction buffer.

Sperm Fertilization Assays

Spawned eggs released naturally from fully mature females (aged >24 months) were freshly collected in FSW. Aliquots of 3 ml FSW containing 10³ spawned eggs were added to the wells of a 16-well plate and kept at 27°C in a water bath. Upon isolation, 10⁵ Tsp as well as the freshly released Ssp, resuspended in 200 μl FSW, were gently added to the egg suspensions. Sequential changes of fertilized eggs including extrusions of polar bodies and occurrence of two-cell embryos were used as indicators of successful fertilization which has been reported in many abalone species (Septo and Cook 1998; Yi et al. 2002; Liu et al. 2004). These parameters were monitored at 8, 15, and 20 min post-sperm addition. The data were expressed as mean±S.D. calculated from six replicates and analyzed statistically using a one-way analysis of variance.

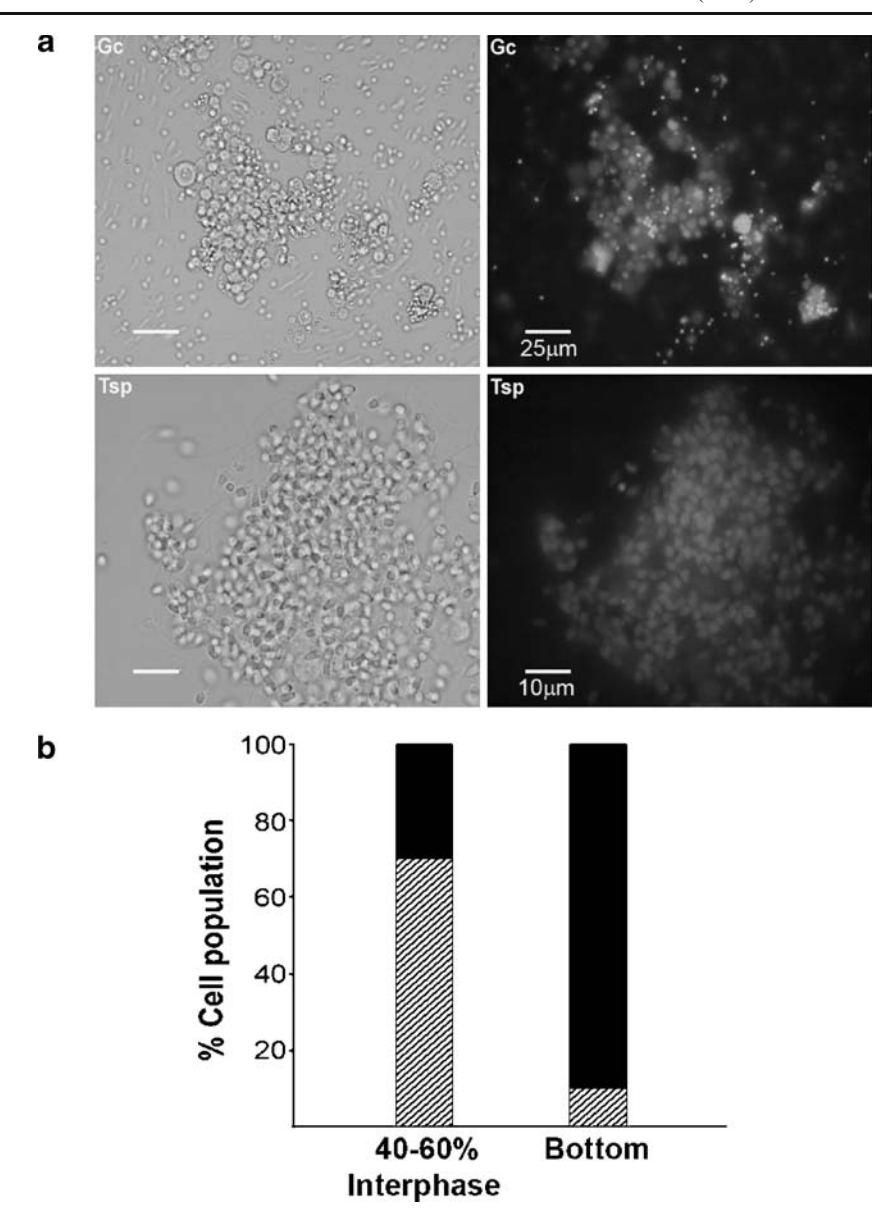
Results

Morphological Comparison Between Tsp and Ssp

Initially, we performed discontinuous Percoll gradient centrifugation to select testicular sperm from the mixed population of other germ cells. It was found that testicular sperm constituted 20–25% of the total population of the isolated germ cells (Fig. 1b, left bar). Upon subjecting the isolated cells to Percoll gradient centrifugation, the proportion of testicular sperm (pelleted fraction) increased to >90% (Fig. 1b, right bar), and the vast majority of these sperm were motile. The major contaminants in this sperm preparation were spermatocytes and early spermatids (~5–7%).



Fig. 1 Separation of H. asinina testicular germ cells using a discontinuous Percoll gradient (20%-80%) centrifugation. a Cells sedimented at the interphase between 40% and 60% and at the bottom of the gradient were subjected to Hoechst 33258 DNA staining and examined under a light microscope. Left, phase contrast micrographs; right, corresponding fluorescent micrographs. b The proportion of Gc (hatched bars) and Tsp (solid bars) collected as in a

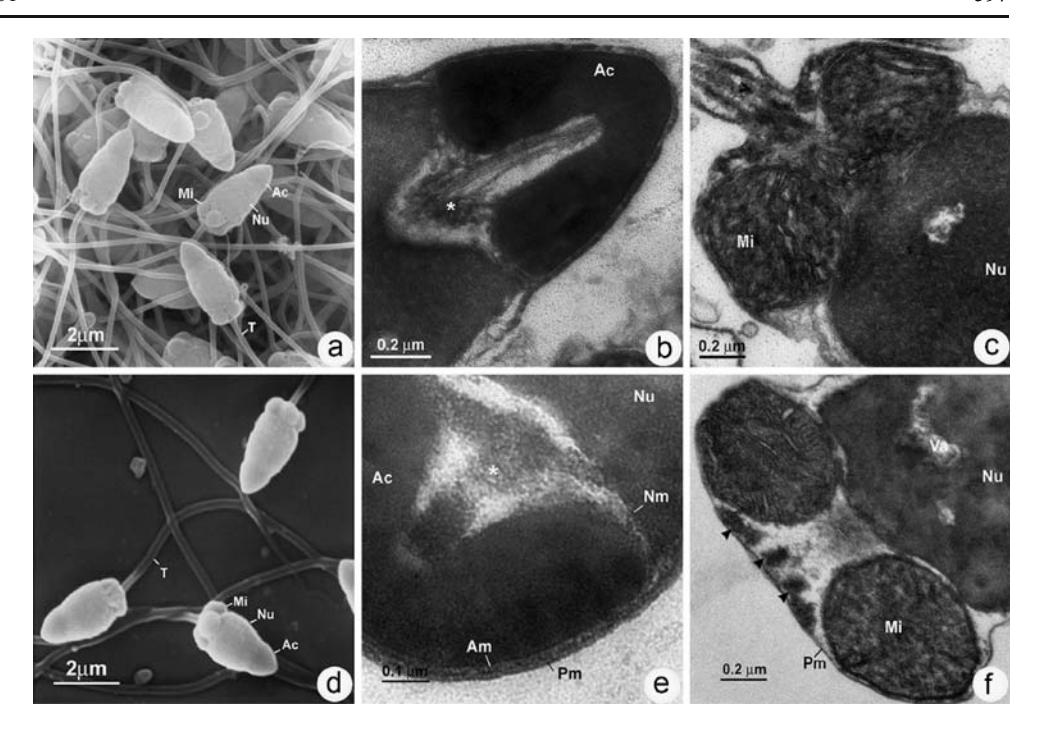


The ultrastructural comparison between Tsp and Ssp was demonstrated in Fig. 2. As observed under SEM, the surface architecture and the cornical contour of the sperm head for both sperm samples were quite similar. However, the width of the posterior part of Tsp sperm head (1.24 \pm 0.03 $\mu m \times 2.78 \pm 0.02~\mu m$) was notably narrower (but not significantly different, P=5.12) than that of Ssp (1.41 \pm 0.03 $\mu m \times 2.80 \pm 0.03~\mu m$), making Tsp appear slightly slender than Ssp (panels a, d). At the TEM level, the plasma membranes (Pm) of both sperm samples were readily distinguishable from the underlying outer acrosomal membrane (Am, panels b, e). There was no apparent difference in the thickness of the outer Pm leaflet in Ssp, which may suggest the adsorption of glycosylated proteins onto the sperm surface. The electron dense acrosomal matrix appeared to be

uniformly distributed throughout the large, U-shaped acrosome in both sperm samples (panels b, e). Despite having large acrosome, there was no evidence to suggest any compartmentalization of the acrosomal matrices in the manner that have been reported for mammalian sperm possessing the large acrosomes (Foster et al. 1997; Kim and Gerton 2003). The acrosome and nuclear membrane of both Tsp and Ssp were separated by subacrosomal space, filled with crystalline-like structures surrounded with electron lucent materials (panels b, e). The nuclei of both sperm samples were occupied by highly condensed chromatin, leaving few vacuolar spaces in between (panels c, f). In the sperm tail, mitochondria were organized into annular structures around the proximal part of the tail. The axonemal complexes were surrounded only by a thin layer of plasma membrane (panels c, f).



Fig. 2 Scanning and transmission electron micrographs of Tsp (upper panels) and Ssp (lower panels). SEM (a and d) showing similar conical sperm heads and three to four spherical mitochondria around the neck and long flagella in both Tsp and Ssp. TEM (b, c, e, and f) showing large U-shaped acrosomal vesicle (Ac) with a uniform electron dense materials (b and e), a crystalline-like structure in the subacrosomal region (asterisk), a highly condensed chromatin with some vacularlike structures (Va) in the sperm nuclei (Nu), and large globular mitochondria (Mi, c and f) in both sperm samples. T sperm tail, Pm plasma membrane, Am acrosomal membrane, Nm nuclear membrane



Profiles of the Membrane Proteins among Different Sperm Samples

Modification of sperm plasma membrane has been known to be one of the major events associated with post-testicular sperm maturation/capacitation process (Yanagimachi 1994; Vanichviriyakit et al. 2004). Two types of membrane proteins (based on their extractability) were analyzed, peripheral (NaCl-extractable) proteins and integral (Triton X-114-partitioning) proteins. NaCl-extractable proteins observed in Gc were mostly intermediate- and slow-migrating proteins ranging from 38 to 200 kDa. In addition, the fast migrating proteins of 15-33 kDa were mainly present in the peripheral proteins of Tsp, but were rarely detected in Gc proteins (Fig. 3, left panel, arrowheads). Compared with Tsp, the peripheral proteins of Ssp possessed at least three additional bands with the molecular masses of 26, 42, and 48 kDa (Fig. 3, left panel, arrows). Notably, the 23 kDa protein was present specifically in the Tsp peripheral proteins, but not in Ssp. For detergent-extractable proteins, two major protein bands of 33 and 130 kDa were apparent in the Gc extracts. Two additional detergent-miscible proteins with the molecular masses of 27 and 52 kDa and a set of 45-50 kDa proteins were visualized in the Tsp extracts, but not in that of Gc (Fig. 3, right panel, arrowheads). In Ssp, at least six additional integral proteins with the molecular masses of 24, 51, 78, 80, 97, and 100 kDa were observed additionally to those found in Tsp (Fig. 3, right panel, arrows).

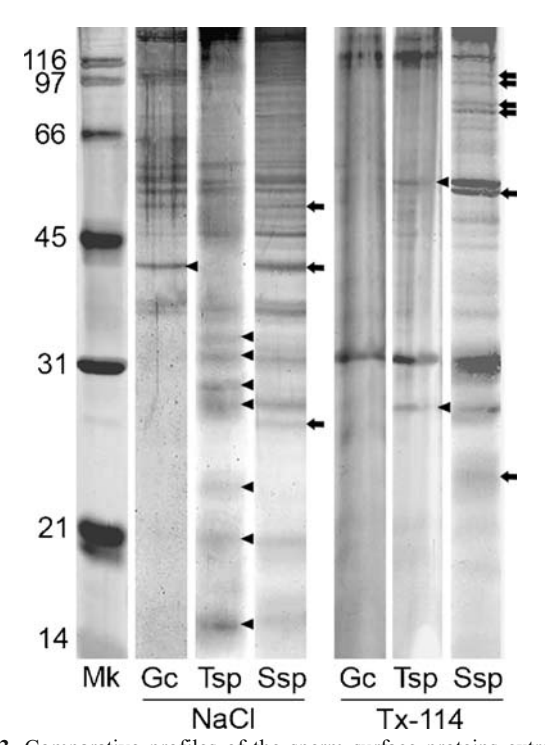


Fig. 3 Comparative profiles of the sperm surface proteins extracted from Gc, Tsp, and Ssp. High salt (NaCl) and detergent (Triton X-114) extracted proteins were resolved by 12.5% SDS–PAGE and visualized by silver staining. *Arrowheads* and *arrows* indicate the major differences in the protein patterns between Gc and Tsp and Tsp and Ssp, respectively. *Mk* molecular weight marker



Activation of Sperm Serine Proteases in Ssp Detergent Extracts

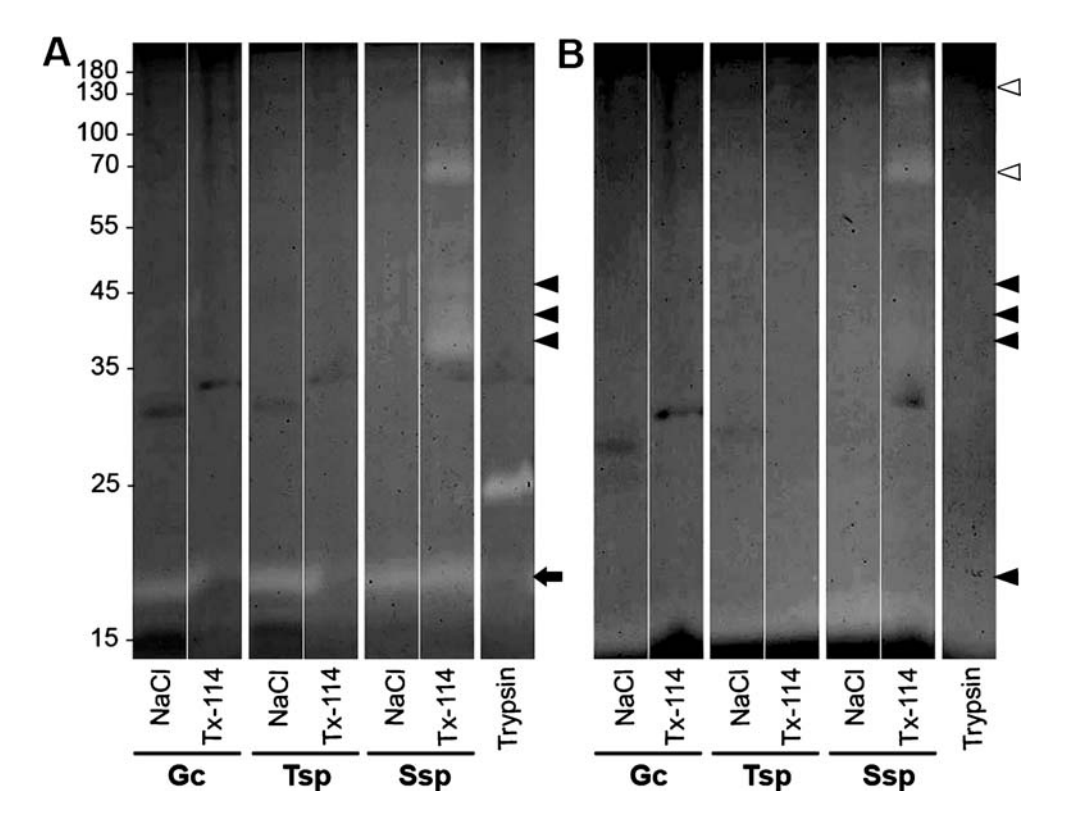
Sperm serine proteases, significant for the acrosome reaction, have been shown to be activated upon sperm transit into female reproductive organs (Lindsay and Clark 1992). This led us to hypothesize that activation of these serine proteases may also be a crucial step for abalone sperm to gain their full fertilizing ability. As shown in Fig. 4A, at least five proteolytically active proteins having the molecular masses of 38, 40, 46, 68, and 130 kDa were present in the detergent extracts of Ssp. It should be noted that these proteolytically active proteins had the different mobility pattern from those proteins that were additionally found in the integral proteins of Ssp compared with Tsp (Fig. 3, right panel, rightmost lane). Conversely, the enzymatic activity was minimal or absent in the detergent fractions of either Gc or Tsp. Notably, the only active protein band that was detectable in the NaCl extracts of all samples was an 18-kDa protein (Fig. 4A, arrow). This protein was also found to be active in the detergent extract of Ssp, but not in Gc or Tsp. Most of the enzyme activities in the aforementioned proteins including trypsin (as a positive control) were abolished upon pretreatment of sperm membrane proteins with either 2 mM PMSF (Fig. 4B) or SBTI (data not shown). However, some residual activity was still visible at the 68- and 130-kDa protein bands (Fig. 4B, empty

arrowheads). Taken together, these results suggested that sperm proteases, mainly serine ones, were activated upon the sperm release into seawater during spawning.

Changes in Protein Tyrosine Phosphorylation in the Sperm Extracts

Enhanced level of protein tyrosine phosphorylation is generally anticipated to be a key characteristic that is tightly related to sperm capacitation in both invertebrates and vertebrates (Vanichviriyakit et al. 2004; Visconti and Kopf 1998). Therefore, we also used this characteristic to detect biochemical changes within the three samples studied. Notably, immunoreactivity of anti-tyrosine phosphate was found to be limited to the small proteins with the molecular masses ranging from 15 to 20 kDa (Fig. 5A). The level of immunoreactive intensity of the phosphorylated proteins was relatively low in Gc, with only a trace amount of the 16-, 17-, and 19-kDa proteins detected. However, the intensity level of these three tyrosine phosphorylated protein bands and the additional 15 and 20 kDa ones were greatly enhanced in the Tsp sample. This high phosphorylation level remained constant in the Ssp sample (Fig. 5A). When an excess amount of phosphotyrosine-BSA was included to demonstrate a specific binding of the antityrosine phosphate antibody, only a background level of the antibody staining was observed (Fig. 5B).

Fig. 4 Proteolytic activity of the extracted membrane proteins in Gc, Tsp, and Ssp. NaCland detergent-extracted proteins of the three samples were resolved in 10% SDS-PAGE containing 0.3% gelatin under non-reducing condition. The resolved proteins were either untreated (A) or treated with 2 mM PMSF (B) before developing enzymatic reactions in the reaction buffer. Trypsin (rightmost lane in each panel) was also co-electrophoresed as a positive control. Clear bands against dark background represent enzymatically active protein bands. Solid and empty arrowheads indicate the diminished and remaining enzyme activities, respectively, upon treatment of the resolved proteins with inhibitors. Note the presence an 18-kDa active protein within the NaCl extracts of all three samples and in the detergent extract of Ssp (arrow)





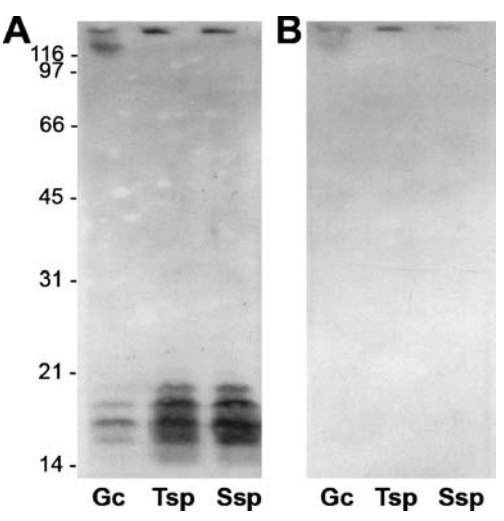


Fig. 5 Detection of protein tyrosine phosphorylation in the different germ cells. **A** Western blotted proteins of the whole cell lysates extracted from Gc, Tsp, and Ssp probed with monoclonal anti-tyrosine phosphate (1:20,000) and a corresponding HRP-conjugated secondary antibody (1: 3,000). **B** Negative control in which the primary antibody was pre-absorbed with a tyrosine phosphate–BSA conjugate

Comparative Fertilizing Abilities of Tsp and Ssp

Figure 6 demonstrated fertilizing abilities of both purified Tsp and Ssp as successful fertilization rates based on protrusion of polar bodies at 8- and 15-min post-insemination and occurrence of two-cell embryos at 20-min post-insemination. Fertilization rates of Tsp at 8 min were \sim 25% compared to \sim 34% in Ssp. Notably, fertilization rates at 15 min were \sim 27% and 77% for Tsp and Ssp, respectively, which were significantly different (P<0.05). However, the percent fertilization rates at 20 min of the Tsp samples greatly increased to \sim 66%, closely approaching to that observed in the Ssp samples (\sim 76%). The implication drawn from these results was that the isolated Tsp sperm possessed a fertilizing ability not dissimilar to Ssp; however, the activation to full fertilizing capacity might be delayed.

Discussion

Based on their ultrastructural features studied herein, H. asinina sperm could be classified as a primitive type because of the following criteria: a very large acrosome covering the anterior part of the nucleus, large-sized mitochondria around the neck region, and a simple structure of the tail consisting of 9 + 2 microtubule doublets surrounded by plasma membrane (Franzen 1983). In general, ultrastructures of Ssp were quite similar to those of the isolated Tsp and also to those sperm residing in the germinal epithelial cords of the testis (Apisawetakan et al. 2000). The only difference that could be detected was

that sperm head contour of Ssp was slightly wider than that of isolated Tsp, especially at the posterior region. A possible explanation of this could be due to the mechanical compression applied to the Tsp sperm head while they were embedded in cytoplasm of supporting epithelium or the swelling of Ssp upon their contact with seawater. It has been reported that a higher level of intermolecular crosslinking of protamines rendering higher compaction of chromosome and sperm head is associated with posttesticular sperm modification (Yanagimachi 1994). In H. asinina, chromatin condensation is also modulated by protamine-like basic nuclear proteins (Suphamungmee et al. 2005), consistent with other mollusks and even mammals (Ausio 1999; Balhorn et al. 1999). However, our results revealing the larger Ssp heads than those of Tsp (Fig. 2) would suggest that a post-testicular cross-linking of protamines resulting in the highly compacted sperm head may not occur in this abalone species.

In this study, we also compared the biochemical and physiological properties of the isolated germ cells (Gc, routinely used for fertilizing the spawned eggs in abalone aquaculture with a variable proportion of developing germ cells), purified testicular sperm (Tsp, having purity >90%), and the naturally spawned sperm (Ssp, having full fertilizing ability). Three lines of experimental evidence shown herein allowed us to imply that capacitation-related mechanisms took place during differentiation of testicular germ cells, which may associate with fertilizing capacity of these cells, particularly Tsp. Firstly, gradual modifications of membrane-associated proteins, both peripheral and integral proteins, could be detected from Gc to Tsp and Ssp (Fig. 3). These sperm membrane alterations noticed

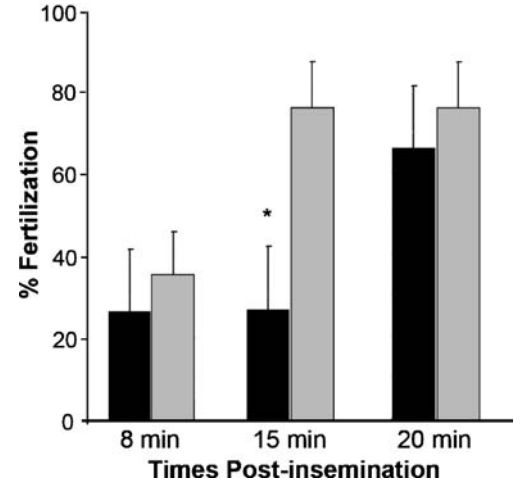


Fig. 6 Comparative fertilization rates of Tsp and Ssp. The rates were determined by the occurrence of polar bodies at 8 and 15 min as well as the presence of two-cell embryos at 20 min under a phase contrast microscope. One thousand eggs were loaded into each well of a 16-well plate, followed by the addition of 10^5 Tsp (*black bars*) and Ssp (*gray bars*). The data were expressed as mean \pm SD from six replicates. *Asterisk* denotes significant difference (P<0.05)



along with the enhanced fertilizing ability are known to be coupled with both sperm maturation and capacitation processes in invertebrates and mammals (Yanagimachi 1994, Vanichviriyakit et al. 2004). Secondly, an enhanced level of protein tyrosine phosphorylation was detectable as early as in Tsp (Fig. 5). Increased phosphorylation in a broad spectrum of sperm proteins has been thought to be a characteristic of downstream-signaling event closely associated with sperm capacitation in many mammals as well as in some invertebrates (Asquith et al. 2004; Naz and Rajesh 2004; Vanichviriyakit et al. 2004; Krapf et al. 2007). Our results reveal for the first time the enhancement of this signal transduction pathway in the isolated Tsp at a level comparable with Ssp. These results suggest that the molecular machineries that mark full fertilizing capability of the sperm are readily present in Tsp (Fig. 5). Thirdly, the activation of sperm serine proteases was observed in the sperm upon spawning into seawater (Fig. 4). This finding was consistent with the activation of serine proteases, particularly trypsin-like enzymes, during sperm transit into the closed-thelycum of female reproductive tracts as part of capacitation process in penaeoid shrimp (Lindsay and Clark 1992; our unpublished results). These shrimp enzymes belong to the acrosomal contents that serve their crucial function in the acrosomal reaction. This function corresponds with the function of the well-studied mammalian acrosomal serine proteases, proacrosin/acrosin (Arboleda and Gerton 1988; Barros et al. 1992; Pasten et al. 2005). Knocking out of this proacrosin/acrosin system has led to a prolonged delay in fertilization process (Baba et al. 1994; Adham et al. 1997; Nayernia et al. 2002). It should be noted that other proteases aside from serine ones (resistant to PMSF with the molecular masses of 68 and 180 kDa; Fig. 4b) were also present in the detergent extracts of Ssp. Identification and physiological function related to fertilization of these proteases still require further investigation.

The high levels of fertilization rate observed for the isolated Tsp, comparable with Ssp (Fig. 6), correlated with the onset of at least two capacitation associated characteristics detected in Tsp, namely, the membrane protein alterations and the enhanced protein tyrosine phosphorylation. The lack of proteolytic activation in the isolated Tsp made them biochemically different from Ssp (Fig. 4). This absence of proteolytic activity in Tsp may account for the delay of fertilization (as gauged from a significant difference in polar body extrusion at 15 min; Fig. 6). However, it appeared not to affect the final fertilizing capacity of Tsp (as deduced from the comparable fertilization rate at 20 min of Tsp and Ssp). In fact, this finding was in agreement with the aforementioned knockout studies of the proacrosin/acrosin system which results in a delayed fertilization time but not fertilizing ability (Baba et al. 1994; Adham et al. 1997; Nayernia et al. 2002). It remains to be proven whether trypsin-like enzymes in the abalone Tsp are activated upon the contact of these sperm with the egg surface. From these results, we believe that the fertilizing ability of abalone sperm is acquired during testicular residence via capacitation-like molecular machineries. These capacitation-related characteristics could be used as biomarkers for predicting sperm fertilizing capability especially in cases when isolated germ cells are used in place of naturally spawned sperm. Moreover, the use of purified Tsp to replace spawned sperm may improve both fertilization rates and consistency in the abalone aquaculture.

Acknowledgments This research was supported by Thailand Research Fund (to PS and WW and Royal Golden Jubilee Ph.D. Scholarship Program to WS) and Mahidol University.

References

Adham IM, Nayernia K, Engel W (1997) Spermatozoa lacking acrosin protein show delayed fertilization. Mol Reprod Dev 46:370–376 Alfaro J, Munoz N, Vargas M, Komen J (2003) Induction of sperm activation in open and closed thelycum penaeoid shrimps. Aquaculture 216:371–381

Apisawetakan S, Sobhon P, Wanichanon C, Linthong V, Kruatrachue M, Upatham ES, Jarayabhand P, Pumthong T, Nugranad J (2000) Ultrastructure of spermatozoa in the testis of *Haliotis asinina* Linnaeus. J Med Appl Malacol 10:101–109

Arboleda CE, Gerton GL (1988) Proacrosin/acrosin during guinea pig spermatogenesis. Dev Biol 125:217–225

Asquith KL, Baleato RM, McLaughlin EA, Nixon B, Aitken RJ (2004) Tyrosine phosphorylation activates surface chaperones facilitating sperm-zona recognition. J Cell Sci 117:3645–3657

Ausio J (1999) Histone H1 and evolution of sperm nuclear basic proteins. J Biol Chem 274:31115–31118

Baba T, Azuma S, Kashiwabara S, Toyada Y (1994) Sperm from mice carrying a targeted mutation of the acrosin gene can penetrate the oocyte zona pellucida and effect fertilization. J Biol Chem 269 (50):31845–31849

Balhorn R, Cosman M, Thornton K, Krishnan VV, Corzett M, Bench G, Kramer C, Lee JD IV, Hud NV, Allen MJ, Prieto M, Meyer-Iese W, Brown JT, Kirz J, Zhang X, Bradbury EM, Maki G, Braun RE, Breed W (1999) Protamine mediated condensation of DNA in mammalian sperm. In: Gagnon C (ed) The male gamete: from basic science to clinical applications. Cache River Press, Vienna IL, pp 55–70

Barros C, Capote C, Perez C, Crosby JA, Becker MI, De Ioannes A (1992) Immunodetection of acrosin during the acrosome reaction of hamster, guinea-pig and human spermatozoa. Biol Res 25:31–40

Bedford JM (1983) Significance of the need for sperm capacitation before fertilization in eutherian mammal. Biol Reprod 28:108–120 Bordier C (1981) Phase separation of integral membrane proteins in

Triton X-114 solution. J Biol Chem 256:1604–1607
Bradford MM (1976) A rapid and sensitive method for the

Bradford MM (1976) A rapid and sensitive method for the quantitation of microgram quantities of protein utilizing the principle of protein-dye binding. Anal Biochem 72:248–254

Dusenbury DB (2000) Selection for high gamete encounter rates explains the success of male and female mating types. J Theor Biol 202:1–10

Encena VC II, Capinpin EC Jr, Bayona NC (1998) Optimal sperm concentration and time for fertilization of the tropical abalone, *Haliotis asinina* Linné 1758. Aquaculture 165:347–352



- Foster JA, Friday BB, Maulit MT, Blobel C, Winfrey VP, Olson GE, Kim KS, Gerton GL (1997) AM67, a secretory component of the guinea pig sperm acrosomal matrix, is related to mouse sperm protein sp56 and the complement component 4-binding proteins. J Biol Chem 272:12714–12722
- Franzen A (1983) Ultrastructural studies of spermatozoa in three bivalve species with notes on evolution of elongated sperm nucleus in primitive spermatozoa. Gamete Res 7:199–214
- Gardner C, Williams H (2002) Maturation in the male giant crab, Pseudocarcinus gigas, and the potential for sperm limitation in the Tasmanian fishery. Mar Freshwater Res 53:661–667
- Giese AC, Kanatani H (1987) Maturation and spawning. In: Giese AC, Pearse JS, Pearse VB (eds) Reproductive Biology of Invertebrates. Boxwood Press, Pacific Grove, CA, pp 251–329
- Griffin FJ, Clark WH Jr (1990) Induction of acrosomal filament formation in the sperm of Sicyonia ingentis. J Exp Zool 254:296–304
- Grubert MA, Mundy CN, Ritar AJ (2005) The effects of sperm density and gamete contact time on the fertilization success of blacklip (*Haliotis rubra*; Leach, 1814) and greenlip (*H. laevigata*; Donovan, 1808) abalone. J Shellfish Res 24:407–413
- Kim KS, Gerton GL (2003) Differential release of soluble and matrix components: evidence for intermediate states of secretion during spontaneous acrosomal exocytosis in mouse sperm. Dev Biol 264 (1):141–152
- Krapf D, Visconti PE, Arranz SE, Cabada MO (2007) Egg water from the amphibian Bufo arenarum induces capacitation-like changes in homologous spermatozoa. Dev Biol 306:516–524
- Laemmli UK (1970) Cleavage of structural proteins during the assembly of the head of bacteriophage T4. Nature 227:680–685
- Levitan DR, Sewell MA, Chia FS (1991) Kinetics of fertilization in the sea urchin *Strongylocentrotus franciscanus*: interaction of gamete dilution, age, and contact time. Biol Bull 181:371–378
- Lindsay LL, Clark WH Jr (1992) Preloading of micromolar intracellular Ca²⁺ during capacitation of *Sicyonia ingentis* sperm, and the role of the pHi decrease during the acrosome reaction. J Exp Zool 262:219–229
- Liu W, Heasman M, Simpson R (2004) Evaluation of cytochalasin B (CB) treatments for triploidy induction in the blacklip abalone, *Haliotis rubra*. Aquaculture Res 35:1062–1075
- Lowry OH, Rosenbrough NJ, Farr AL, Randall RJ (1951) Protein measurement with the Folin phenol reagent. J Biol Chem 193:265–275

- Mastro R, Hall M (1999) Protein delipidation and precipitation by trin-butylphosphate, acetone, and methanol treatment for isoelectric focusing and two-dimensional gel electrophoresis. Anal Biochem 273:313–315
- Meidel SK, Yund PO (2001) Egg longevity and time-integrated fertilization in a temperate sea urchin (*Strongylocentrotus droebachiensis*). Biol Bull 201(1):84–94
- Nayernia K, Adham IM, Shamsadin R, Müller C, Sancken U, Engel W (2002) Proacrosin-deficient mice and zona pellucida modifications in an experimental model of multifactorial infertility. Mol Hum Reprod 8:434–440
- Naz RK, Rajesh PB (2004) Role of tyrosine phosphorylation in sperm capacitatation/acrosome reaction. Reprod Biol Endocinol 2:75
- Pasten C, Morales P, Kong M (2005) Role of the sperm proteasome during fertilization and gamete interaction in the mouse. Mol Reprod Dev 71:209–219
- Rios M, Barros C (1997) Trypsin-like enzymes during fertilization in the shrimp *Rhynchocinetes typus*. Mol Reprod Dev 46:581– 586
- Septo NK, Cook PA (1998) Induction of triploidy in the South African abalone using cytochalasin B. Aquaculture Int 6:161–169
- Suphamungmee W, Apisawetakan S, Weerachatyanukul W, Wanichanon C, Sretarugsa P, Poomtong T, Sobhon P (2005) Basic nuclear protein pattern and chromatin condensation in the male germ cells of a tropical abalone, *Haliotis asinina*. Mol Reprod Dev 70:211–221
- Vanichviriyakit R, Kruevaisayawan H, Weerachatyanukul W, Tawipreeda P, Withyachumnarnkul B, Pratoomchat B, Chavadej J, Sobhon P (2004) Molecular modification of *Penaeus monodon* sperm in female thelycum and its consequent responses. Mol Reprod Dev 69:356–363
- Visconti PE, Kopf GS (1998) Regulation of protein phosphorylation during sperm capacitation. Biol Reprod 59:1–6
- Yanagimachi R (1994) Mammalian fertilization. In: Knobil E, Neill JD (eds) Physiology of reproduction. 2nd edn. Raven, NY, pp 189–317
- Yi JH, Lefievre L, Gagnon C, Anctil M, Dube F (2002) Increase of cAMP upon release from prophase arrest in surf clam oocytes. J Cell Sci 115:311–320
- Yund PO (2000) How severe is sperm limitation in natural populations of marine free-spawners? Trends Ecol Evol 15(1):10–13



Induction of the Acrosome Reaction in Black Tiger Shrimp (*Penaeus monodon*) Requires Sperm Trypsin-Like Enzyme Activity¹

Hathairat Kruevaisayawan,^{3,4} Rapeepun Vanichviriyakit,^{3,4} Wattana Weerachatyanukul,^{2,4} Sitthichai Iamsaard,^{4,5} Boonsirm Withyachumnarnkul,^{4,5} Ajoy Basak,^{6,7,8} Nongnuj Tanphaichitr,^{3,6,7,9} and Prasert Sobhon^{3,4}

Department of Anatomy⁴ and Center of Excellence for Shrimp Molecular Biology and Biotechnology (Centex Shrimp),⁵ Faculty of Science, Mahidol University, Bangkok 10400, Thailand Chronic Disease,⁶ Ottawa Health Research Institute, Ottawa, Ontario K1Y 4E9, Canada Departments of Biochemistry/Microbiology/Immunology,⁷ Medicine,⁸ and Obstetrics and Gynecology,⁹ University of Ottawa, Ottawa, Ontario K1H 8M5, Canada

ABSTRACT

Trypsin-like enzymes in egg water (EW), a natural acrosome reaction (AR) inducer, are known for their importance in shrimp AR. In this report, we describe a unique phenomenon of the AR of black tiger shrimp (Penaeus monodon) sperm. It was completed within 45-60 sec and comprised only the acrosomal exocytosis and depolymerization of the sperm head anterior spike. We used peptidyl fluorogenic substrates to show the presence of trypsin-like enzymes in P. monodon EW and sperm, but minimal activities of chymotrypsin-like enzymes. In sperm, these trypsin-like enzymes existed both on the sperm surface and in the acrosome. The acrosomal enzyme was revealed as a 45kDa band by fluorogenic substrate in-gel zymography. Although EW possessed high trypsin-like enzyme activities, they were not essential for the AR induction; EW pretreated with an irreversible trypsin inhibitor, or heat-inactivated EW (HI-EW), to abolish the trypsin-like activities could still induce the AR. The HI-EW-induced AR was inhibited by the presence of a membrane impermeant soybean trypsin inhibitor (SBTI) in the sperm suspension, indicating the significance of sperm-borne trypsin-like enzymes (on the surface and/or in the acrosome) in this AR process. However, pretreatment of sperm with SBTI followed by its removal from the suspension still allowed the AR to occur within 5 min of sperm exposure to HI-EW. Since trypsin-like activity of the SBTI-pretreated sperm surface at 5 min after SBTI removal was at the minimal level, our results suggest the importance of the acrosomal trypsin-like enzyme in the AR process.

acrosome reaction, egg water, fertilization, gamete biology, P. monodon, sperm, trypsin

Received: 25 October 2007. First decision: 21 November 2007. Accepted: 27 March 2008.

© 2008 by the Society for the Study of Reproduction, Inc.

ISSN: 0006-3363. http://www.biolreprod.org

INTRODUCTION

In penaeoid shrimp, spermatophores have to be inserted into the female seminal receptacle (called thelycum) before the release of sperm together with eggs during spawning [1]. It has been shown previously that sperm gain fertilizing ability during their storage in the thelycum [2, 3]. Unlike sperm of other marine invertebrates, penaeoid sperm are nonflagellated and immotile [4, 5]. The success of fertilization in these shrimp thus relies on two key steps: contact of the sperm anterior spike with the egg outer vestment and the subsequent acrosome reaction (AR). The AR process involves a triggered fusion of the sperm plasma membrane with the outer acrosomal membrane, leading to the release of the acrosomal vesicles and soluble content. Thereafter, the AR spermatozoon interacts, fuses, and incorporates into the egg proper. In Sicyonia ingentis, the AR has been shown to be a biphasic process. During the first phase, the anterior spike of the sperm becomes depolymerized upon contacting the vitelline envelope (VE), leading to an acrosomal exocytosis. The second phase involves the formation of the acrosomal filament, which binds to the egg plasma membrane, followed by gamete plasma membrane fusion [5-7]. These two distinct events are temporally separated, and can be induced by two different inducers [7]. While the event in the first AR phase is common in all penaeoid sperm, formation of the acrosomal filament during the second AR phase cannot be detected in some penaeoid shrimp, including Penaeus aztecus, Penaeus setiferus, and Penaeus stylirostris [8].

In Penaeus monodon, detailed information of the AR has not yet been described. Our preliminary work indicates that the AR in P. monodon differs drastically from that of S. ingentis in both timing and morphological alterations [9]. The AR occurring as part of the fertilization process of P. monodon takes only a few minutes compared with \sim 45–60 min in S. ingentis [10]. This rapid process makes it difficult to detect the various steps of morphological changes during the AR in this species. Overall structural alterations during the AR in P. monodon, as detected at the light microscopic level, include depolymerization of the anterior spike, in conjunction with the swelling and rupturing of the acrosomal vesicle. However, the formation of the acrosomal filament during the AR is not notable in P. monodon sperm. Therefore, spike depolymerization and rupture of the acrosomal vesicle are used to mark completion of AR in this species.

Egg water (EW), a flocculent material in seawater that is generated during egg spawning, has been commonly used for in vitro induction of sperm AR in several aquatic species,

¹Supported by funding from the National Science and Technology Development Agency of Thailand to B.W., the Thailand Research Fund to W.W. and P.S., Thailand Research Fund-Royal Golden Jubilee Ph.D. Program grant PHD/0275/2545 to R.V., and from the Commission on Higher Education to H.K. and S.I.

²Correspondence: Wattana Weerachatyanukul, Department of Anatomy, Faculty of Science, Mahidol University, Rama 6 Rd., Payathai, Bangkok 10400, Thailand. FAX: 66 2 354 7168;

e-mail: scwwy@mahidol.ac.th
³These authors contributed equally to this work.

including sea urchins [11, 12], sturgeons [13], and shrimp [10]. EW of penaeoid shrimp is made up of components released from the female during spawning, including the outermost layer of the eggs, VE, cortical rods (CRs), which are the egg jelly components embedded in the egg surface crypts, and some thelycal (T) substances. In S. ingentis, the trypsin-like proteolytic activity in EW is important for acrosomal filament formation during the second AR phase [7, 14]. The given explanation is that trypsin may hydrolyze enzymes or channel proteins in the inner acrosomal membrane, thus activating filament formation [14]. Whether or not these EW enzymes are involved in any steps of the AR induction in P. monodon remains to be addressed. In this study, we determined whether EW trypsin-like enzymes were involved in any steps of the AR induction in P. monodon. Alternatively, EW may be involved in the initial part of AR induction, simply through its binding to the sperm surface. Furthermore, since sperm of many invertebrate species have been known to contain trypsin-like enzymes [14–16], we investigated their existence and possible involvement in P. monodon sperm AR induction.

MATERIALS AND METHODS

Sample Collection

Collection of EW was carried out at the Bangkok Aquaculture Farm Company, Nakhon Sri Thammarat Province, Thailand. Female shrimp possessing mature ovaries (stage IV) were individually placed in a 500-L plastic tank. In order to exclude sperm factors in the EW, only shrimp that had not been inseminated were used in this study. The shrimp were held firmly over a 500-ml container and allowed to spawn their eggs into filtered seawater. After swirling gently to settle the eggs to the bottom, seawater without spawned eggs was collected and designated as EW. This EW was centrifuged ($10\,000 \times g$, $15\,$ min, 4° C) to remove particulates, and kept at -80° C until use. Proteins in the EW were quantified with a Bradford's reagent (Sigma, St. Louis, MO) [17].

To collect T sperm , inseminated females were anesthetized under ice, and the thelyca located at the fifth pair of walking legs were carefully removed and placed in calcium-free artificial seawater (CFASW; 423 mM NaCl, 9 mM KCl, 23 mM MgCl₂, 9.3 mM MgSO₄, 2.1 mM NaHCO₃, pH 7.8). Subsequently, they were teased with dissecting forceps to release sperm masses and fluid. The T-sperm suspension was filtered through a 212-µm metal sieve (Endecotts, London, UK) to remove aggregates, washed (500 \times g, 5 min), and resuspended in CFASW at the final concentration of 1×10^7 sperm/ml before use. T fluid (TF) was also collected from the female shrimp, which had not been inseminated, following the dissecting method described above. This fluid was centrifuged (12 000 \times g, 10 min, 4°C) to remove any small particulates, assayed for the protein concentration as mentioned above and kept frozen at $-80^\circ\mathrm{C}$ until use.

CRs were isolated from mature ovaries according to the method described by Lynn and Clark [18]. Briefly, pieces of ovaries were homogenized in an isolation medium (IM; 500 mM NaCl, 9 mM CaCl₂, 14 mM KCl, 15 mM MgCl₂, and 10 mM Tris-HCl, pH 7.6) containing 30% sucrose. The homogenate was centrifuged (1000 \times g, 5 min, 4°C). The pellet containing CRs was resuspended in IM, and the suspension was overlaid onto 60% sucrose in IM and centrifuged (8000 \times g, 60 min, 4°C). The white pellet containing mainly CRs was washed four times with IM. As in physiological conditions, isolated CRs were left overnight (4°C) in artificial seawater (ASW; same compositions as CFASW, but with 9.3 mM CaCl₂, pH 7.8) to obtain soluble materials. Solubilization of CRs was also facilitated by brief sonications (100 W, 15 sec, 4°C, three times) before the overnight incubation. Protein concentration of the solubilized CRs was measured as described above.

Induction of the Sperm AR with EW

Isolated T-sperm in CFASW were pelleted and resuspended in ASW. The sperm were then treated with various concentrations of EW (1–64 $\mu g/ml$) for 5 min or with 16 $\mu g/ml$ EW for various time periods (0–600 sec) at room temperature to induce the AR. Alternatively, EW treated with amidino-PMSF (APMSF; a trypsin inhibitor) (APMSF-EW) or heat-inactivated EW (HI-EW) (see below) was used in place of native EW in the AR induction. Treated sperm were fixed with 4% paraformaldehyde in ASW and the percentages of unreacted (with an intact long anterior spike) and reacted (without the anterior spike) sperm were scored under a phase contrast microscope. The percentage of

spontaneous AR was assessed from sperm treated with ASW. Approximately 200 sperm were counted for each data point. Each experiment was repeated at least three times with different sperm samples.

Electron Microscopy of Acrosome Intact and Reacted Sperm

Sperm were fixed with 2% glutaraldehyde and 4% paraformaledehyde in ASW (pH 7.8, 2 h, 4°C). They were then postfixed in 1% ${\rm OsO_4}$ in ASW, dehydrated in increasing percentages of cold ethanol, and finally embedded in Spurr's resin (EMS, Fort Washington, PA). Thin sections (\sim 70 nm) were cut and mounted on formvar-coated copper grids and counterstained with lead citrate and uranyl acetate before being viewed under an FEI Tecni-20 transmission electron microscope (FEI-USA, Hillboro, OR) at 80 kV.

Binding of Fluorescently Labeled EW to the Sperm Surface

EW was conjugated to an Alexa-488 fluorescent reactive dye (Molecular Probes, Eugene, OR) according to the manufacturer's procedures. Since EW initiated AR very rapidly (see Fig. 1C), we used aldehyde-fixed AI sperm for the EW-sperm binding experiments. T-sperm collected in CFASW were fixed with 4% paraformaldehyde in ASW (1 h, room temperature). Fixed sperm were washed twice with ASW and blocked with 4% BSA containing 0.1 M glycine in ASW (30 min, room temperature). The sperm were incubated (15 min, room temperature) with 16 µg/ml fluorescently labeled EW, washed twice (500 × g, 10 min) to eliminate unbound EW, plated on a slide, and topped with a coverslip before being observed under a Nikon Eclipse epifluorescent microscope equipped with a Nikon DXM 1200 CCD camera (Nikon Corp., Kanagawa, Japan). T-sperm were also incubated with Alexa-488 EW in the presence of a 50-fold unlabeled EW.

Effects of Protease Inhibitors on the EW-Induced AR

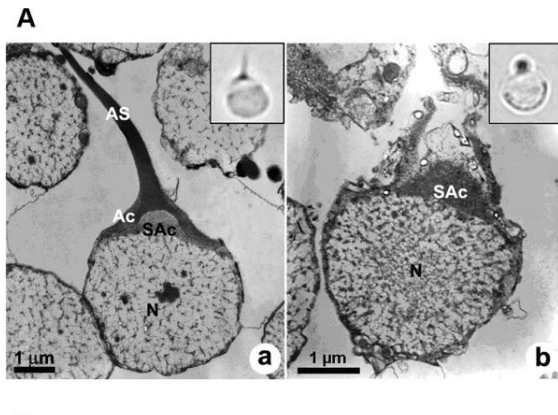
To test whether AR induction was dependent on protease activities, various concentrations of protease inhibitors (all from Sigma) were preaded to EW prior to coincubation with T-sperm resuspended in ASW. These inhibitors included the following: 1) serine protease inhibitors, PMSF (0.1–1 mM), APMSF (0.2–1 mM), soybean trypsin inhibitor (SBTI; 0.1–0.4 mM); 2) cysteine protease inhibitor, E-64 (1–100 μ M); 3) aspartic protease inhibitor, pepstatin A (1–10 μ M); and 4) metalloprotease inhibitor, EGTA (0.25–1 mM). The percentage of the AR response was analyzed according to the aforementioned protocol.

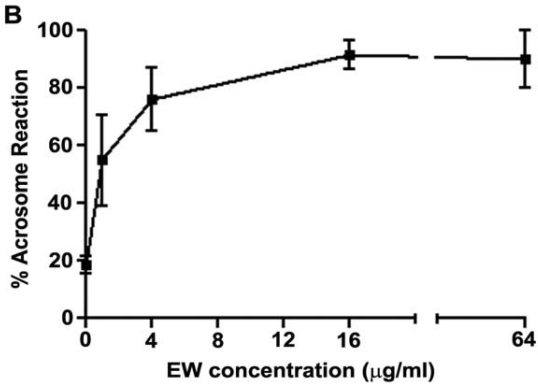
To determine whether EW-derived proteases, especially trypsin-like ones, were mediators of AR, HI-EW or APMSF-EW was used in place of native EW to treat sperm. HI-EW was prepared by heating EW to 100°C for 2 h, followed by freezing at -20°C overnight. The activity of this HI-EW was examined with a trypsin-specific fluorogenic substrate (as described below) in parallel with native EW. The remaining activity of HI-EW was compared with that of native EW. APMSF-EW was prepared by preincubating EW with 0.5 mM APMSF at 4° C for 2 h. The mixture was washed and concentrated ($10\,000 \times g$, 15–30 min, 4°C) three times with ASW through a Microcon YM-10 centrifugal device (Millipore, Bedford, MA) to remove unbound APMSF, which came down in the flow-through fraction. Native EW that washed and concentrated in a similar fashion as APMSF-EW served as an experimental sham control. The remaining activity of APMSF-EW was then determined and compared with that of the EW sham control, HI-EW, APMSF-EW, and sham-EW were used to treat the sperm in place of native EW and the number of AR sperm was scored as described above.

In an alternative experiment, sperm-borne trypsin-like enzymes of acrosome-intact (AI) sperm were inhibited with 0.4 mM membrane impermeant SBTI (15 min, room temperature). The excess amount of the inhibitor was washed from sperm by centrifugation ($500 \times g$, 5 min, twice). Aliquots of this sperm suspension were then induced to undergo AR with 16 μ g/ml HI-EW (5 min, room temperature), and assayed for the AR responses following the protocol described above. Another aliquot of sperm was used for trypsin-like enzyme assays at various time points after the removal of SBTI.

Enzyme Assays

Serine protease assay was performed according to the previously described method [19] with some modifications. Fluorogenic-4-methylcoumarin-7-amide (MCA) substrates were used in these assays. These included a final concentration of 20 µM of Boc-Gln-Ala-Arg-MCA (Boc = t-butyloxycarbonyl; Peptide Institute, Louisville, KY) for trypsin-like enzymes, and Suc-Ala-Ala-Pro-Phe-MCA (Suc = succinyl; Bachem, Torrance, CA) for chymotrypsin-like enzymes. All assays were performed at room temperature in a final volume of





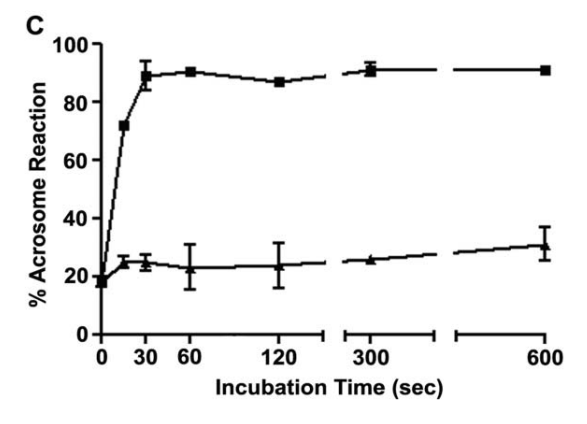


FIG. 1. **A**) Transmission electron micrographs of the AI (**a**) and AR (**b**) sperm after 5-min induction with EW. Inset in each figure represents the corresponding phase contrast micrograph. Increases in the AR responses were dependent on the concentration (**B**) of and incubation time with EW (**C**, square symbol). Triangles in **C** represent spontaneous AR when ASW was used in place of EW for sperm incubation. Data in this figure and the remainder are expressed as mean \pm SD from three replicates performed on different sperm samples. Ac, Acrosome; AS, anterior spike; N, nucleus; Sac, subacrosomal region.

 $100~\mu l$ in a 96-well, flat-bottom black plate (Corning Inc., Corning, NY). The samples included EW-related samples (native EW, HI-EW, and APMSF-EW) and T-sperm-related samples (untreated live sperm and SBTI-treated live sperm, AR sperm, and acrosomal vesicles and content). The reaction mixture was comprised of $10~\mu l$ of each sample, $10~\mu l$ of 0.2~mM substrate solution in 10% dimethyl sulfoxide, and $80~\mu l$ of buffer A (10 mM CaCl $_2$, 0.001% Triton X-100 in 50~mM Tris-HCl, pH 7.5) for trypsin-like enzyme assay, or buffer B (10 mM CaCl $_2$ in 50~mM Tris-HCl, pH 8.0) for chymotrypsin-like enzyme assay. Fluorescent 7-amino-4-methylcoumarin (AMC), the released product from substrate hydrolysis, was monitored spectrofluorometrically at various time points with a Spectra Max Gemini XS (Molecular Dynamics, Sunnydale, CA), with excitation and emission wavelengths of 360~and 470 nm, respectively. The measured raw fluorescence units were converted to the amount of free AMC released by using an AMC standard curve. One unit of the

enzyme activity was defined as a picomole of AMC released per hour at 25°C from Boc-Gln-Ala-Arg-MCA for trypsin-like activity or from Suc-Ala-Ala-Pro-Phe-MCA for chymotrypsin-like activity. Specific activity of the enzyme was defined as unit activity per microgram protein.

Characterization of a Trypsin-Like Acrosomal Enzyme by Fluorogenic Substrate in-Gel Zymography

The released acrosomal vesicles and content of P. monodon sperm were collected as a supernatant of T-sperm that were induced to undergo the AR by HI-EW, as described above. This AR supernatant collected from 5×10^6 sperm possessed 1500 U of trypsin like activity, when Boc-Gln-Ala-Arg-MCA was used as the substrate (see the enzyme assay method above). The supernatant of AI sperm (sham-treated with ASW) was also collected from the same number of sperm and used as a negative control; it contained only 100 U of trypsin-like activity. The zymography method described by Yasothornsrikul and Hook [20] was used to characterize the trypsin-like enzyme in the supernatant of AR sperm. An SDS-10% polyacrylamide gel was copolymerized with 200 μM Boc-Gln-Ala-Arg-MCA in 0.375 Tris-HCl, pH 8.8, and 0.4% SDS. The separation gel was allowed to polymerize in the dark at room temperature. When polymerization of the separation gel was complete, the stacking gel, consisting of 4% polyacrylamide, 0.330 mM Tris-HCl, pH 6.8, and 0.1% SDS, was cast and polymerized. Subsequently, 10 µl of the supernatant from AR or AI sperm, or purified trypsin (0.5 ng of 8000 U; Roche Applied Science, Indianapolis, IN) was mixed with 10 μl of 2× Laemmli sample loading buffer [21] without heating, and then loaded into the gel well. Electrophoresis was performed in the dark at 4°C at a constant current of 10 mA until completed. The gel was then washed in 2.5% Triton X-100 solution to remove SDS for 15 min at room temperature, followed by washing seven times in cold distilled water (5 min for each wash). The gel was subsequently incubated in trypsin zymography developing buffer (200 mM NaCl, pH 7.5, 20 mM Hepes, 10 mM CaCl₂ and 0.005% Triton X-100) at 37°C for 30 min. Fluorescent bands indicating trypsin activity were immediately observed and recorded with an Ultraviolet Transilluminator (Alpha Innotech Inc, San Leandro, CA).

RESULTS

Induction of the AR with EW

The morphology of the AI and AR P. monodon sperm are shown in Figure 1A. Transmission electron microscopy revealed the presence of electron-dense materials in the anterior spike, and moderately electron-dense materials in the acrosome and subacrosomal region of the AI sperm (Fig. 1A, a). Within 5 min of EW addition, the anterior spike completely disappeared along with the rupture of the acrosome (Fig. 1A, b). The subacrosomal region of the AR sperm became somewhat larger and more electron dense compared with that of the AI sperm (Fig. 1A, b versus Fig. 1A, a). There was no evidence for the acrosomal filament formation (as seen in S. ingentis) [22], even at the longer incubation time period (>10 min) (data not shown). At the light microscopic level, the disappearance of the anterior spike and the presence of dark subacrosomal materials in the AR sperm were evident. These features were thus used to differentiate between AI and reacted sperm in all experiments described below.

The ability of a natural inducer, EW, to induce the AR in P. monodon sperm was concentration dependent (Fig. 1B). Within 5 min of sperm treatment with 1 and 4 μ g/ml EW, the AR levels were 54.9 \pm 15.7% and 76.1 \pm 11.0%, respectively. At 16 μ g/ml of EW, the maximal AR response was reached (90.1 \pm 9.9%). This EW concentration was therefore selected for all subsequent experiments. When ASW was used in place of EW, \sim 20% of sperm underwent spontaneous AR.

Time-dependent AR induction of *P. monodon* sperm by EW is demonstrated in Figure 1C. Within 15 sec of the EW treatment, $71.9 \pm 0.9\%$ of sperm underwent AR, whereas only $25.0 \pm 2.0\%$ of sperm treated with ASW became AR. The percentage of AR sperm increased to the maximal value of 89.3 \pm 4.9% within 30 sec of EW incubation time, and remained

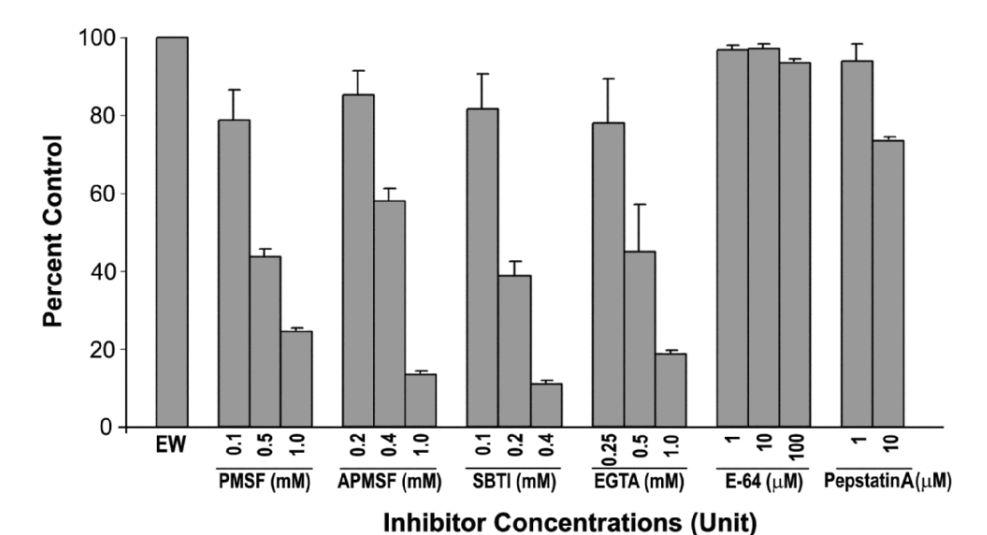


FIG. 2. Effects of various protease inhibitors on the EW-induced AR. T-sperm ($\sim 5 \times 10^5$) were incubated at room temperature with EW (16 µg/ml) in 50 µl ASW in the presence of various concentrations of different protease inhibitors (PMSF, APMSF, SBTI, EGTA, E-64, and pepstatin A). The AR levels obtained from control sperm (incubated with EW without any inhibitors) were assigned as 100%, and the AR extent of sperm incubated with EW in the presence of the protease inhibitor was expressed as percent of control. Data are expressed as mean \pm SD of results of three or more replicate experiments.

constant afterwards. In contrast, the spontaneous AR rate of sperm incubated with ASW remained at $\sim\!25\%$ -30% within 5 min of the ASW incubation. We therefore chose the 5-min incubation period for subsequent experiments.

Trypsin-Like Proteases Mediated AR Induction in Shrimp Sperm

We investigated the possible involvement of proteases in sperm AR induction. Results shown in Figure 2 indicate that inhibitors of trypsin (PMSF, APMSF, and SBTI) inhibited EW-induced AR in a dose-dependent manner. Notably, SBTI at 0.4 mM decreased EW-induced AR to only 12% of the control values. PMSF and APMSF at 1 mM also exerted marked inhibition (75%–85%) of the EW-induced AR. Inclusion of EGTA, a specific Ca $^{2+}$ chelator and metalloprotease inhibitor, also showed a dose-dependent inhibitory effect, and, at 1.0 mM EGTA, the inhibition of the EW-induced AR was $\sim\!80\%$. E-64 and pepstatin A, inhibitors of cysteine and aspartic proteases, respectively, exerted no or very low inhibitory effects on sperm AR induction at all concentrations tested.

Existence of Trypsin-Like Enzymes in EW

Among serine proteases, trypsin and chymotrypsin have been shown to be significant for sperm AR induction [15, 23]. We thus investigated the existence and physiological functions of these two proteases in EW. Results in Table 1 show that EW demonstrated trypsin-like activity. It selectively hydrolyzed the trypsin-specific substrate (Boc-Gln-Ala-Arg-MCA), with a specific activity of 30.7 U/µg protein. In contrast, EW possessed minimal chymotrypsin-like activity when testing with suc-Ala-Ala-Pro-Phe-MCA as the substrate (i.e., 0.2 U/µg protein).

Further attempts were made to determine the source of trypsin-like activity in the two major components of EW, CRs, and TF. Comparatively, high trypsin-like activity (171.0 U/µg protein) was detected in TF, whereas minimal trypsin-like activity (2.4 U/µg protein) was present in isolated CRs (Table 1). These results suggest that the enzymatic activity detected in EW was mainly derived from TF.

Trypsin-Like Enzymes in EW Were Not Involved in the AR Induction

Previous evidence has indicated that EW trypsin-like enzymes mediate the AR induction in S. ingentis [7]. This

prompted us to determine whether this mechanism also held true in $P.\ monodon$ sperm. Activity of trypsin-like enzymes in EW was abolished by either HI-EW or APMSF-EW. The remaining trypsin-like activities of HI-EW and APMSF-EW were 1.5 and 1.9 U/µg protein, respectively, compared with that of native EW (Table 1). Surprisingly, treatment of sperm with HI-EW or APMSF-EW produced AR responses of 84% and 82%, respectively, a result that was similar to that observed in sperm treated with native EW (\sim 90%) (Fig. 3). The percentage of spontaneous AR in these experiments was \sim 16%. This result indicated that trypsin-like activity involved in AR induction was not derived from EW.

Binding of EW to the Sperm Surface

Binding of the EW to the sperm surface may initiate sperm signaling events leading to the AR. Our results showed that fluorescently labeled EW bound to the entire sperm surface as well as the anterior spike (Fig. 4, a and b) in the overall sperm population. A slight difference in fluorescence intensity was noted among individual sperm. A background level of fluorescent staining was observed when an excess amount of unlabeled EW was included in the sperm-EW coincubates to compete with fluorescently labeled EW in sperm binding (Fig. 4, c and d); this indicated specific interaction of EW to the sperm surface.

Presence of Sperm Trypsin-Like Enzymes and Their Putative Roles in AR Induction

Inhibitor studies indicated the significance of trypsin-like enzymes in sperm AR induction (Fig. 2). However, since

TABLE 1. Trypsin- and chymotrypsin-like activities in egg water (EW)-related samples.

	Specific activity (units/µg protein)						
Sample	Trypsin (Boc-Gln-Ala-Arg-MCA)	Chymotrypsin (Suc-Ala-Ala- Pro-Phe-MCA) ^a					
Native EW	30.7 ± 0.5	0.2 ± 0.1					
Heat-inactivated EW	1.5 ± 1.9	NA					
APMSF-treated EW	1.9 ± 0.1	NA					
Thelycal fluid	171.0 ± 4.1	NA					
Cortical rods	2.4 ± 0.1	NA					

^aNA = Data not available

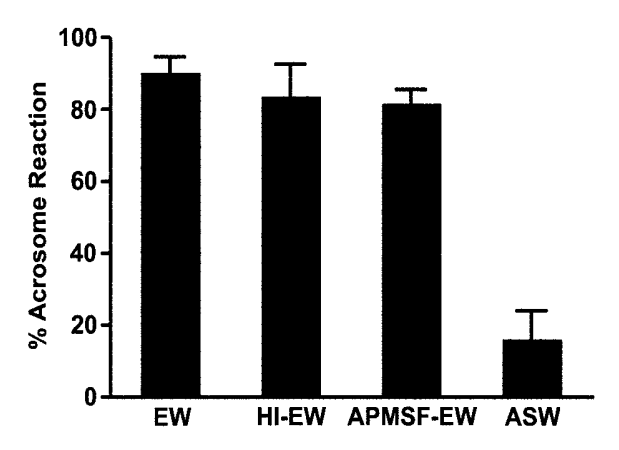


FIG. 3. EW with very low trypsin-like activity could still induce sperm AR. Native EW, HI-EW, or AMPSF-EW (see *Materials and Methods* for their preparation) was added to 50 μ l T-sperm suspension ($\sim \! \! 5 \times 10^5$ sperm). Note that HI-EW and APMSF-EW, having very low trypsin activity (Table 1), were able to induce the AR to the same extent as native EW. Spontaneous AR was assessed in sperm exposed to ASW.

APMSF-EW and HI-EW could still induce the AR, the trypsin-like enzymes participating in the AR induction would have belonged to sperm, and they could be localized, either on the sperm surface or in the acrosome. Results show that live AI sperm did possess trypsin-like activity $(77.1 \pm 11.4 \text{ U}/10^6 \text{ sperm})$, which would reflect the presence of trypsin-like enzymes on the AI sperm surface. The supernatant of AI sperm contained trypsin-like activity of only $11.8 \pm 9.9 \text{ U}/10^6 \text{ sperm}$, and this may reflect a low degree of trypsin-like enzyme release from sperm. When these live AI sperm were treated with a membrane-impermeable SBTI, the trypsin-like activity measured at 30 sec after SBTI removal was $2.2 \pm 0.6 \text{ U}/10^6 \text{ (Table 2)}$, indicating the marked inhibition of SBTI on sperm

FIG. 4. Binding of Alexa-488-labeled EW to aldehyde-fixed sperm. Approximately 5 \times 10^5 T-sperm in 50 μl were incubated (room temperature) with 16 $\mu g/ml$ Alexa-488-labeled EW in the presence (\boldsymbol{c} and \boldsymbol{d}) and the absence (\boldsymbol{a} and \boldsymbol{b}) of 50-fold excess of unlabeled EW. \boldsymbol{a} and \boldsymbol{c}) Fluorescent micrographs. \boldsymbol{b} and \boldsymbol{d}) Corresponding phase contrast micrographs. Bars = 10 μm .

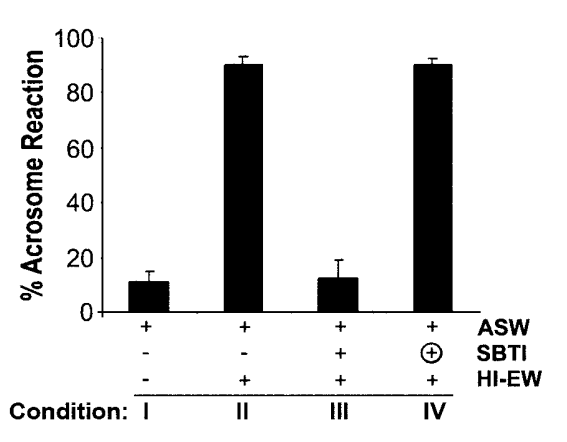
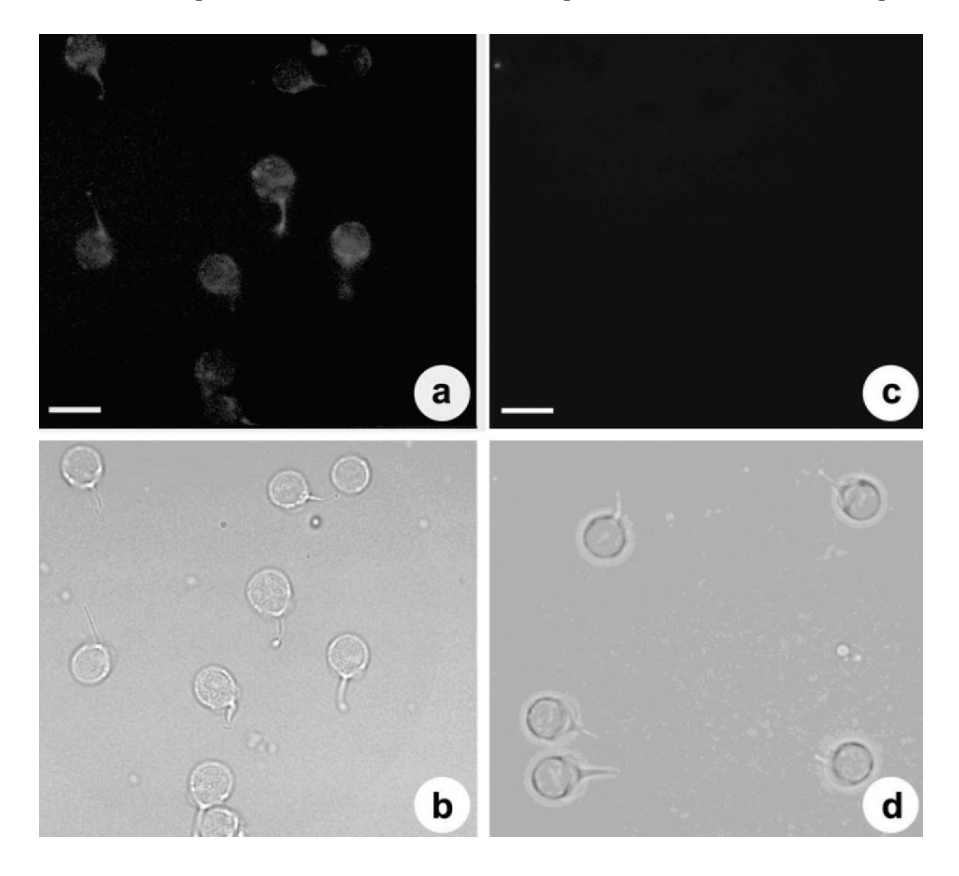


FIG. 5. Decreases in sperm surface trypsin-like activity did not affect the ability of HI-EW to induce the AR. Approximately 5×10^5 T-sperm in 50 μl were induced to undergo the AR by 16 $\mu g/ml$ HI-EW (condition II) or ASW (condition I, control). SBTI (0.4 mM) present in the coincubate (condition III) inhibited the HI-EW-induced AR. Under condition IV, T-sperm were pretreated with cell-impermeant SBTI (denoted by the encircled "plus" symbol) to inhibit surface trypsin-like enzymes (see <code>Materials</code> and <code>Methods</code>) prior to incubation with HI-EW. Note that the same extent of the AR was still observed in these SBTI-pretreated sperm as that occurring in untreated sperm (condition II).

surface trypsin. At 5 and 10 min after the removal of the excess amount of SBTI from sperm, the sperm surface trypsin-like activity was still relatively low (i.e., 6.8 ± 3.4 and 12.9 ± 6.0 U/ 10^6 sperm, respectively [<16% of the activity of untreated control sperm]). However, this enzyme activity was restored to 46.4 ± 13.8 and 71.7 ± 8.5 U/ 10^6 sperm 30 and 60 min post-SBTI removal, respectively (Table 2). AR sperm induced by HI-EW also possessed trypsin-like enzyme activity, but to a lesser extent than AI sperm (53.2 \pm 8.5 U/ 10^6 sperm).



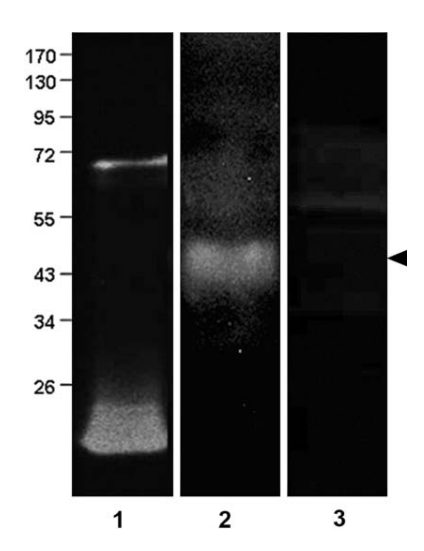


FIG. 6. Characterization of sperm acrosomal trypsin-like protease. The supernatant of 5×10^6 AR sperm containing acrosomal vesicles and content (lane 2) and the supernatant of the same number of AI sperm (lane 3), as well as 0.5 ng purified trypsin (lane 1), were subjected to fluorogenic substrate in-gel zymography with Boc-Gln-Ala-Arg-MCA as the substrate. The fluorescent bands (arrowhead) were indicative of trypsin-like activities.

However, the supernatant of these HI-EW-treated sperm (containing acrosomal vesicles and soluble content) showed a significant level of trypsin-like activity (84.0 \pm 27.9 U/10⁶ sperm).

To determine which trypsin-like enzymes (i.e., those at the sperm surface versus those in the acrosome) were significant for AR induction, the sperm surface enzymes were inhibited by pretreating AI live sperm with 0.4 mM of cell-impermeant SBTI. These SBTI-treated sperm still contained low surface trypsin activity within 5-10 min after SBTI removal by centrifugation (Table 2). Significantly, the SBTI-pretreated sperm were still responsive to HI-EW following 5-min exposure to this inducer; 88.3% of these sperm underwent AR (Fig. 5, fourth bar), a rate that was comparable to that observed with untreated sperm incubated with either HI-EW or native EW (Fig. 5, second bar; Fig. 3, first bar). However, when SBTI was present throughout the HI-EW-sperm coincubation, the AR rate was only \sim 12%, similar to the spontaneous AR rate (Fig. 5, first and third bars). All of these results suggest that the sperm surface trypsin-like enzymes may

TABLE 2. Recovery of trypsin-like activities of SBTI-pretreated acrosome intact sperm.

Time after SBTI removal (min)	Activities (units/10 ⁶ sperm)
0.5 5 10 30 60	2.2 ± 0.6 6.8 ± 3.4 12.9 ± 6.0 46.4 ± 13.8 71.7 ± 8.5

not be essential for the AR induction. Instead, the trypsin-like enzyme(s) in the acrosome would play a more pertinent role in inducing AR in *P. monodon* sperm.

To further characterize the trypsin-like enzyme(s) in the acrosome, the supernatant of the HI-EW-treated sperm, containing the acrosomal vesicles and soluble content, was subjected to fluorogenic substrate in-gel zymography. Figure 6 indicates that this supernatant generated a major fluorescent band (indicating the presence of a trypsin-like activity) of a 45-kDa molecular mass. As expected, purified trypsin generated a major fluorescent band at 21 kDa and a minor fluorescent band at 69 kDa (possibly due to the polymerization of the enzyme). In contrast, the supernatant of the AI sperm treated with ASW showed no fluorescent bands in the zymogram (Fig. 6).

DISCUSSION

We report here that the AR induction in *P. monodon* sperm involved EW binding and enzymatic action of sperm trypsinlike enzymes. In spite of an extremely short period of AR in this species, two morphological changes—spike depolymerization and the rupture of the acrosome (Fig. 1A)—were recognized and, therefore, used as criteria for determining a complete AR in P. monodon. Serine proteases, particularly trypsin- and chymotrypsin-like enzymes, have been shown to play significant roles in sperm AR induction [15, 23]. In this study, we also demonstrated the physiological relevance of trypsin-like proteases in this process in *P. monodon* sperm (Fig. 2). This was deduced from our results showing that the EWinduced AR was inhibited by trypsin inhibitors (APMSF, PMSF, and SBTI). We used fluorogenic substrates specific for trypsin and chymotrypsin to show that P. monodon sperm and their acrosomal vesicles and content contained substantial levels of trypsin-like activity, but minimal amounts of chymotrypsin-like activity. The results of inhibitor studies suggest that metalloproteases (an inhibitor of which is EGTA) may also be important for sperm AR induction. However, this

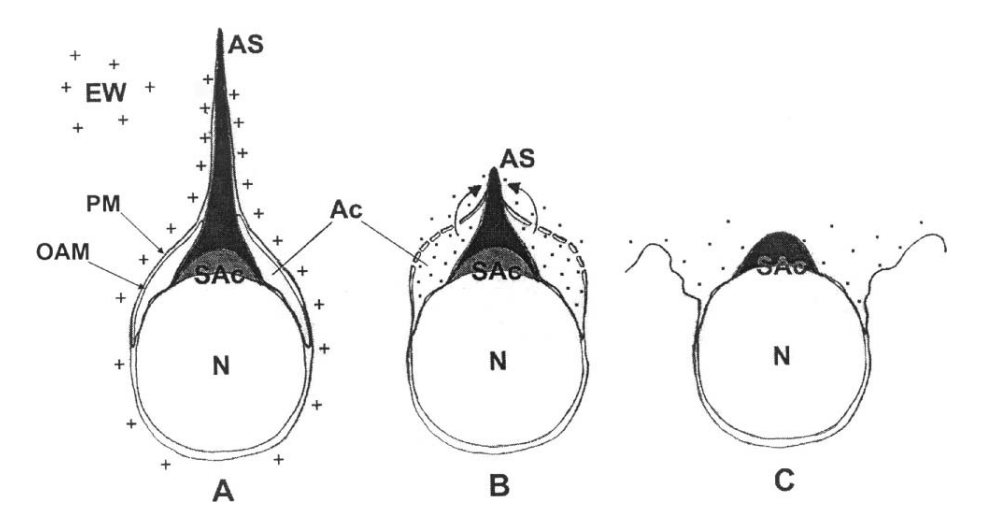


FIG. 7. Pictorial diagram postulating the temporal events of the EW-induced AR in P. monodon. A) Components in EW (initially bind to the sperm surface. This binding may trigger the fusion of the sperm plasma membrane (PM) and the outer acrosomal membrane (OAM), creating pores on the membrane overlying the acrosome (Ac). This would lead to a leakage of trypsin-like enzymes (dots) from the sperm acrosome. Depolymerization of the anterior spike (AS) may then occur due to the hydrolytic activity of the released trypsin-like enzymes (B). Shortly afterwards, the anterior spike was completely depolymerized along with the rupturing of the entire acrosome (C). N, Nucleus; Sac, subacromal region.

inhibition can also be due to the effect of EGTA on chelating extracellular calcium, the role of which during the AR process has been extensively documented [22, 24].

The significance of trypsin-like proteases in AR induction has long been reported in many invertebrates, including sea urchins [15] and the penaeoid shrimp, S. ingentis [7, 14]. However, the mechanisms of these enzymes in the AR response in the two shrimp species, S. ingentis and P. monodon, are dissimilar. The proteolytic activity in S. ingentis specifically mediates the acrosomal filament formation [7, 14]. This mechanism does not apply to P. monodon sperm, since such a morphological change does not occur in sperm undergoing the AR in this species. EW trypsin-like proteases of S. ingentis is involved in the AR induction, whereas EW trypsin-like enzymes of P. monodon appear to be unimportant for this event. This observation stems from the fact that denatured EW (HI-EW) or APMSF-EW was still capable of inducing AR responses to a similar extent to that of native EW (Fig. 3). Therefore, trypsin-like proteases essential for the AR induction in *P. monodon* likely belonged to sperm. We provide the results here indicating that trypsin-like enzymes existed both on the sperm surface and in the acrosome, the latter of which was revealed as a 45-kDa band in the zymogram (Fig.

Our results also revealed that sperm AR was inhibited when SBTI was present throughout sperm-EW coincubates (Figs. 2 and 5), while the AR was still inducible with 5-min exposure of SBTI-treated sperm with HI-EW (Fig. 5). Since the surface of SBTI-pretreated sperm contained only minimal levels of trypsin-like activity within 5-10 min after SBTI removal (Table 2), our AR results shown in Figure 5 (condition IV) suggest that the sperm surface trypsin activity might not be essential for AR induction (Fig. 5). Rather, the trypsin-like activity in the acrosomal vesicles/content may be more pertinent for sperm AR in P. monodon shrimp. In fact, the presence of a 45-kDa trypsin-like enzyme was observed in this study (Fig. 6). In the cases in which PMSF and APMSF were used for incubation with sperm, these cell-permeant inhibitors could readily reach the acrosome and inhibit the trypsin-like activity in this organelle. However, for the sperm incubation with SBTI, it would reach the trypsin-like enzyme(s) in the acrosome once pores on the sperm surface membranes were formed via fusion between the sperm plasma membrane and the outer acrosomal membrane at the onset of AR. Our results also suggest that the participation of these acrosomal trypsin enzymes in AR events was downstream of the initial interaction between the EW and the sperm head plasma membrane, which may lead to the fusion between the sperm plasma membrane and outer acrosomal membrane. This would allow the release of the acrosomal trypsin-like enzyme, which might be responsible for the digestion of the sperm anterior spike. Our ongoing work involves the purification and proteomic analyses of this acrosomal 45-kDa trypsin-like protease. We intend to discern its peptide sequence which will then be comapred with that of acrosomal trypsin-like enzymes of invertebrate animals (ascidians [16] and abalones [25]), known to be involved in enzymatic and nonenzymatic egg coat digestion, respectively. In addition, comparison will be made with acrosin and testis serine protease 5, two well-characterized serine proteases in the mammalian sperm acrosome that are believed to engage in sperm acrosomal matrix dispersion and zona pellucida digestion, respectively [26, 27].

Recently, sperm proteasomes have been shown to be involved in egg jelly-induced AR [28, 29] and vitelline layer hydrolysis [29] in sea urchins. Proteasomes have also been found in mammalian sperm, and play similar roles in AR

induction, as observed in sea urchin gametes and in sperm-zona pellucida interaction [30, 31]. The 26S proteasome is a large protein complex, consisting of a 19S regulatory particle and a 20S core particle. Based on their substrate specificity, three threonine proteases, present in the latter particle, are categorized to be trypsin-like, chymotrypsin-like, and peptidylglutamyl peptide hydrolyzing enzymes. The confinement of these three different enzymes within the 20S particle may accelerate the hydrolysis of their common substrates, which are usually ubiquitinated [32]. While it is tempting to speculate that the trypsin-like enzyme found in the acrosome of *P. monodon* sperm may be a component of proteosomes, evidence available so far argues against this possibility. First, the molecular masses of proteases in the 20S proteasome particle are usually in the range of 20-30 kDa [33]. Second, our unpublished results also revealed relatively low chymotrypsin-like activity, both in the acrosome and on the sperm surface of this shrimp species. Experiments are ongoing in our laboratory to determine whether the 20S α subunits of the proteasome exist in the sperm lysate of P. monodon.

Despite the deficit in proteolytic activity, HI-EW still possessed high competency in inducing AR (Fig. 3). The initial step of the AR induction was likely dependent on the direct interaction of EW components with sperm (Fig. 4). These EW constituents were derived from TF and egg components, including the egg jelly (originated from the CR precursor upon spawning [34, 35]) and the egg VE. Both the egg jelly in echinoderms [36–38] and VE in shrimp [39, 40] have been known to engage in AR induction, presumably through their binding to the sperm surface. Since *P. monodon* sperm that were stored in the thelycum and continuously exposed to TF (T-sperm) only had a minimal level of spontaneous AR (as described previously here), EW components from the CR and VE may be of greater importance in the sperm binding that leads to AR induction.

The significance of EW components and sperm acrosomal trypsin-like proteases in the acrosomal exocytosis in *P. monodon* is summarized pictorially in Figure 7. Initially, EW components bind specifically to the sperm membrane receptors (Fig. 7A). This ligand-receptor binding would likely induce the downstream signaling events that lead to the fusion of the sperm plasma membrane and the acrosomal membrane. The acrosomal trypsin-like enzymes that are then released through the membrane pores may be responsible for dissociating the sperm anterior spike (Fig. 7B). Subsequently, the acrosome is completely ruptured, leaving a dense spherical mass lying in place of the anterior spike against the nuclear pole of the AR sperm (Fig. 7C). Whether the dense spherical material is analogous to the acrosomal filament of *S. ingentis*, or a protease-resistant remnant of the depolymerized spike, is currently under investigation.

ACKNOWLEDGMENTS

The authors would like to thank Dr. Athula Wikramanayake for his valuable comments and proof reading of this manuscript, and Dr. Boonyarath Pratoomchat, Department of Aquatic Science, Faculty of Science, Buraphar University, for kindly providing shrimp samples.

REFERENCES

- Clark WH Jr, Yudin AI, Griffin FJ, Shigekawa K. The control of gamete activation and fertilization in the marine penaeidae, Sicyonia ingentis. In: Engels W (ed.), Advances in Invertebrate Reproduction, 3rd ed. Amsterdam: Elsevier Science Publishers; 1984:459–472.
- Alfaro J, Munoz N, Vargas M, Komen J. Induction of sperm activation in open and closed thelycum penaeoid shrimps. Aquaculture 2003; 216:371– 381.

- Vanichviriyakit R, Kruevaisayawan H, Weerachatyanukul W, Tawipreeda P, Withyachumnarnkul B, Pratoomchat B, Chavadej J, Sobhon P. Molecular modification of *Penaeus monodon* sperm in female thelycum and its consequent responses. Mol Reprod Dev 2004; 69:356–363.
- Kleve MG, Yudin AI, Clark WH Jr. Fine structure of the unistellate sperm of the shrimp, Sicyonia ingentis (Natantia). Tissue Cell 1980; 12:29–45.
- Clark WH Jr, Kleve MG, Yudin AI. An acrosome reaction in natantian sperm. J Exp Zool 1981; 218:279–291.
- Griffin FJ, Shigekawa K, Clark WH Jr. Formation and structure of the acrosomal filament in the sperm of Sicyonia ingentis. J Exp Zool 1988; 246:94–102.
- Griffin FJ, Clark WH Jr. Induction of acrosomal filament formation in the sperm of Sicyonia ingentis. J Exp Zool 1990; 254:296–304.
- Clark WH Jr, Griffin FJ. Acquisition and manipulation of penaeoidean gametes. In: McVew J (ed.), Handbook of Techniques for Crustacean Aquaculture, vol. 1, 2nd ed. Boca Raton: CRC Press; 1993:133–152.
- Pongtippatee-Taweepreda P, Chavadaj J, Plodpai P, Pratoomchart B, Sobhon P, Weerachatyanukul W, Withyachumnarnkul B. Egg activation in the black tiger shrimp *Penaeus monodon*. Aquaculture 2004; 234:183– 198.
- Griffin FJ, Clark WH Jr, Crowe JH, Crowe LM. Intracellular pH decreases during the in vitro induction of the acrosome reaction in the sperm of Sicyonia ingentis. Biol Bull 1987; 173:311–323.
- Dan JC. Studies on the acrosome. I. Reaction to egg-water and other stimuli. Biol Bull 1952; 103:54–66.
- Afzelius BA, Murray A. The acrosomal reaction of spermatozoa during fertilization or treatment with egg water. Exp Cell Res 1957; 12:325–337.
- Cherr GN, Clark WH Jr. An egg envelope component induces the acrosome reaction in sturgeon sperm. J Exp Zool 1985; 234:75–85.
- Lindsay LL, Clark WH Jr. Protease-induced formation of the sperm acrosomal filament. Develop Growth Differ 1992; 34:189–197.
- Levine AE, Walsh KA. Involvement of an acrosin-like enzyme in the acrosome reaction of sea urchin sperm. Dev Biol 1979; 72:126–137.
- 16. Sawada H. Ascidian sperm lysin system. Zoolog Sci 2002; 19:139-151.
- Bradford MM. A rapid and sensitive method for the quantitation of microgram quantities of protein utilizing the principle of protein-dye binding. Anal Biochem 1976; 72:248–254.
- Lynn JW, Clark WH Jr. Physiological and biochemical investigations of the egg jelly release in *Penaeus aztecus*. Biol Bull 1987; 173:451–460.
- Zimmerman M, Ashe B, Yurewicz EC, Patel G. Sensitive assays for trypsin, elastase, and chymotrypsin using new fluorogenic substrates. Anal Biochem 1977; 78:47–51.
- Yasothornsrikul S, Hook VY. Detection of proteolytic activity by fluorescent zymogram in-gel assays. Biotechniques 2000; 28:1166– 1168,1170,1172–1163.
- Laemmli UK. Cleavage of structural proteins during the assembly of the head of bacteriophage T4. Nature 1970; 227:680–685.
- Clark WH Jr, Griffin FJ. The morphology and physiology of the acrosome reaction in the sperm of the decapod, Sicyonia ingentis. Develop Growth Differ 1988; 30:451–462.
- Morales P, Socias T, Cortez J, Llanos MN. Evidences for the presence of chymotrypsin-like activity in human spermatozoa with a role in the acrosome reaction. Mol Reprod Dev 1994; 38:222–230.

- Collins F, Epel D. The role of calcium ions in the acrosome reaction of sea urchin sperm: regulation of exocytosis. Exp Cell Res 1977; 106:211–222.
- Lewis CA, Talbot CF, Vacquier VD. A protein from abalone sperm dissolves the egg vitelline layer by a nonenzymatic mechanism. Dev Biol 1982; 92:227–239.
- Yamagata K, Murayama K, Okabe M, Toshimori K, Nakanishi T, Kashiwabara S, Baba T. Acrosin accelerates the dispersal of sperm acrosomal proteins during acrosome reaction. J Biol Chem 1998; 273: 10470–10474.
- Honda A, Yamagata K, Sugiura S, Watanabe K, Baba T. A mouse serine protease TESP5 is selectively included into lipid rafts of sperm membrane presumably as a glycosylphosphatidylinositol-anchored protein. J Biol Chem 2002; 277:16976–16984.
- Matsumura K, Aketa K. Proteasome (multicatalytic proteinase) of sea urchin sperm and its possible participation in the acrosome reaction. Mol Reprod Dev 1991; 29:189–199.
- Yokota Y, Sawada H. Sperm proteasomes are responsible for the acrosome reaction and sperm penetration of the vitelline envelope during fertilization of the sea urchin *Pseudocentrotus depressus*. Dev Biol 2007; 308:222–231.
- Pasten C, Morale P, Kong M. Role of sperm proteasome during fertilization and gamete interaction in the mouse. Mol Reprod Dev 2005; 71:209–219.
- Sutovsky P, Manandhar G, McCauley TC, Caamaño JN, Sutovsky M, Thompson WE, Day BN. Proteasomal interference prevents zona pellucida penetration and fertilization in mammals. Biol Reprod 2004; 71:1625–1637.
- Carrard G, Bulteau AL, Petropoulos I, Friguet B. Impairment of proteasome structure and function in aging. Int J Biochem Cell Biol 2002; 34:1461–1474.
- Heinemeyer W, Fischer M, Krimmer T, Stachon U, Wolf DH. The active sites of the eukaryotic 20S proteasome and their involvement in subunit precursor processing. J Biol Chem 1997; 272:25200–25209.
- Bradfield JY, Berlin RL, Rankin SM, Keeley LL. Cloned cDNA and antibody for an ovarian cortical granule polypeptide of the shrimp *Penaeus* vannamei. Biol Bull 1989; 177:344–349.
- 35. Clark WH Jr, Yudin AI, Lynn JW, Griffin FJ, Pillai MC. Jelly layer formation in Penaeoidean shrimp eggs. Biol Bull 1990; 178:295–299.
- Alves AP, Mulloy B, Diniz JA, Mourao PA. Sulfated polysaccharides from the egg jelly layer are species-specific inducers of acrosomal reaction in sperm of sea urchins. J Biol Chem 1997; 272:6965–6971.
- Alves AP, Mulloy B, Moy GW, Vacquier VD, Mourao PA. Females of the sea urchin *Strongylocentrotus purpuratus* differ in the structures of their egg jelly sulfated fucans. Glycobiology 1998; 8:939–946.
- Vilela-Silva AC, Castro MO, Valente AP, Biermann CH, Mourao PA. Sulfated fucans from the egg jellies of the closely related sea urchins Strongylocentrotus droebachiensis and Strongylocentrotus pallidus ensure species-specific fertilization. J Biol Chem 2002; 277:379–387.
- Clark WH Jr, Griffin FJ, Wikramanayake AH. Prefusion events of spermoocyte interaction in the marine shrimp, *Sicyonia ingentis*. Semin Dev Biol 1994; 5:225–231.
- Wikramanayake AH, Clark WH Jr. Two extracellular matrices from oocytes of the marine shrimp Sicyonia ingentis that independently mediate only primary or secondary sperm binding. Dev Growth Differ 1994; 36:89–101.



Contents lists available at ScienceDirect

General and Comparative Endocrinology

journal homepage: www.elsevier.com/locate/ygcen



Changes in the levels of serotonin and dopamine in the central nervous system and ovary, and their possible roles in the ovarian development in the giant freshwater prawn, *Macrobrachium rosenbergii*

Yotsawan Tinikul ^a, A. Joffre Mercier ^b, Nantawan Soonklang ^a, Prasert Sobhon ^{a,*}

ARTICLE INFO

Article history: Received 8 May 2008 Revised 14 July 2008 Accepted 22 July 2008 Available online 5 August 2008

Keywords:
Macrobrachium rosenbergii
Serotonin
Dopamine
HPLC
CNS
Ovary
Vitellin

ABSTRACT

Serotonin or 5-hydroxytryptamine (5-HT) and dopamine (DA) are the two key neurotransmitters that control gonadal development in decapod crustaceans. This study investigated changes in the levels of 5-HT and DA in the CNS and ovary during different phases of the ovarian cycle of the freshwater prawn, Macrobrachium rosenbergii. The levels of 5-HT and DA were quantified by using High Performance Liquid Chromatography with electrochemical detection (HPLC-ECD). Moreover, changes of vitellogenin (Vg) concentrations in the hemolymph after treatment with 5-HT and DA (at doses of 2.5×10^{-6} and 2.5×10^{-7} mol per prawn) were also examined. 5-HT exhibited a gradual increase in concentration in the brain and thoracic ganglia from ovarian stage I (0.12 ± 0.01 nmol/mg, 0.22 ± 0.01 nmol/mg, respectively) to reach a maximum $(0.66 \pm 0.03 \text{ nmol/mg}, 1.48 \pm 0.03 \text{ nmol/mg}, respectively)$ at ovarian stage IV. In contrast, DA in the brain and thoracic ganglia showed the highest concentrations at ovarian stage II $(0.20 \pm 0.01 \text{ nmol/mg}, 1.27 \pm 0.06 \text{ nmol/mg}, respectively)$ and then decreased to the lowest concentrations $(0.06 \pm 0.01 \text{ nmol/mg}, 0.28 \pm 0.04 \text{ nmol/mg}, \text{ respectively})$ at ovarian stage IV. The ovarian concentration of 5-HT was 0.53 ± 0.11 nmol/mg at ovarian stage I and gradually increased to 1.63 ± 0.16 nmol/mg at ovarian stage IV. In contrast, the concentration of DA was highest at ovarian stage I $(29.05 \pm 1.31 \text{ nmol/mg})$, and lowest at the ovarian stage IV $(11.43 \pm 0.74 \text{ nmol/mg})$. Injecting 5-HT into prawns significantly increased Vg concentration in the hemolymph at ovarian stage IV compared to control groups, and injecting DA into prawns had the opposite effect. The inverse relationship between 5-HT and DA levels in neural ganglia and ovaries, and their opposing effects on hemolymph Vg levels suggest that these two transmitters play opposite regulatory roles in controlling ovarian maturation and oocyte development in this species.

© 2008 Elsevier Inc. All rights reserved.

1. Introduction

The giant freshwater prawn, *Macrobrachium rosenbergii*, is an important food source that is cultured in Thailand and other Asian countries (Sandifer and Smith, 1985). Reproduction of this as well as other decapod crustaceans is regulated by various neurohormones that are synthesized and released from the X-organ-sinus gland complex located in the eyestalks (Chen et al., 2003). The synthesis and release of these neurohormones are believed to be regulated by biogenic amines (Ridchardson et al., 1991), particularly 5-HT and DA that are present in the CNS of these crustaceans (Kerkut et al., 1966; Butler and Fingerman, 1983; Laxmyr, 1984; Fingerman et al., 1994). Several previous studies have reported a stimulatory effect of 5-HT on gonadal maturation in some decapods, including *Procambarus clarkii* (Kulkarni et al., 1992), *Penaeus*

monodon (Wongprasert et al., 2006), and M. rosenbergii (Meeratana et al., 2006). It was suggested that 5-HT stimulates gonadal maturation by inhibiting the release of gonad-inhibiting hormone (GIH) and/or by enhancing the release of gonad-stimulating hormone (GSH), whereas DA plays the opposite role (Sarojini et al., 1995; Fingerman, 1997). 5-HT and the rate limiting enzymes (tryptophan hydroxylase and 5-hydroxy-L-tryptophan decarboxylase) involved in its synthesis were found at measurable levels in several regions of the CNS of a crustacean, Panulirus homarus (Kirubagaran et al., 2005). Moreover, 5-HT and DA have been detected by HPLC in various regions of the CNS of Pacifastacus leniusculus (Elofsson et al., 1982; Laxmyr, 1984), the eyestalks of P. clarkii (Alvarez et al., 2005), and the intestinal nerve of P. clarkii (Mercier et al., 1991). Major tissues that exhibited a high level of 5-HT are the optic ganglion, cerebral ganglion, circumoesophageal connectives, stomatogastric ganglion, and thoracic ganglia (Aramant and Elofsson, 1976; Beltz et al., 1984). However, quantification of the levels of these two neurotransmitters in correlation with different phases of the

^a Department of Anatomy, Faculty of Science, Mahidol University, Rama VI Road, Ratchathewi, Bangkok 10400, Thailand

^b Department of Biological Sciences, Brock University, St. Catharines, Ont., Canada L2S 3A1

^{*} Corresponding author. Fax: +66 2 354 7168. E-mail addresses: scpso@mahidol.ac.th, anatch2002@yahoo.com (P. Sobhon).

decapod crustacean ovarian cycle has not yet been performed. In this study, we have investigated changes in 5-HT and DA concentrations in various parts of the CNS and the ovary during various phases of the ovarian maturation in *M. rosenbergii*. Moreover, hemolymph vitellogenin (Vg) concentrations were also determined during various phases of ovarian cycle following the treatments with 5-HT and DA in order to assess possible effects of these two neurotransmitters on ovarian maturation more directly.

2. Materials and methods

2.1. Experimental animals

Mature female freshwater prawns (each weighing on average about $30.88 \pm 3.6 \, \mathrm{g}$) were obtained from commercial farms in Chonburi Province, Thailand. The animals were kept in outdoor circular concrete tanks, each with 1.50 m diameter with the water depth at 0.80 m, and about 30% of water changed every 2 days. The prawns were fed commercial food pellets twice per day. Aeration was given all day. Small plastic cages were added in every tank (30 per tank) for molting animals to hide in and avoid being killed from the cannibalistic behavior of this species. The prawns were acclimatized under a photoperiod of 12:12 h light–dark for two weeks before beginning the experiments.

2.2. Determination of ovarian stages

The changing phases of the ovarian cycle in female broodstock could be observed directly and classified into five stages based on the size, color, and histology of the ovary as reported by Chang and Shih (1995) and Meeratana and Sobhon (2007). Stages 0 and I were spawn and spent phases, respectively, when the ovaries appeared white and indistinct when observed through the carapace (Fig. 1A). In stage II (proliferative) a small yellow mass of ovary could be observed dorsally under the carapace (Fig. 1B). In stage III (premature), the ovary became orange (Fig. 1C). In stage IV (mature), the reddish-orange ovary extended from behind the eye posteriorly to the first abdominal segment (Fig. 1D). These ovarian stages were confirmed by histological study (Fig. 1E–H) based on the criteria described by Meeratana and Sobhon (2007).

2.3. Chemicals and standard solutions

5-HT, DA, and all other chemicals used in the experiments were obtained from Sigma Chemical Co. (St. Louis, MO, USA). Standard solutions were freshly prepared by dissolving 5-HT and DA in ice-cold 0.1 M perchloric acid on the day of analysis and were stored in ice between injections onto the HPLC system.

2.4. Sample preparations

The brain (supraesophageal ganglion), the five thoracic ganglia (combined), the six abdominal ganglia (combined), and the ovaries were collected at mid-day from ten animals at each ovarian stage (as defined by Meeratana and Sobhon, 2007). Each organ was carefully dissected, and its wet mass was weighed. Samples were placed in 50 μ l 0.1 M perchloric acid. The mixture was then sonicated and centrifuged at 14,000g at 4 °C. The supernatants were then collected and filtered through a 0.22 μ m Spin-x centrifugal filter tube before injection onto the HPLC column. Detection and quantification of 5-HT and DA in the CNS and ovaries were performed by using High Performance Liquid Chromatography with

electrochemical detection (HPLC-ECD). The average concentrations of 5-HT and DA were estimated in four replicates.

2.5. Quantification of 5-HT and DA by HPLC

HPLC method used in this study was adapted from Mercier et al. (1991) and Molaei and Lange (2003). Each tissue sample was dissected, weighed and placed in 50 µl of 0.1 M perchloric acid and was prepared as described above (Section 2.4). Supernatants from the extracts were injected onto a Brownlee C₁₈-Aquapore OD-300 HPLC column (250 \times 4.6 mm i.d.). 5-HT and DA were detected electrochemically using a completely isocratic mode for the determination of the neurotransmitters. A glassy carbon electrode served as the working electrode and was used with an Ag/AgCl reference electrode. The detector potential was set at +0.8 V versus an Ag/AgCl reference electrode. The sensitivity of the detector was maintained at 100 nA with full scale deflection. The mobile phase consisted of 75 mM NaH₂PO₄, 0.3 mM sodium octylsulphate, 50 µM EDTA, 2.5% acetonitrile, and 4% methanol. The pH was adjusted to 2.75 with orthophosphoric acid. The flow rate was kept constant at 0.7 ml/min. The mixture was sonicated, centrifuged at 14,000g at 4 °C. The supernatants were collected and then filtered through a 0.22 µm Spin-x centrifugal filter tube before injection. Samples were injected into a 20 µl injection loop. The signals from the electrochemical detector were recorded and integrated using data analysis software (Millennium, Waters). 5-HT and DA levels were quantified using the external standard method. Peaks corresponding to 5-HT and DA were detected in the extracts at the same elution times as their corresponding standards. The identities of the peaks in each sample were further verified by spiking the tissue extracts with known amounts of 5-HT and DA standards. All samples were freshly prepared and analyzed within the same day. The Bio-Rad (Mississauga, Canada) Protein Assay System was employed for protein determination in the extracts according to Bradford (1976).

2.6. Effects of 5-HT and DA on Vg levels

Female prawns at ovarian stage I were divided into six groups (four experimental groups and two control groups) of 28 animals each. Prawns in the experimental groups were injected with 5-HT at doses of 2.5 \times 10⁻⁶, 2.5 \times 10⁻⁷ mol of 5-HT/prawn or DA at doses of 2.5 \times 10⁻⁶, 2.5 \times 10⁻⁷ mol of DA/prawn. 5-HT and DA were dissolved in crustacean physiological saline (CPS) containing the following: NaCl 29 g, KCl 0.71 g, CaCl₂ · 2H₂O 2.38 g, MgSO₄ · 7H₂O 3.16 g, NaHCO₃ 0.5 g, MgCl₂ · 6H₂O 0.17 g, HEPES 4.76 g in 11 of distilled water. The injected volumes of 5-HT and DA were 0.10 ml. All prawns tolerated the injected doses of neurotransmitters without showing any abnormal behavior. All injections were performed at 4-day intervals, covering a period of 49 days. The effects of the neurotransmitter-treated groups were compared with two control groups of 28 animals each. In the first control group, the animals were untreated and served as a negative control (NC). The second control group was a vehicle-injected control (VIC) in which each animal was injected with 0.1 ml of CPS. Animals in each group were identified by tying plastic loops of different colors around the eyestalk. The injections were performed by intramuscular route at the lateral aspect of the second abdominal segment by using a 1 ml syringe (NIPRO) fitted with 26G $\times \frac{1}{2}$ $(0.45\times12\;mm)$ thin-wall needles (NIPRO). The weight and total length of the prawns were measured on every treatment day, before injection. The total length was evaluated from the base of eyestalk to the telson (Eyestalk base-telson length, EBTL).

The hemolymph of treated and control prawns was collected from the substernal hemolymph sinus at 4-day intervals. Each

¹ For interpretation of color mentioned in this figure the reader is referred to the web version of the article.

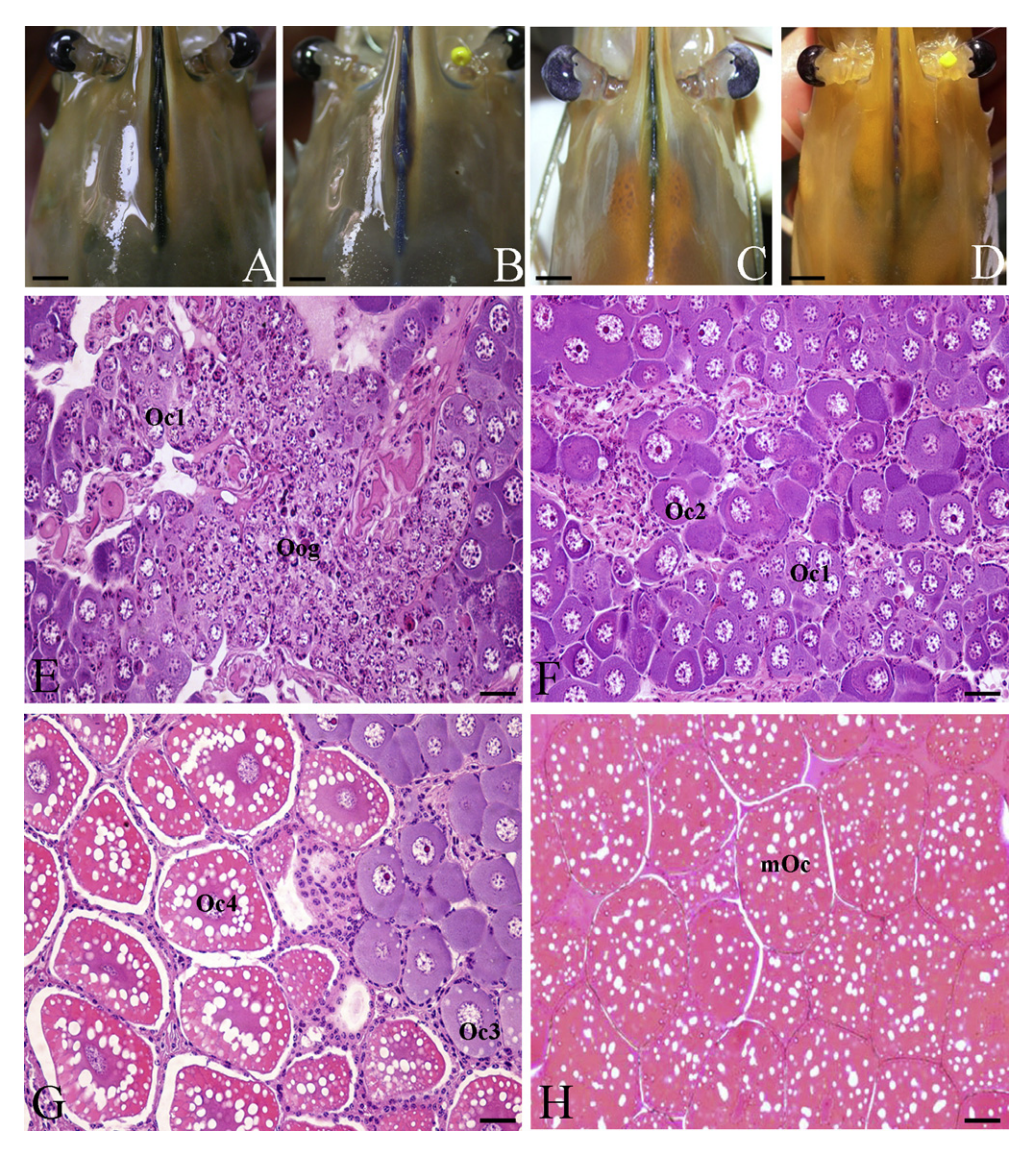


Fig. 1. Top views of female giant freshwater prawn, *M. rosenbergii*, showing ovary at various stages: (A) stage I, (B) stage II, (C) stage II, (D) stage IV. (E–H) Light micrographs of H&E-stained ovarian sections showing histology of various stages of ovarian cycle (I–IV) and steps of oocyte development. Oog, oogonia; Oc1, early previtellogenic oocyte; Oc2, late previtellogenic oocytes; Oc3, early vitellogenic oocytes; Oc4, late vitellogenic oocytes; mOc, mature oocytes (classified according to Meeratana and Sobhon 2007). Scale bars = 1 cm (A–D). Scale bars = 50 μm (E–H).

100 μ l sample of hemolymph was mixed together with 100 μ l of anticoagulant (containing 0.45 M NaCl, 0.1 M glucose, 30 mM sodium citrate, 26 mM citric acid, 20 mM EDTA in distilled water, pH 4.5; Kwok and Tobe, 2006). The sample was then centrifuged at 2000 rpm at 4 °C, for 10 min. The supernatants were collected and then stored at -80 °C until Vg assays.

2.6.1. Production of anti-vitellin antibody and Enzyme-Linked Immunosorbent Assay (ELISA) to determine the hemolymph vitellogenin (Vg) levels

The anti-vitellin antibody was prepared according to Chen and Kuo (1998). Briefly, frozen ovarian samples were homogenized and centrifuged. The supernatant was concentrated by concentrator (Centreprep-30, Amicon Inc., USA), and then vitellin protein was fractionated by HPLC using UV-detector, and further concentrated by ultrafiltration. The purity of vitellin was then determined using polyacrylamide gel electrophoresis. A 250 μ g of purified vitellin was further dissolved in 300 μ l of 0.1 M PBS, emulsified with an equal volume of Freund's adjuvant and injected into each of the two New Zealand white rabbits (purchased from the Animal

Care Unit, Mahidol University with the approval of the Animal Ethics Committee). The titers of the rabbit immune sera were determined by ELISA following the standard protocol. Serum providing high titer was used in ELISA (anti-vitellin was shown to cross-react with hemolymph vitellogenin (Vg), Chen and Kuo, 1998).

An indirect ELISA technique was used to determine hemolymph Vg levels. In the assay, polystyrene microtiter plates were coated with 100 μl of 1.25 μg/ml hemolymph diluted in coating buffer (15 mM Na₂CO₃, 35 mM NaHCO₃ pH 9.6) for 2 h at 37 °C. After incubation, the excess antigen was washed using analytical grade dH₂O three times, 1 min each. Non-specific bindings were blocked with 100 μl of blocking buffer containing 0.25% bovine serum albumin (BSA) in 0.01 M PBS, pH 7.2 and 0.05% Tween 20, at 37 °C for 2 h. After washing three times, the plate was incubated in the primary antibody (anti-vitellin) diluted at 1:2000 in the diluent containing 0.25% BSA in 0.01 M PBS, pH 7.2 and 0.05% Tween 20. One hundred μl of primary antibody was added to each well and incubated at 37 °C for 2 h. The plate was washed as described above, and then 100 μl of HRP-conjugated goat anti-rabbit IgG (Zymed Co., San Francisco, CA, USA) diluted to 1:4000 in blocking solution was added

to each well, and incubated at 37 °C for 1 h. After washing three times, the color reaction was developed by adding 100 μl of O-phenylenediamine dihydrochloride (OPD, Sigma, St. Louis, MO, USA) substrate solution (3 mg OPD in 7.5 ml substrate buffer and 3 μl $H_2O_2)$ to each well, and incubating at 37 °C for 30 min in a dimly lit room. Finally, 100 μl of 6 N H_2SO_4 was added to stop the enzymatic reaction, and the optical density (OD) was measured at 492 nm in an automatic spectrophotometer (Titertex Multiscan Flow Laboratories, Pty. Ltd., Australia). A negative control sample was prepared in parallel by using rabbit pre-immune serum in place of primary antibody. The Vg concentrations were calculated from a standard curve established from known concentrations of Vg.

2.7. Statistical analysis

Experimental data were analyzed with the SPSS program using one-way analysis of variance (ANOVA) and Tukey's post hoc test. A probability value less than 0.05 (P < 0.05) indicated the statistical significance. Data were presented as means \pm SEM.

3. Results

The 5-HT and DA peaks in the extracts of the brain (supraesophageal ganglion), thoracic ganglia, abdominal ganglia, and ovary showed the same elution times as their corresponding standards. Additionally, the spiked peaks and the peaks of corresponding

standards appeared at the same position when 5-HT and DA were added to each sample (Fig. 2).

3.1. Changes in the 5-HT concentration in the CNS and ovary

From HPLC-ECD analyses, the concentrations of 5-HT and DA in the organ extracts were expressed as nmol per mg protein (Fig. 3 and 4). The concentration of 5-HT in the brain and thoracic ganglia exhibited a gradual increase from ovarian stage I to stage IV. At stage I, the concentration of 5-HT in the brain was $0.12 \pm$ 0.01 nmol/mg, and it gradually increased through the ovarian stage II $(0.18 \pm 0.01 \text{ nmol/mg})$, ovarian stage III $(0.44 \pm 0.05 \text{ nmol/mg})$, and finally reached the highest level $(0.66 \pm 0.03 \text{ nmol/mg})$ in stage IV, which was approximately a 5.7-fold increase over stage I. A similar pattern was observed in the thoracic ganglia, where the 5-HT concentration was 0.22 ± 0.01 nmol/mg at ovarian stage I, 0.69 ± 0.02 nmol/mg at stage II, 1.06 ± 0.01 nmol/mg at stage III, and finally 1.48 ± 0.03 nmol/mg at stage IV, showing approximately a 6.7-fold increase. In the abdominal ganglia, 5-HT concentration increased from ovarian stage I to stage II $(0.08 \pm 0.01,$ 0.21 ± 0.01 nmol/mg, respectively), and then declined at ovarian stage III $(0.06 \pm 0.01 \text{ nmol/mg})$. When compared within a tissue, the concentration of 5-HT was about 4 and 5 times higher in the brain at ovarian stage III and IV (P < 0.05) than in the brain at ovarian stage I, respectively. The concentration of 5-HT was about 3, 5, 7 times higher in the thoracic ganglia at ovarian stage II, III, and IV (P < 0.05) than in the thoracic ganglia at ovarian stage I, respec-

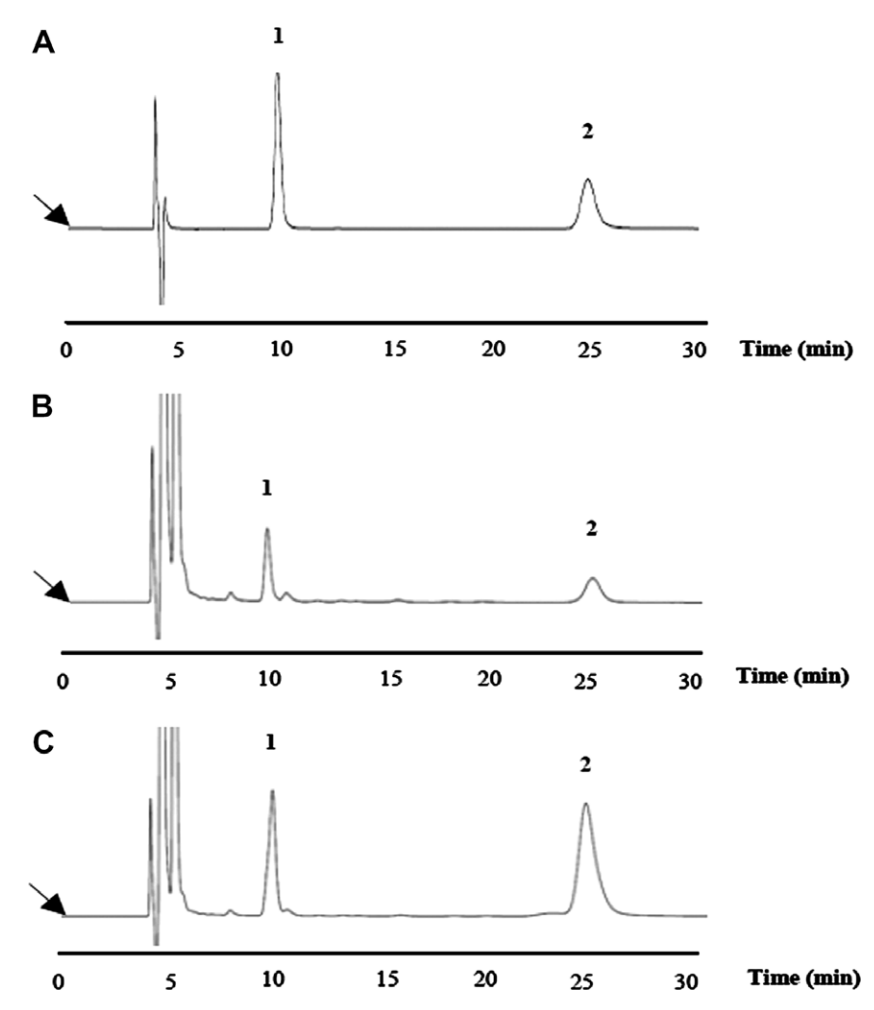


Fig. 2. (A) HPLC chromatogram of standards at 0.7 ml/min flow rate. Solutes: (1) DA; (2) 5-HT. (B) HPLC chromatogram of the brain extract. (C) The brain extract was spiked with DA and 5-HT standards. Samples were injected at the start of each recording trace (arrows).

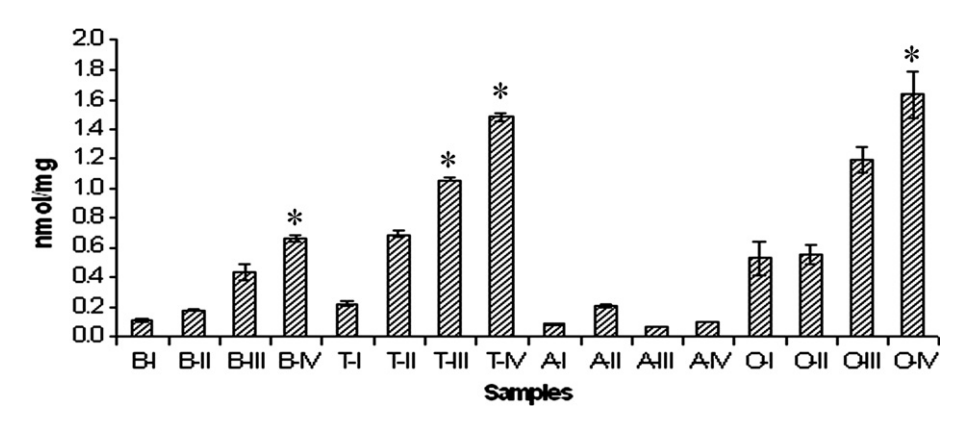


Fig. 3. A graph illustrating the changing concentrations of 5-HT in the brain, thoracic ganglia, abdominal ganglia, and ovary during various stages of the ovarian cycle (stage I–IV). The concentration is expressed as nmol/mg of protein in the organ extract. Numbers are means ± SEM. Asterisks indicate significant differences at *P* < 0.05 in an analysis of variance. B-I to IV are the concentration of 5-HT in brain at ovarian stages I–IV. T-I to IV are the concentration of 5-HT in abdominal ganglia at ovarian stages I–IV. O-I to IV are the concentration of 5-HT in ovarian stages I–IV.

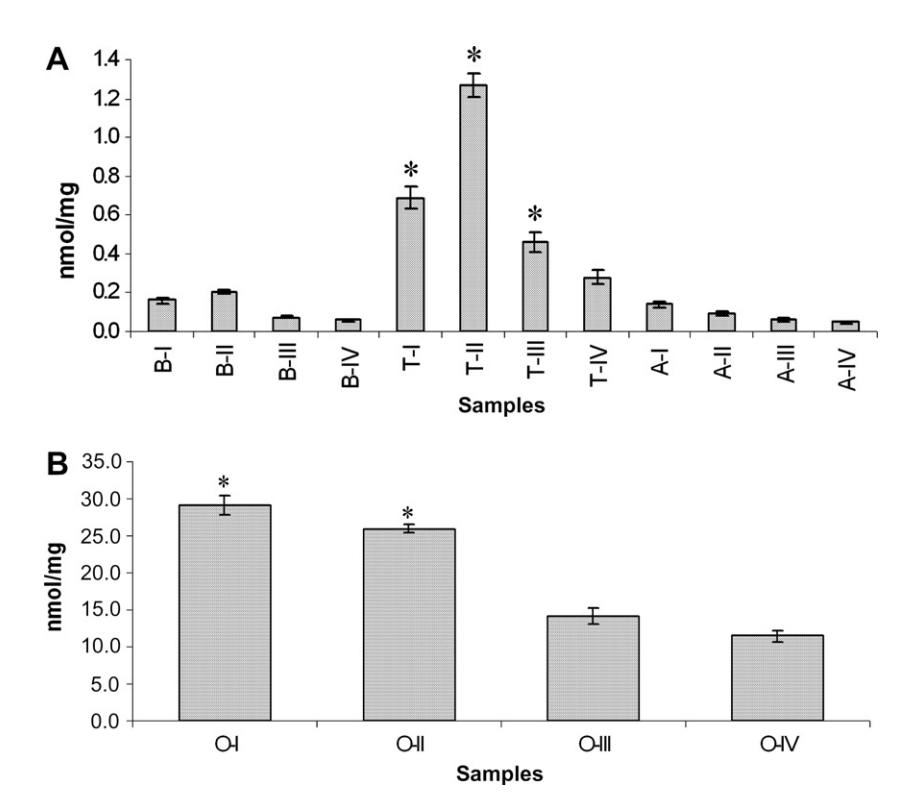


Fig. 4. Graphs illustrating: (A) the changing concentrations of DA in the brain, thoracic ganglia, and abdominal ganglia; (B) the changing concentrations of DA in the ovaries. The concentration is expressed as nmol/mg of protein in the organ extract. Numbers are means ± SEM. Asterisks indicate significant differences at *P* < 0.05 in an analysis of variance. B-I to IV are the concentration of DA in brain at ovarian stages I–IV. T-I to IV are the concentration of DA in thoracic ganglia at ovarian stages I–IV. A-I to IV are the concentration of DA in abdominal ganglia at ovarian stages I–IV. O-I to IV are the concentration of DA in ovarian stages I–IV.

tively. The level of 5-HT in the thoracic ganglia at any one ovarian stage was about two times higher than in the brain, and about 15 times higher than in abdominal ganglia when compared at ovarian stage IV. These results were statistically significant (P < 0.05). In the ovaries, the 5-HT concentration showed a gradual increase from a low level at ovarian stage I ($0.53 \pm 0.11 \text{ nmol/mg}$) to the highest level ($1.63 \pm 0.16 \text{ nmol/mg}$) at ovarian stage IV (Fig. 3).

3.2. Changes in DA concentration in the CNS and ovary

In the brain, the concentration of DA (Fig. 4A) increased slightly from ovarian stage I to stage II (0.16 ± 0.01 , and 0.20 ± 0.01 nmol/mg, respectively) and then declined at ovarian stages III and IV (at

 0.08 ± 0.01 , and 0.06 ± 0.01 nmol/mg, respectively). The concentration of DA in the thoracic ganglia also increased from ovarian stage I $(0.69\pm0.06~\text{nmol/mg})$, became highest in stage II $(1.27\pm0.06~\text{nmol/mg})$, and then decreased in ovarian stages III and IV, $(0.46\pm0.05,~\text{and}~0.28\pm0.04~\text{nmol/mg},~\text{respectively})$. In the abdominal ganglia, DA concentration was highest $(0.14\pm0.02~\text{nmol/mg})$ in ovarian stages I and then decreased from ovarian stages II to IV $(0.09\pm0.01,~0.06\pm0.01,~0.05\pm0.01~\text{nmol/mg},~\text{respectively})$. At ovarian stages I to III, the concentration of DA in the thoracic ganglia was 6-fold higher (P<0.05) than in the brain. When compared to the abdominal ganglia, the DA concentration in the thoracic ganglia was higher by 14-fold, 7-fold, and 6-fold at stage I, II, and III, respectively (P<0.05). When compared within a tissue, the concentration

of DA was about 2.5 and 3 times higher in the brain at ovarian stage II than in the brain at ovarian stage III and IV. The concentration of DA was about 2.7 and 4.5 times higher in the thoracic ganglia at ovarian stage II (P < 0.05) than in the thoracic ganglia at ovarian stage III and IV, respectively. The highest and the lowest concentrations of DA in each part of CNS were comparable to those of 5-HT, but the stages at which these occurred were in reverse. In the ovaries, the highest concentration of DA was detected at the ovarian stage I ($29.05 \pm 1.31 \, \text{nmol/mg}$), and it declined to the lowest level ($11.43 \pm 0.74 \, \text{nmol/mg}$) at ovarian stage IV (Fig 4B). Additionally, the concentration of DA was about 2 to 3 times higher in ovarian stage I and II (P < 0.05) than in the ovarian stage IV (Fig. 4B).

3.3. Changes in Vg concentrations after treatment with 5-HT and DA

The Vg concentrations in the hemolymph of female prawns after injection with various doses of 5-HT and DA during various stages of ovarian cycle were expressed in mg/ml of hemolymph as means \pm SEM. The Vg concentration in the NC group exhibited gradual increases from ovarian stage I to reach maximum at stage IV, which were 1.76 ± 0.25 , 3.19 ± 0.49 , 5.88 ± 0.94 , 9.90 ± 1.02 mg/ml, respectively. A similar pattern was also observed in the VIC group, whose Vg concentrations were 1.54 ± 0.13 , 3.04 ± 0.24 , 6.02 ± 0.68 , 9.37 ± 0.93 mg/ml, respectively, from ovarian stage I to stage IV (Fig. 5A and B).

The Vg concentrations after treatment with 2.5×10^{-6} or 2.5×10^{-7} mol of 5-HT/prawn exhibited a gradual increase from ovarian stage I to stage IV (Fig. 5A). At stage I, the Vg concentrations were 2.50 ± 0.15 and 2.33 ± 0.12 mg/ml, respectively, for the two 5-HT doses. Vg concentration gradually increased through ovarian stage II $(8.89 \pm 1.10 \text{ and } 7.99 \pm 0.82 \text{ mg/ml, respectively})$ and ovarian stage III (16.96 ± 2.01) and 14.37 ± 1.59 mg/ml, respectively), and finally reached the highest level (24.95 ± 1.88 and $20.33 \pm 1.60 \,\text{mg/ml}$, respectively) in stage IV, which was approximately at 10-fold increase over stage I. The Vg concentrations of prawns treated with 2.5×10^{-6} mol 5-HT/prawn were about 3, 3, and 2-3 times higher than those of control groups at ovarian stage II-IV. These results were statistically significant (P < 0.05). The Vg concentrations of prawns treated with 2.5×10^{-7} mol 5-HT/prawn were about 2-3, 2-3, and 2 times higher than those of control groups at ovarian stage II-IV (P < 0.05). The Vg concentration of prawns treated with either dose of 5-HT at ovarian stage IV was approximately a 14-fold higher that of control groups at ovarian stage I (P < 0.05). Furthermore, injection of 5-HT shortened the ovarian maturation periods (OMP) by about 10 days compared to control groups (OMP, ~29 days for 5-HT vs. ~39 days for NC). The gonado-somatic (GSI) index (i.e., ovarian size) was also significantly increased by about 2.5 fold, when compared to those of the control groups (Tinikul et al., in press).

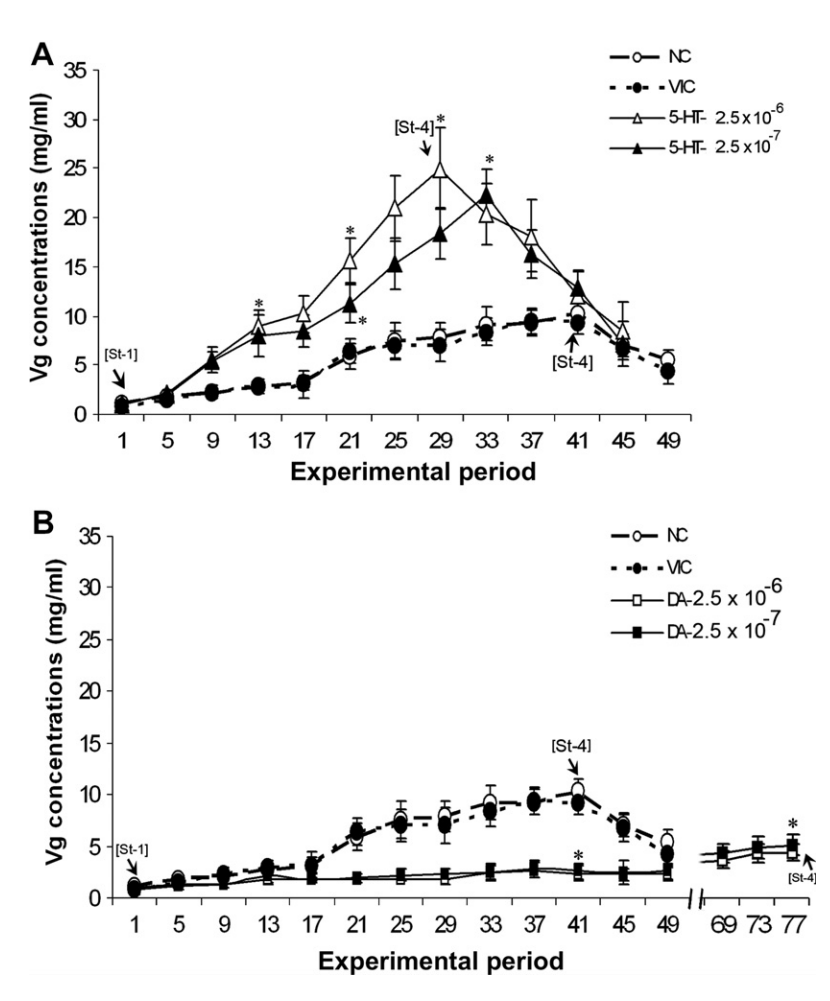


Fig. 5. A graph illustrating the concentrations of hemolymph vitellogenin (Vg) during various phases of the ovarian cycle following administrations of 5-HT (A) and DA (B). The doses of 5-HT and DA were given at 2.5×10^{-6} and 2.5×10^{-7} moles per prawn. The concentration is expressed as mg/ml of hemolymph. Numbers are expressed as means \pm SEM. Asterisks indicate significant differences P < 0.05, when compared between the experimental groups (5-HT and DA) and the control groups. St-1, at ovarian stage I; St-4, at ovarian stage IV.

In contrast, Vg concentrations after treatment with DA at 2.5×10^{-6} or 2.5×10^{-7} mol of DA/prawn increased slightly from ovarian stage I (1.84 \pm 0.36 and 2.06 \pm 0.21 mg/ml, respectively) to stage II (2.66 ± 0.18 and 2.77 ± 0.16 mg/ml, respectively), and then slightly increased at ovarian stages III (3.01 ± 0.71 and 3.58 ± 0.83 mg/ml, respectively), and stage IV (3.88 ± 0.65 and 4.49 ± 0.9 mg/ml, respectively). The Vg concentrations of prawns treated with DA ($2.5 \times 10^{-6} \text{ mol/prawn}$) were about 2 and 2.5 times lower than those of control groups at ovarian stage III and IV. These results were statistically significant (P < 0.05). The Vg concentrations of prawns treated with DA $(2.5 \times 10^{-7} \text{ mol/})$ prawn) were about 1 and 2 times lower than those of control groups at ovarian stage III and IV (P < 0.05) (Fig. 5B). However, prawns treated with DA showed longer ovarian maturation period (OMP ~64-67 days) as well as decreased ovarian size (Tinikul et al., in press).

4. Discussion

The present investigation documents how endogenous levels of 5-HT and DA change in the ovaries and nervous system in M. rosenbergii during the ovarian cycle. Variations in the concentration of 5-HT in the ovaries appear to be correlated with changes in brain and thoracic ganglia throughout the four stages of the cycle. Specifically, 5-HT levels rose steadily in all three structures from ovarian stage I to ovarian stage IV. In contrast, levels of DA in the brain, thoracic ganglia, and ovaries were high in ovarian stages I and II, and declined in ovarian stages III and IV. Thus, changes in DA concentration in the brain, thoracic ganglia, and ovaries were essentially opposite to those of 5-HT. This suggests that the two transmitters may play opposite roles in regulating ovarian maturation. Maximal DA levels occurred in stage I in the ovaries and in stage II in the brain and thoracic ganglia. Thus, the relationship between DA levels in the ovaries, brain and thoracic ganglia does not appear to be as tightly correlated as for 5-HT. Changes in DA and 5-HT levels in the abdominal ganglia during various stages of the ovarian cycle were not statistically significant.

The distribution of 5-HT has been extensively mapped using immunohistochemistry on the CNS of various crustaceans, including the crayfish, *Cherax destructor* (Sandeman et al., 1988), *P. leniusculus* (Elofsson, 1983), *P. clarkii* (Real and Czternasty, 1990), the lobster, *Homarus americanus* (Beltz and Kravitz, 1983), and squat lobster, *Munida quadrispina* (Antonsen and Paul, 2001). As well, DA was reported to be present in various regions of the CNS, including the lobster, *Homarus gammarus* (Cournil et al., 1994), the spiny lobster, *Panulirus argus* (Schmidt and Ache, 1997), the blue crab, *Callinectes sapidus* (Wood and Derby, 1996), and several crayfish species (Tierney et al., 2003).

Although immunohistochemistry is a useful method for visualizing and mapping neuronal populations containing biogenic amines, it is not an effective method for estimating and comparing the quantities of these neurotransmitters in various regions of the CNS. HPLC is a better method for this purpose, as pointed out by Hardie and Hirsh (2006). In the crayfish, P. clarkii, levels of biogenic amines were quantified in various regions of the CNS, eyestalk, and intestinal nerve using HPLC (Mercier et al., 1991; Kulkarni et al., 1992; Alvarez et al., 2005). In this species, the total concentration of 5-HT in the brain (0.581 \pm 0.36 μ g/g) was higher than in the eyestalks (0.299 \pm 0.15 μ g/g) (Cervantes et al., 1999). In the spiny lobster, P. homarus, the level of 5-HT was higher in thoracic ganglia than in the brain at ovarian stage IV, and as a result it was suggested that 5-HT could be involved in controlling the ovarian development (Kirubagaran et al., 2005). In the lobsters, Palinurus interruptus, H. americanus, and the crab, Cancer irroratus, major tissues that exhibited high levels of 5-HT were the optic ganglion, cerebral ganglion, circumoesophageal connectives,

stomatogastric ganglion, and thoracic ganglia (Aramant and Elofsson, 1976; Beltz et al., 1984). However, fluctuations in the levels of both 5-HT and DA in correlation with different phases of the ovarian cycle have not been previously reported. The present study demonstrates that in the freshwater prawn, *M. rosenbergii*, the levels of 5-HT and DA in the brain, thoracic ganglia and ovaries fluctuate in opposite directions during the ovarian cycle. Specifically, 5-HT levels rose with ovarian maturation, and DA levels fell. Our results agree with those reported earlier in *P. clarkii* and in *P. homarus* by Cervantes et al. (1999) and Kirubagaran et al. (2005), but these authors reported only 5-HT levels. Chen et al. (2003) was the first to report the possible involvement of DA in ovarian development in *M. rosenbergii*, but they did not show the variation pattern of DA in various regions of CNS and ovary as reported here.

The effects of 5-HT and DA on regulation of ovarian maturation in crustaceans have been extensively reported (Martinez and Rivera, 1994; Sarojini et al., 1995; Meeratana et al., 2006). 5-HT induces ovarian maturation in several species, including the crayfish, P. clarkii, the lobster, H. americanus (Kulkarni et al., 1992; Fingerman, 1997), the giant freshwater prawn, M. rosenbergii (Meeratana et al., 2006), the black tiger shrimp, P. monodon (Wongprasert et al., 2006), P. vannamei (Vaca and Alfaro, 2000), and Litopenaeus vannamei and Litopenaeus stylirostris (Alfaro et al., 2004). Treatment of the crayfish, P. clarkii, with 5-HT causes significant increases in ovarian index and oocyte diameter (Kulkarni et al., 1992). Kulkarni et al. (1991) reported that brain and thoracic ganglia of *P. clarkii* stimulated incorporation of leucine into ovarian protein. In the freshwater prawn, M. rosenbergii, treatment with 5-HT also showed a significant increase in the gonadosomatic (GSI) index (Meeratana et al., 2006). In L. stylirostris, the combined injection of 5-HT and spiperone elicited higher rates of ovarian maturation compared to application of 5-HT alone (Alfaro et al., 2004). Furthermore, the ovaries of prawns injected with the culture medium of 5-HT-primed thoracic ganglia exhibited an increase in the number of oocytes developing to vitellogenic and mature stages. These findings suggest that 5-HT and/or other hormonal factors from the thoracic ganglia could be major factors that stimulate the ovarian maturation (Meeratana et al., 2006). 5-HT might act indirectly by stimulating the release of some other putative gonadotrophic factor, such as gonad-stimulating hormone (GSH) from the thoracic ganglion, and/or by inhibiting the release of gonad-inhibiting hormone (GIH) from the optic lobe, whereas DA plays the opposite role (Kulkarni et al., 1992; Sarojini et al., 1995; Fingerman, 1997). In the freshwater prawn, M. rosenbergii, it was suggested that the inhibitory action of DA could be on the thoracic ganglia through inhibition of vitellogenesis-stimulating hormone (VSH) release, but not at the eyestalk level through stimulation of VIH release from the X-organ-sinus gland complex (Chen et al., 2003). Our finding that the thoracic ganglia contained high levels of 5-HT and DA implies that this part of CNS may play a leading role in controlling the prawn's ovarian maturation, and that the brain may play a secondary role. In contrast, the abdominal ganglia, which had the lowest levels and least fluctuation of both 5-HT and DA levels, may not be involved in this controlling process.

In crustaceans, vitellogenesis is an important process in the female reproductive cycle (Okumura, 2004), which is characterized by the appearance in the hemolymph of vitellogenin (Vg), the precursor of the major yolk protein, vitellin (Vn) (Tsukimura, 2001). Thus, hemolymph Vg level is an important indicator of ovarian maturation. Extracts of the brain and thoracic ganglia stimulate ovarian vitellogenin synthesis and the development of secondary oocytes in the crayfish, *P. leniusculus* and *P. clarkii* (Elofsson et al., 1982; Sarojini et al., 1995), the crab, *Uca pugilator* (Chang, 1985), and the shrimp, *Paratya compressa* (Takayanagi et al., 1986). In the present study, injection of 5-HT and DA, respectively, increased

or decreased levels of hemolymph Vg in *M. rosenbergii*. Vg concentrations of prawns treated with 5-HT were higher at all ovarian stages, especially stage IV, compared to control groups, whereas prawns treated with DA exhibited lower Vg concentrations when compared to those of 5-HT and control groups. These results indicate causal relationships, with 5-HT stimulating Vg synthesis and DA inhibiting Vg synthesis. Taken together with fluctuations in 5-HT and DA levels, the present data suggest that ovarian maturation involves increases in levels of 5-HT and decreases in levels of DA in the CNS and ovary.

In this study, the concentration of 5-HT in the ovary was lowest at ovarian stage I and gradually increased to ovarian stage IV. In contrast, the concentration of DA was highest at ovarian stage I and lowest at the ovarian stage IV. Fluctuations in the level of these two neurotransmitters were also in opposite directions as in the brain and thoracic ganglia. However, the levels of DA in the ovaries were much higher than those of 5-HT at each phase of the ovarian cycle. There have been previous reports on the roles of 5-HT and DA in the oocyte maturation. In mouse, the existence and expression of a 5-HT receptor (5-HT1D) in oocytes implies that 5-HT may be involved in the regulation of oocyte maturation (Vasela et al., 2003). Moreover, increasing levels of 5-HT have been detected in human ovarian follicular fluid in association with the ovulatory cycle (Bodis et al., 1992). In marine memertean worms, 5-HT causes increases in cAMP in immature oocytes, which stimulates meiotic division and maturation of oocytes (Stricker and Smythe, 2001). In bivalves, Spisula sp., 5-HT stimulates the completion of meiotic division of isolated cultured oocytes (Hirai et al., 1988). The mechanism by which 5-HT releases oocytes from prophase I arrest appears to involve a G-protein coupled receptor that results in the increase of IP-3 and intracellular Ca²⁺ levels (Gobet et al., 1994). In P. monodon, 5-HT1 receptors were expressed in the membrane of mature oocytes in stages III and IV of the ovarian cycle (Ongvarrasopone et al., 2006), which suggest that 5-HT may play a critical role in regulating oocyte maturation in this penaeoid shrimp as well. As a significantly high level of 5-HT appeared in the ovary from stage I to IV in M. rosenbergii, and 5-HT was also detected in late and mature oocytes (unpublished observation), we propose that 5-HT may play similar role in the oocyte maturation in this species.

The expression of DA in the ovary appears to be phylogenetically conserved feature (Buznikov, 1991). In sea urchins, the ability of both unfertilized and fertilized eggs to take up DA was demonstrated, and it was shown that the uptake of DA was more prominent before fertilization (Carginale et al., 1995). In the grey mullet, Mugil cephalus, DA was found to inhibit the proliferation of early stages of vitellogenic oocytes and the final stage of oocyte maturation and ovulation (Aizen et al., 2005). In the European eel, Anguilla anguilla, and in teleost fish, it was demonstrated that DA could inhibit the release of luteinizing hormone (LH) (Peter et al., 1986; Vidal et al., 2004). Consequently, the oocytes fail to mature and ovulate (Yaron, 1995). Even though the role of DA is not as well defined as that of 5-HT, it is possible that in M. rosenbergii DA might also delay oocyte maturation by promoting the meiotic arrest at the end of prophase stage. This, however, needs to be further studied.

Acknowledgments

This research was supported by the Thailand Research Fund (Royal Golden Jubilee Ph.D. Program (Grant No. PHD/0171/2547) to Yotsawan Tinikul and Prasert Sobhon, Senior Research Scholar Fellowship to Prasert Sobhon), and the Commission on Higher Education (Research Group Development Grant to Prasert Sobhon). We would like to express our special thanks to Dr. Angela Lange (University of Toronto, Canada), Dr. Jeffrey Atkinson (Brock University, Canada), Dr. Wattana Weerachatyanukul, Ms. Ruchanok Cheota-

cha, Ms. Rapeepun Kongtoom, Ms. Jaruwan Poljaroen, Mrs. Pornsawan Duangsuwan, and Mr. Ittipon Phoungpetchara for useful suggestions and assistance in the HPLC work.

References

- Aizen, J., Meiri, I., Tzchori, I., Levavi-Sivan, B., Rosenfeld, H., 2005. Enhancing spawning in the grey mullet (*Mugil cephalus*) by removal of dopaminergic inhibition. Gen. Comp. Endocr. 142, 212–221.
- Alfaro, J., Zuniga, G., Komen, J., 2004. Induction of ovarian maturation and spawning by combined treatment of serotonin and a dopamine antagonist, spiperone in *Litopenaeus stylirostris* and *Litopenaeus vannamei*. Aquaculture 236, 511–522.
- Alvarez, R.A., Villalobos, M.G.P., Rosete, G.C., Sosa, L.R., Arechiga, H., 2005. Dopaminergic modulation of neurosecretory cells in the crayfish. Cell. Mol. Neurobiol. 25, 345–370.
- Antonsen, B.L., Paul, D.H., 2001. Serotonergic and octopaminergic systems in the squat lobster *Munida quadrispina* (Anomura, Galatheidae). J. Comp. Neurol. 439, 450–468.
- Aramant, R., Elofsson, R., 1976. Monoaminergic neurons in the nervous system of crustaceans. Cell Tissue. Res. 170, 231–251.
- Beltz, B.S., Kravitz, E.A., 1983. Mapping of serotonin-like immunoreactivity in the lobster nervous system. J. Neurosci. 3, 585–602.
- Beltz, B.S., Eisen, J.S., Flamm, R., Harris, R.M., Hooper, S.L., Marder, E., 1984. Serotonergic innervation and modulation of the stomatogastric ganglion of three decapod crustaceans (*Palinurus interruptus*, *Homarus americanus*, and *Cancer irroratus*). J. Exp. Biol. 87, 285–313.
- Bodis, J., Torok, A., Tinnberg, H.R., Volker, H., Hamori, M., Cledon, P., 1992. Influence of serotonin on progesterone and estradiol secretion by cultured human granulosa cells. Fertil. Steril. 57, 1008–1011.
- Bradford, M.M., 1976. A rapid and sensitive method for the quantitation of microgram quantities of protein utilizing the principle of protein-dye binding. Anal. Biochem. 72, 248–254.
- Butler, T.A., Fingerman, M., 1983. Concentration of neurotransmitters in the central nervous system of *Uca panacea* and *Callinectes sapidus*. Am. Zool. 23, 954–958.
- Buznikov, G.A., 1991. The biogenic amines as regulators of early (pre-nervous) embryogenesis. Adv. Exp. Med. Biol. 296, 33–48.
- Carginale, V., Borrelli, L., Capasso, A., Parisi, E., 1995. Changes in dopamine uptake and developmental effects of dopamine receptor inactivation in the sea urchin. Mol. Reprod. Dev. 40, 379–385.
- Cervantes, O.C., Battelle, B.A., Moles, M.L.F., 1999. Rhythmic changes in the serotonin content of the brain and eyestalk of crayfish during development. J. Exp. Biol. 202, 2823–2830.
- Chang, E.S., 1985. Hormonal control of molting in decapod crustacean. Am. Zool. 25, 179–185.
- Chang, C.F., Shih, T.W., 1995. Reproductive cycle of ovarian development and Vitellin profiles in the freshwater prawns, *Macrobrachium rosenbergii*. Invertebr. Reprod. Dev. 27, 11–20.
- Chen, Y.N., Kuo, C.M., 1998. Purification and characterization of vitellin from the freshwater giant prawn, Macrobrachium rosenbergii. Zool. Stud. 37, 126–136.
- Chen, Y.N., Fan, H.F., Hsieh, S.L., Kuo, C.M., 2003. Physiological involvement of DA in ovarian development of the freshwater giant prawn, *Macrobrachium rosenbergii*. Aquaculture 228, 383–395.
- Cournil, I., Helluy, S.M., Beltz, B.S., 1994. Dopamine in the lobster Homarus gammarus: I Comparative analysis of dopamine and tyrosine hydroxylase immunoreactivities in the nervous system of the juvenile. J. Comp. Neurol. 344, 455–469.
- Elofsson, R., Laxmyr, L., Rosengren, E., Hansson, C., 1982. Identification and quantitative measurement of biogenic amines and DOPA in the central nervous system and hemolymph of the crayfish *Pacifastacus leniusculus* (Crustacea). Comp. Biochem. Physiol. C71, 195–201.
- Elofsson, R., 1983. 5-HT-like immunoreactivity in the central nervous system of the crayfish, *Pacifastacus leniusculus*. Cell Tissue. Res. 232, 231–236.
- Fingerman, M., Nagabhushanam, R., Sarojini, R., Reddy, P.S., 1994. Biogenic amines in crustaceans: identification, localization, and roles. J. Crustacean. Biol. 14 (3), 413–437.
- Fingerman, M., 1997. Roles of neurotransmitters in regulating the reproductive hormone release and gonadal maturation in decapod crustaceans. Invertebr. Reprod. Dev. 31, 47–54.
- Gobet, I., Durocher, Y., Lecler, C., Moreau, M., Guerrier, P., 1994. Reception and transduction of the serotonin signal responsible for meiosis reinitiation in oocytes of the Japanese clam *Ruditapes philippinarum*. Dev. Biol. 164, 540–549.
- Hardie, S.L., Hirsh, J., 2006. An improved method for the separation and detection of biogenic amines in adult *Drosophila* brain extracts by high performance liquid chromatography. J. Neurosci. Meth. 153, 243–249.
- Hirai, S., Kishimoto, T., Kadam, A.L., Kanatani, H., Koide, S.S., 1988. Induction of spawning and oocyte maturation by 5-hydroxytryptamine in the surf clam. J. Exp. Zool. 245, 318–321.
- Kerkui, G.A., Sedden, C.B., Walker, R.J., 1966. The effect of DOPA, a-methyl DOPA and reserpine on the DA content of the brain of the snail, *Helix aspersa*. Comp. Biochem. Physiol. 18, 921–930.
- Kirubagaran, R., Peter, D.M., Dharani, G., Vinithkumar, N.V., Sreeraj, G., Ravindran, M., 2005. Changes in vertebrate-type steroids and 5-hydroxytryptamine during ovarian recrudescence in the Indian spiny lobster, *Panulirus homarus*. New Zeal. J. Mar. Fresh. 39, 527–537.

- Kulkarni, G.K., Glade, L., Fingerman, M., 1991. Oogenesis and effects of neuroendocrine tissues on in vitro synthesis of protein by the ovary of the red swamp crayfish *Procambarus clarkii* (Girard). J. Crustac. Biol. 11, 513–522.
- Kulkarni, G.K., Nagabhushanam, R., Amaldoss, G., Jaiswal, R.G., Fingerman, M., 1992. In vitro stimulation of ovarian development in the red swamp crayfish, *Procambarus clarkii* (Girard), by 5-hydroxytryptamine. Invertebr. Reprod. Dev. 21, 231–240.
- Kwok, R., Tobe, S.S., 2006. Hemolymph clotting in crustaceans: implications for neuropeptide extraction from invertebrate hemolymph. Peptides 27, 590–596.
- Laxmyr, L., 1984. Biogenic amines and DOPA in the central nervous system of decapod crustacean. Comp. Biochem. Physiol. C77, 139–143.
- Martinez, G., Rivera, A., 1994. Role of monoamines in the reproductive process of Argopecten purpurarus. Invertebr. Reprod. Dev. 25, 167–174.
- Meeratana, P., Withyachumnarnkul, B., Damrongphol, P., Wongprasert, K., Suseangtham, A., Sobhon, P., 2006. Serotonin induces ovarian maturation in giant freshwater prawn broodstock, *Macrobrachium rosenbergii* de Man. Aquaculture 260, 315–325.
- Meeratana, P., Sobhon, P., 2007. Classification of differentiating oocytes during ovarian cycle in the giant freshwater prawn, *Macrobrachium rosenbergii* de man. Aquaculture 270, 249–258.
- Mercier, A.J., Orchard, I., Schmoeckel, A., 1991. Catecholaminergic neurons supplying the hindgut of the crayfish *Procambarus clarkii*. Can. J. Zool. 69, 2778–2785.
- Molaei, G., Lange, A.B., 2003. The association of serotonin with the alimentary canal of the African migratory locust, *Locusta migratoria*: distribution, physiology and pharmacological profile. J. Insect. Physiol. 49, 1073–1082.
- Okumura, T., 2004. Perspectives on hormonal manipulation of shrimp reproduction review. JARQ 38, 49–54.
- Ongvarrasopone, C., Roshorm, Y., Somyong, S., Pothiratana, C., Petchdee, S., Tangkhabuanbutra, J., Sophasan, S., Payim, S., 2006. Molecular cloning and functional expression of the *Penaeus monodon* 5-HT receptor. Biochim. Biophys. Acta 1759, 328–339.
- Peter, R.E., Chang, J.P., Nahorniak, C.S., Omeljaniuk, R.J., Sokolowska, M., Shih, S.H., Billard, R., 1986. Interactions of catecholamines and GnRH in regulation of gonadotropin secretion in teleost fish. Recent. Prog. Horm. Res. 42, 513–548.
- Real, D., Czternasty, G., 1990. Mapping of serotonin-like immunoreactivity in the ventral nerve cord of crayfish. Brain Res. 521, 203–212.
- Ridchardson, H.G.D., Decaraman, M., Fingerman, M., 1991. The effect of biogenic amines on ovarian development in fiddler crab, *Uca pugilator*. Comp. Biochem. Physiol. C99, 53–56.
- Sandifer, P.A., Smith, T.J., 1985. Freshwater prawn: crustacean and mollusk aquaculture in the United States. A publishing company, Inc., West port, USA. pp. 1–15.

- Sandeman, D.C., Sandeman, R.E., Aitken, A.R., 1988. Atlas of serotonin containing neurons in the optic lobes and brain of the crayfish, *Cherax destructor*. J. Comp. Neurol. 269. 465–478.
- Sarojini, R., Nagabhushanam, R., Fingerman, M., 1995. Mode of action of the neurotransmitter 5-hydroxytryptamine in stimulating ovarian maturation in the red swamp crayfish, *Procambarus clarkii*: an in vivo and in vitro study. J. Exp. Zool. 271, 395–400.
- Schmidt, M., Ache, B.W., 1997. Immunocytochemical analysis of glomerular regionalization and neuronal diversity in the olfactory deutocerebrum of the spiny lobster. Cell Tissue. Res. 287, 541–563.
- Stricker, S.A., Smythe, T.L., 2001. 5-HT causes increase in cAMP that stimulates, rather inhibits, oocyte maturation in marine memertean worms. Development 128, 1415–1427.
- Takayanagi, H., Yamamoto, Y., Takeda, N., 1986. An ovary stimulating pheromone in the freshwater shrimp, *Paratya compressa*. J. Exp. Zool. 240, 397–400.
- Tierney, A.J., Kim, T., Abrams, R., 2003. Dopamine in crayfish and other crustaceans: distribution in the central nervous system and physiological functions. Microsc. Res. Techniq. 60, 325–335.
- Tinikul, Y., Soonthornsumrith, B., Phoungpetchara, I., Meeratana, P., Poljaroen, J., Duangsuwan, P., Soonklang, N., Mercier, A.J., Sobhon, P. in press. Effects of serotonin, dopamine, octopamine, and spiperone on ovarian maturation and embryonic development in the giant freshwater prawn, Macrobrachium rosenbergii (De Man), Crustaceana.
- Tsukimura, B., 2001. Crustacean vitellogenesis: its role in oocyte development. Amer. Zool. 41, 465–476.
- Vaca, A.A., Alfaro, J., 2000. Ovarian maturation and spawning in the white shrimp, *Penaeus vannamei*, by serotonin injection. Aquaculture 182, 373–385.
- Vasela, J., Rehak, P., Mihalik, J., Czikkova, S., Pokorny, J., Koppel, J., 2003. Expression of serotonin receptors in mouse oocytes and preimplatation embryos. Physiol. Rev. 52, 223–228.
- Vidal, B., Pasqualini, C., Belle, N.L., Holland, M.C.H., Sbaihi, M., Vernier, P., Zohar, Y., Dufour, S., 2004. Dopamine inhibits luteinizing hormone synthesis and release in the juvenile European Eel: a neuroendocrine lock for the onset of puberty1. Biol. Reprod. 71, 1491–1500.
- Wongprasert, K., Asuvapongpatana, S., Poltana, P., Tiensuwan, M., Withyachumnarnkul, B., 2006. Serotonin stimulates ovarian maturation and spawning in the black tiger shrimp *Penaeus monodon*. Aquaculture 261, 1447–1454
- Wood, D.E., Derby, C.D., 1996. Distribution of dopamine-like immunoreactivity suggests a role for dopamine in the courtship display behavior of the blue crab *Callinectes sapidus*. Cell Tissue. Res. 285, 321–330.
- Yaron, Z., 1995. Endocrine control of gametogenesis and spawning induction in the carp. Aquaculture 129, 49–73.

REGULAR ARTICLE

Changes in distribution of basic nuclear proteins and chromatin organization during spermiogenesis in the greater bandicoot rat, *Bandicota indica*

Pakawadee Worawittayawong · Chris Leigh · Wattana Weerachatyanukul · Sirikul Manochantr · Prasert Sobhon · William G. Breed · Prapee Sretarugsa

Received: 20 December 2007 / Accepted: 30 June 2008 / Published online: 23 August 2008 © Springer-Verlag 2008

Abstract Male germ cells of the greater bandicoot rat, *Bandicota indica*, have recently been categorized into 12 spermiogenic steps based upon the morphological appearance of the acrosome and nucleus and the cell shape. In the present study, we have found that, in the Golgi and cap phases, round spermatid nuclei contain 10-nm to 30-nm chromatin fibers, and that the acrosomal granule forms a huge cap over the anterior pole of nucleus. In the acrosomal phase, many chromatin fibers are ~50 nm thick; these then thickened to 70-nm fibers and eventually became 90-nm chromatin cords that are tightly packed together into highly condensed chromatin, except where nuclear vacuoles occur. Immunocytochemistry and immunogold localization with anti-histones, anti-transition protein2, and anti-protamine antibodies suggest that histones remain throughout sperm-

iogenesis, that transition proteins are present from step 7 spermatids and remain until the end of spermiogenesis, and that protamines appear at step 8. Spermatozoa from the cauda epididymidis have been analyzed by acid urea Triton X-100 polyacrylamide gel electrophoresis for basic nuclear proteins. The histones, H2A, H3, H2B, and H4, transitional protein2, and protamine are all present in sperm extracts. These findings suggest that, in these sperm of unusual morphology, both transition proteins and some histones are retained, a finding possibly related to the unusual nuclear form of sperm in this species.

Keywords Chromatin organization · Sperm basic nuclear proteins · Immunocytochemistry · Spermiogenesis · *Bandicota indica* (Rodentia)

This work was supported by grants from the Thailand Research Fund (RGJ/PHD/00196/2541 and BGJ/37/2543) to Prapee Sretarugsa and Pakawadee Worawittayawong and by a University of Adelaide grant to William G. Breed.

P. Worawittayawong · W. Weerachatyanukul · P. Sobhon · P. Sretarugsa (⋈)
Department of Anatomy, Faculty of Science, Mahidol Un

Department of Anatomy, Faculty of Science, Mahidol University, Rama 6 Road, Rajdhevee,

Bangkok 10400, Thailand e-mail: scpsr@mahidol.ac.th

P. Worawittayawong · C. Leigh · W. G. Breed (☒)
Discipline of Anatomical Sciences, School of Medical Sciences,
The University of Adelaide,
Adelaide 5005, South Australia
e-mail: bill.breed@adelaide.edu.au

S. Manochantr Department of Anatomy, Faculty of Medicine, Thammasart University, Rangsit Campus, Pathumthani 12120, Thailand

Introduction

Mammalian spermiogenesis involves the differentiation of spermatids into highly polarized spermatozoa during which time the remodeling and repackaging of the sperm nuclear proteins occurs (Balhorn et al. 1984; Courtens and Loir 1981; Oko et al. 1996). In common laboratory rodents, the chromatin organization, as seen by transmission electron microscopy (TEM), appears early in spermiogenesis as 50-nm fibers, which later aggregate into 100-nm cords that then become highly compacted in the mature sperm nuclei (Ploen and Courtens 1986; Biggiogera et al. 1992; Balhorn et al. 1999; Wanichanon et al. 2001). During chromatin condensation, transition proteins (TPs) initially replace most of the histones. They are then largely, or completely, replaced by protamines (Grimes et al. 1977; Oliva and Dixon 1991; Meistrich 1989; Biggiogera et al. 1992; Wouters-Tyrou et al. 1998; Oko et al. 1996; Corzett et al.



2002) with the TPs probably preparing the chromatin for association with protamines and playing a role in bringing about DNA condensation (Oko et al. 1996; Yu et al. 2000; Brewer et al. 2002; for reviews, see Meistrich et al. 2003; Kimmins and Sassone-Corsi 2005; Pradeepa and Rao 2007). In the spermatid nuclei of laboratory rodents, TPs appear before histone removal is complete (Zhao et al. 2004), and in the rat, TPs appear concurrently with the condensation of chromatin (Oko et al. 1996). In the mouse, histones are replaced by TPs in step 11 to 13 spermatids, the TPs then being replaced by protamines (Yu et al. 2000; Meistrich et al. 2003; Zhao et al. 2004) so that mature sperm lack TPs (Oko et al. 1996; Pradeepa and Rao 2007). Protamines, which are small, highly positively charged, arginine-rich proteins, bind to the phosphate backbone of DNA and initiate DNA coiling (Balhorn 1982; Allen et al. 1993; Balhorn et al. 1999). In some mammal species, two groups of protamines occur. Protamine 1, which is relatively highly conserved, is invariably present, whereas protamine 2 is found only in a few species. The reason for this difference in abundance of protamine 2 is not clear, but to date, no obvious relationship appears to exist between the ratio of protamine 1 and protamine 2 and that of nuclear shape (Balhorn 1989; Queralt et al. 1995; Corzett et al. 2002).

Unlike most murine rodents in which sperm heads have falciform-shaped nuclei (Retzius 1909; Friend 1936; Bishop and Austin 1960; Lalli and Clermont 1981; Breed 2004), those of the greater bandicoot rat, *Bandicota indica*, have a globular-shaped nucleus that is capped by an extremely large acrosome (Breed 1993, 1998, 2004; Worawittayawong et al. 2005). The reason for this dramatic difference in sperm nuclear shape is not clear but may be related to differences in sperm chromatin organization and its nuclear protein profile. In the present study, we show that, in the greater bandicoot rat, both filamentous and globular patterns of chromatin packaging occur during spermiogenesis, and that the mature sperm nucleus appears to contain, in addition to protamine, a TP and some histones.

Materials and methods

Antibodies and chemicals

Rabbit polyclonal anti-H2A, anti-H2B, and anti-H4 antibodies were donated by Dr. Sylviane Muller (IBMC, France), and anti-H3 IgG was purchased from Santa Cruz Biotechnology (Santa Cruz, Calif., USA). Rabbit polyclonal anti-TP2 antibody, originally from Alfonso and Kistler (1993), was kindly provided by Dr. Richard Oko (Department of Anatomy and Cell Biology, Ontario, Canada), and monoclonal antibody against human protamine was from Dr. Rod Balhorn (Lawrence Livermore National Laboratory, Livermore, Calif., USA). Chemicals used

in these experiments were purchased from Sigma-Aldrich (St. Louis, Mo., USA) unless mentioned otherwise.

TEM and measurement of chromatin fibers of spermatids

Greater bandicoot rats were caught in rice fields in the northem parts of Thailand and acclimatized for a few days before use. After anesthesia, the testes were removed from the animals, and small pieces of tissue were immediately fixed in 3% glutaraldehyde and 3% paraformaldehyde in 0.1 M phosphate buffer, pH 7.4, at 4°C, overnight. Some of the tissue was then post-fixed in 1% osmium tetroxide (1 h, 4°C), washed in phosphate buffer, dehydrated by being passed through a graded series of ethanols, and embedded in TAAB epoxy resin. Ultrathin sections were cut, mounted on copper grids, stained with uranyl acetate and lead citrate, and observed with a Philips CM100 transmission electron microscope at 80 kV.

Sizes of chromatin fibers at each spermatid step were measured in ten randomly selected areas of each nucleus. At least ten nuclei at each step of spermiogenesis were measured by Adobe Photoshop software at high resolution by using a modified method as described in Manochantr et al. (2005) with a catalase crystal (lattice spacing: 87.5 Å) as a standard.

Immunohistochemistry of spermatids

For immunohistochemistry, testes were removed, fixed in Bouin's fixative overnight, and processed for paraffin embedding. Sections (5 µm thick) were cut, deparaffinized by being passed through a decreasing series of ethanols, and immersed in 1% saturated lithium carbonate in 70% ethanol to eliminate residual picric acid. Endogenous peroxidase activity was minimized by immersion in 1% H₂O₂ in 70% ethanol. The sections were then pre-blocked with 0.1 M glycine and 4% bovine serum albumin (BSA) in 0.1 M phosphate-buffered saline (PBS), and permeabilized with 1% Triton X-100 in PBS for 15 min. Sections were incubated in either antihistones, anti-TP2, or anti-protamine antibodies at a dilution of 1:100 (1 h, in a humidified chamber). For controls, the primary antibodies were omitted, or the sections were treated with pre-immune sera. Sections were washed twice in 0.1 M TRIS-buffered saline (TBS) containing 0.05% Tween 20 (TBST) and subsequently exposed to the corresponding horseradish peroxidase (HRP)-conjugated secondary antibodies at a dilution of 1:400 (1 h, room temperature). The peroxidase reaction products were obtained by incubating tissue sections in 0.03% H₂O₂, 0.3% NiCl₂, and 0.05% diaminobenzidine tetrahydrochloride (DAB) in TBS and washed in distilled water. Sections were dehydrated by being passed through ethanols, cleared in xylene, and a coverslip placed on top. All images were acquired with a Nikon Eclipse E600 microscope equipped with a Nikon DXM 1200 charge-coupled device camera.



Immunoelectron microscopy of spermatids

Small pieces of testes were fixed in 4% paraformaldehyde and 1% glutaraldehyde in 0.1 M phosphate buffer, pH 7.4. They were then dehydrated and processed for embedding in LR White resin (London Resin, Berkshire, UK). Thin sections were cut with a diamond knife, mounted on Formvar-coated nickel grids, placed on drops of 0.1 M glycine solution in PBS, and blocked with 5% normal goat serum (NGS) in TBST (20 min, in a humidified chamber). They were then incubated (4°C, overnight) with one of the primary antibodies (goat anti-rabbit antibody for H2A) H2B, H3, and TP, and goat anti-mouse antibody for protamine) at a dilution of 1:10 in 1% NGS-TBST, washed with NGS-TBST, incubated in the corresponding secondary antibodies coupled with 10-nm gold particles at a dilution of 1:20 (2 h, in a humidified chamber), and washed repeatedly in NGS-TBS and distilled water. For negative controls, the primary antibody was omitted. The sections were then stained with uranyl acetate and observed with a Phillips CM100 transmission electron microscope at 80 kV.

Extraction of basic nuclear proteins from spermatozoa from the cauda epididymidis

Extraction was performed according to the protocol described by Platz et al. (1975) and Manochantr et al. (2005). Briefly, sperm were gently squeezed from the cauda epididymidis, washed in cold PBS, and then centrifuged at 600g for 10 min before being resuspended in sodium-magnesium TRIS (SMT) solution (250 mM sucrose, 2 mM MgCl₂, and 10 mM TRIS-HCl, pH 7.4). The sperm were then pelleted (600g, 10 min), demembranated with 0.5% Triton X-100 in SMT solution, and centrifuged (1500g, 10 min) to obtain the sperm nuclear fraction. Nuclei from chick erythrocytes were prepared similarly.

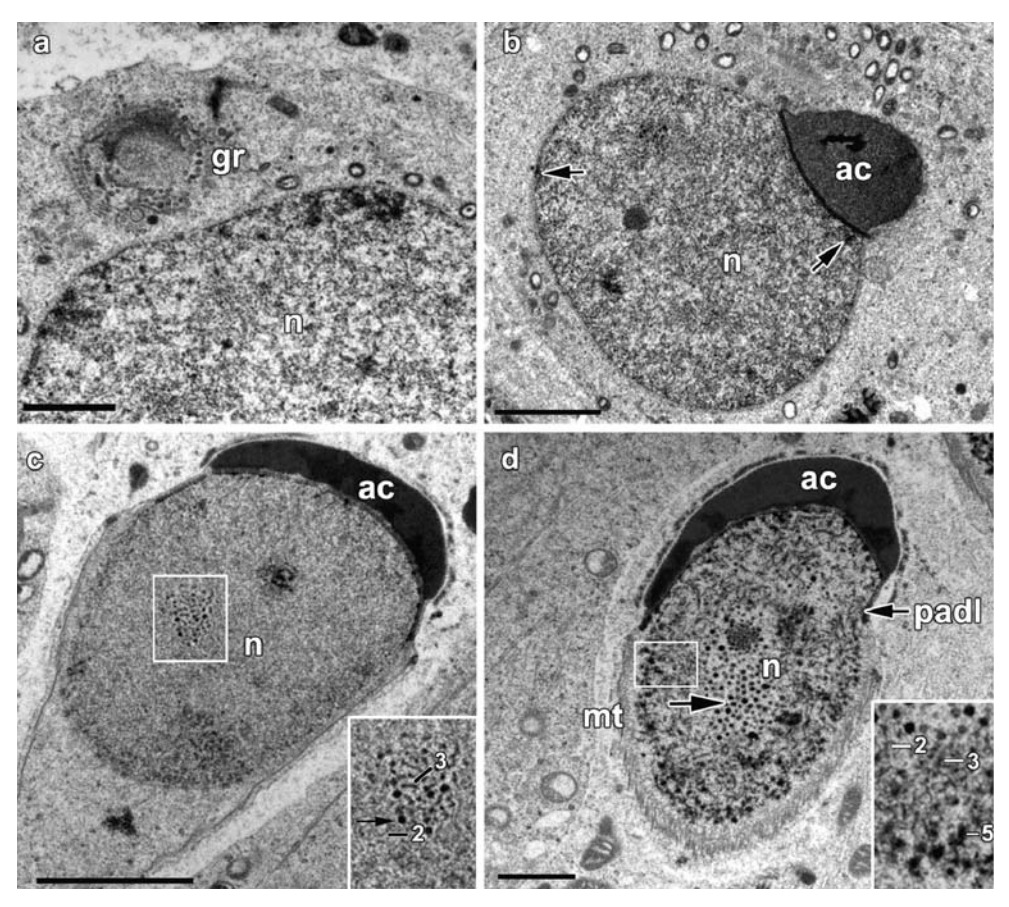
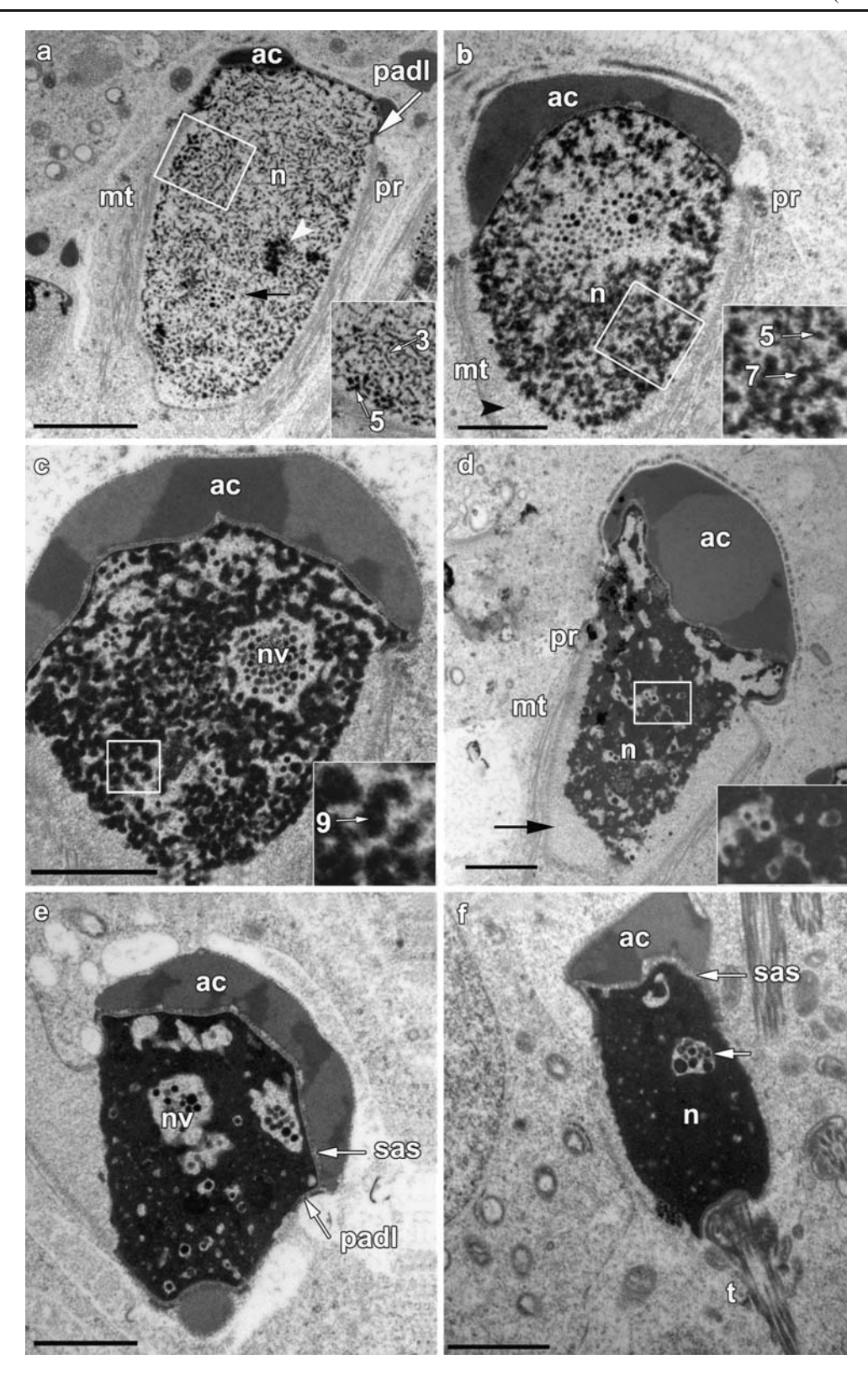


Fig. 1 Transmission electron micrographs of early developing spermatids of *Bandicota indica* testis. **a** A Golgi phase spermatid showing numerous small electron-dense proacrosomal granules (*gr*); the nucleus (*n*) contains 10-nm and 20-nm chromatin threads. **b** An early cap phase spermatid showing a large acrosomal granule (*ac*) attached to the nuclear envelope in the anterior region of nucleus (*n*); condensed chromatin is located just beneath the acrosome and close to other regions of the nuclear envelope (*arrows*). **c** Early acrosome phase spermatid showing cap-shaped acrosome (*ac*) and homogeneous

electron-dense chromatin; 30-nm chromatin fibers (3) have started to appear in the middle (*inset*) and posterior (*arrow*) regions (2 20-nm fibers). **d** An early acrosome phase spermatid showing abundant 30-nm chromatin fibers throughout much of the nucleus (n) and thicker chromatin (50-nm fibers) located peripherally. Spherical electron-dense particles lie in the vacuole situated centrally (*arrow*). *Inset*: Three different types of chromatin fibers of 20 (2), 30 (3), and 50 (5) nm (padl postacrosomal dense lamina, mt microtubule). Bars 1 μ m (a, b, d), 2 μ m (c)





The nuclear fractions of sperm and chick erythrocytes were treated with reducing agent (5 M guanidine HCl, 0.3 M β -mercaptoethanol, and 10 mM dithiothreitol, 0.5 M TRIS-HCl, pH 8.5). To obtain a nuclear suspension, a final

concentration of 0.25 N HCl was added, and incubation was carried out for 1 h to extract the basic nuclear proteins (BNPs). Nuclear remnants were then eliminated by centrifugation (12,000g, 15 min), and the nuclear proteins in



Fig. 2 Transmission electron micrographs of late spermatids in the B. indica testis. a Early acrosome phase showing chromatin fibers of 30 nm (3) throughout the nucleus (n) with 50-nm fibers (5) at the periphery and a localized central region (arrowhead, see also inset). b Mid-acrosome phase spermatid showing 50-nm fibers (5, inset) throughout the nucleus (n) with some 70-nm peripheral chromatin cords (7, inset); a small region of electron-lucent material occurs posteriorly (arrowhead). c Mid-acrosome phase spermatid showing large chromatin cords of 90 nm in thickness (9, inset) with spherical electron-dense particles in the nuclear vacuole (nv); the acrosome (ac) has two regions of different electron density. d Late acrosome phase spermatid showing 90-nm chromatin cords with small region of electron-lucent material posteriorly (arrow). e, f Maturation phase spermatids showing extensive homogeneous electron-dense chromatin, except where nuclear vacuoles (nv) are present (mt microtubules, padl postacrosomal dense lamina, pr perinuclear ring, sas subacrosomal space, t tail). Bars 2 μ m (a), 1 μ m (b-f)

supernatant were precipitated with 80% trichloro-acetic acid (60 min). The precipitate was recovered by centrifugation (12,000g, 10 min), washed twice with cold acidified acetone (-70°C; 2,000:1, v/v: acetone/12 N HCl) and subsequently with cold acetone, and then air-dried.

Acid urea Triton X-100 polyacrylamide gel electrophoresis and immunoblotting of spermatozoa from the cauda epididymidis

BNPs of cauda sperm were separated by 17% acid urea Triton X-100 polyacrylamide gel electrophoresis (AUT-PAGE; 2.5 M urea, 6 mM Triton X-100, and 5% acetic

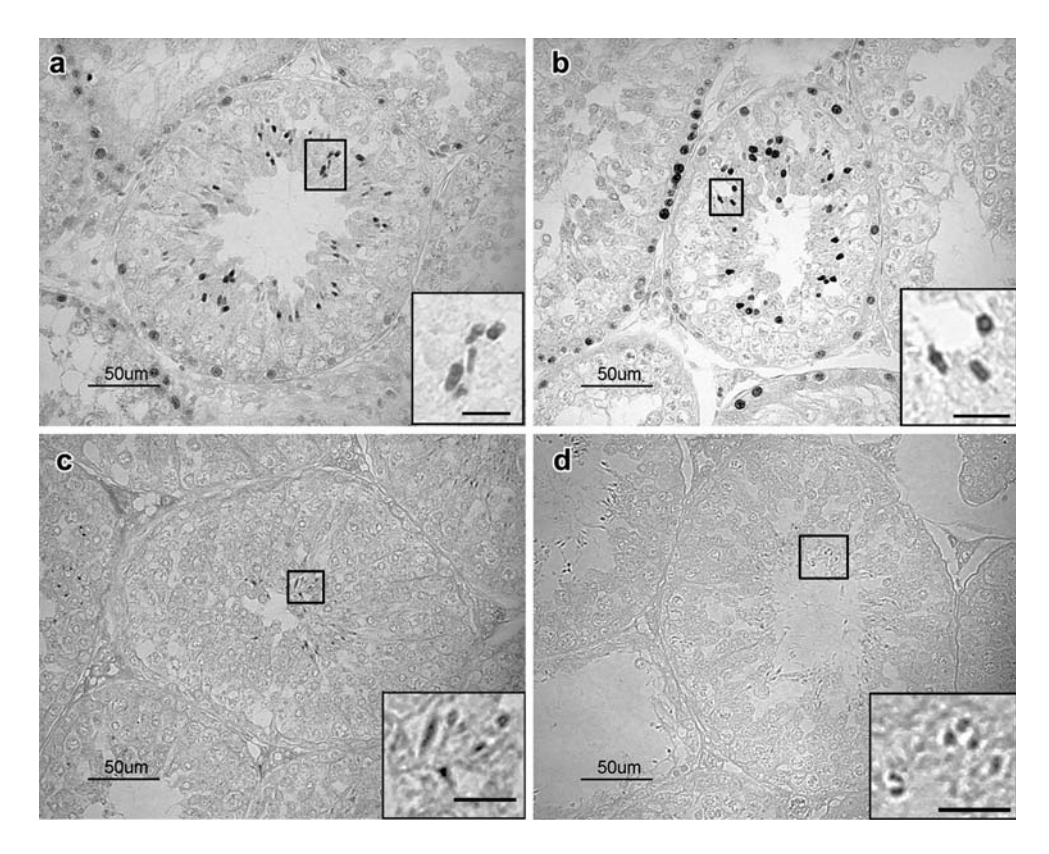
Fig. 3 Immunocytochemistry of BNPs in seminiferous tubules of B. indica. a, b Sections stained with anti-H2B antibody or anti-H3 antibody, respectively, showing the positive staining of many of the nuclei of spermatogonia lying on the basement membrane of the seminiferous tubules and also in some of the spermatids near the lumen (insets in a, b). c, d Sections stained with antibodies against transition protein2 (TP2) or protamine, respectively, demonstrating positive staining in the nuclei of the late spermatids and spermatozoa (insets in c, d). Bar 5 μm (insets)

acid; Zweidler 1978). Protein samples were isolated from cauda epididymal sperm and chick erythrocytes, and standard protein markers were dissolved in sample buffer (9 M urea, 0.9 N acetic acid, 5% mercaptoethanol, and 0.2% pyronine-G). Electrophoresis was carried out at a constant current, and some of the gels were stained with Coomassie brilliant blue R-250. Proteins on the other duplicated gels were transferred onto nitrocellulose membrane by using 0.9 N acetic acid, pH 2.3, as the transfer buffer. Non-specific binding of antibodies was blocked with skimmed milk in TBST. The membranes were then flooded with either anti-TP2 or anti-protamine antibodies at a dilution of 1:10,000 (1 h, room temperature), and washed in TBST. Subsequently, the proteins were exposed to the corresponding HRP-conjugated secondary antibodies at a dilution of 1:20,000 (1 h, room temperature) and visualized by enhanced chemiluminescence (ECL) using an ECL Kit (Amersham Pharmacia, Buckinghamshire, UK).

Results

Ultrastructure of spermatids and chromatin organization

We have previously categorized *B. indica* spermatids into 12 steps by light microscopy based on their appearance and the patterns of the germ cell associations (Worawittayawong et al. 2005). In the present study, we extend these





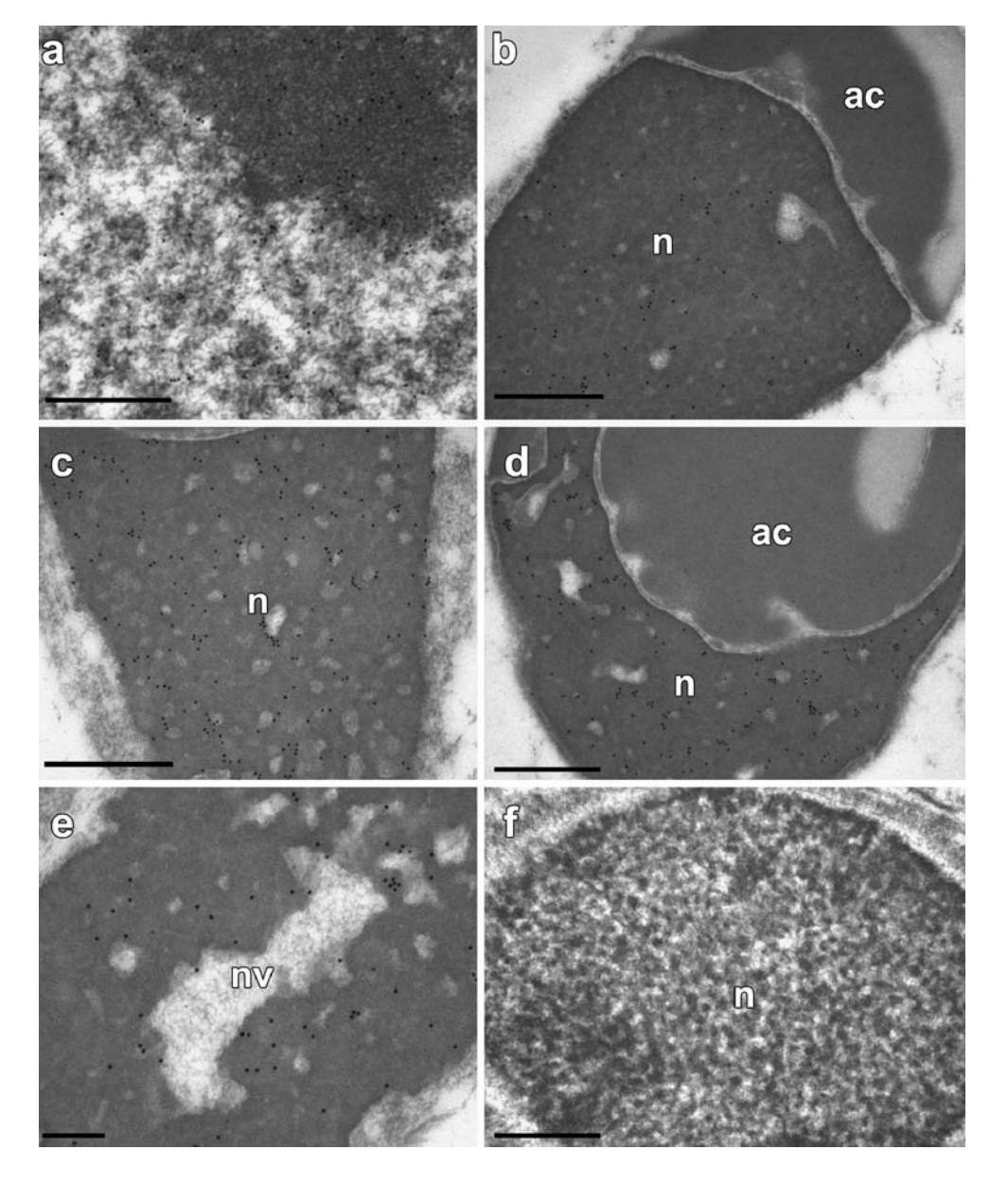
observations by determining the ultrastructural organization of the spermatids with special emphasis on chromatin organization.

The formation of the acrosomal granule, by the attachment of Golgi-body-derived vesicles to the outer nuclear envelope, was characteristic of the Golgi phase (steps 1–2) spermatids (Fig. 1a), similar to that in most mammalian species (Biggiogera et al. 1992; Courtens et al. 1991; Dooher and Bennett 1973; Loir and Courtens 1979). In the early cap phase (steps 3–4) of *B. indica* spermatids, the acrosomal granule became extremely large (Breed 1993) (see Fig. 1b), and the acrosomal matrix developed two regions of differing electron density (Fig. 2c-f) suggesting compartmentalization of the acrosomal contents in the granule. Thickening of the nuclear envelope occurred close to the acrosomal granule with an elongation of the

Fig. 4 Transmission electron micrographs of gold-immunolabeled nuclei of B. indica spermatocyte and spermatids after immunostaining with anti-histones antibodies (n nucleus). Immunostaining with the anti-H2B antibody demonstrated gold particles scattered throughout the condensing nuclear chromatin of a pachytene primary spermatocyte) serving as the positive control for histone (a and of a step 12 spermatid (b). Immunostaining with the anti-H3 antibody revealed numerous gold particles in the step 10 (c) and step 12 (d) late spermatids. The acrosome (ac in b, d) exhibited no labeling. No immunogold labeling occurred in the nuclear vacuole (nv in e) or in the control section (f). Bars 500 nm (a-d, f), 200 nm (e)

acrosomal granule taking place during the late cap and acrosomal phases (steps 5–9), with the manchette forming around the nuclear periphery (Figs. 1c,d, 2a-d).

In the Golgi phase and early cap phase (steps 1–4) spermatids (Fig. 1a,b), the nuclear chromatin initially appeared as 10-nm and 20-nm scattered granules. In spermatids of the late cap phase (step 5), condensed 30-nm fibers of nucleochromatin began to appear in the central nuclear region (Fig. 1c). Whereas these chromatin fibers spread throughout the nucleus of the spermatids of early acrosome phase (steps 6–7), higher order condensation of chromatin fibers with a diameter of about 50 nm appeared close to the nuclear periphery at a distance from the acrosomal granule (Figs. 1d, 2a, insets). Vacuoles with electron-dense particles surrounded by an electron-lucent region often occurred near the center of the nuclei of these





spermatids (Fig. 2b). In the mid-acrosome phase (step 8) spermatids, 50-nm diameter fibers were dispersed throughout much of the nucleus with larger 70-nm diameter fibers being present peripherally (Fig. 2b, inset). All chromatin fibers reached their maximal thickness of about 90 nm in spermatids of the late acrosome phase (step 9), leaving some spaces filled with unidentified material scattered randomly throughout the nucleus (Fig. 2c, inset). The thick chromatin cords in spermatids of the maturation phase (step 10–12) then associated with each other to become highly condensed chromatin patches, with the vacuoles containing the spherical electron-dense particles becoming reduced in size (Fig. 2d-f) as was the overall volume of the nucleus.

Distribution of BNPs in spermatids during spermiogenesis

Intense immunoreactivity to antibodies against histones H2B (Fig. 3a) and H3 (Fig. 3b) was detectable in some of the spermatogonia lining the base of seminiferous tubules. Similar immunostaining by both anti-H2B and anti-H3 was also observed in various spermatids in the adluminal compartment of the tubules (Fig. 3a,b, insets) indicating that these two histones were retained until late differentiation. At the TEM level, as in primary spermatocytes (Fig. 4a), deposition of gold particles was seen in spermatids from the late cap phase (step 9) to the late

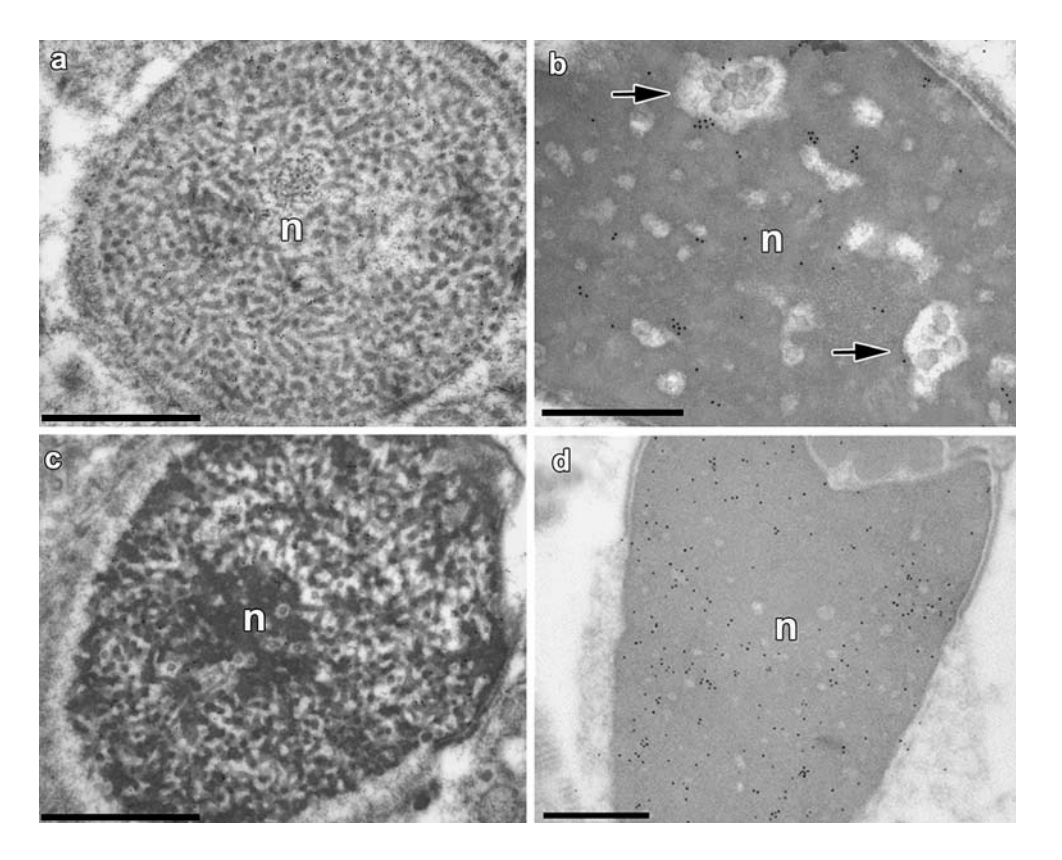
maturation phase after staining with histone antibodies (Fig. 4b-d). There was an absence of labeling against both anti-histones in the nuclear vacuoles of the late differentiating spermatid nuclei (Fig. 4e) and in the negative controls (Fig. 4f).

Immunoreactivity with anti-TP2 was initially found in step 7 spermatids and remained throughout nuclear maturation (Figs. 3c, 5a,b), whereas staining with the anti-protamine antibody was detected from the mid-acrosomal phase (step 8; Figs. 3d, 5c,d). At the TEM level, some deposition of gold particles initially appeared at step 7 after anti-TP2 staining (Fig. 5a) and in step 8 spermatids after anti-protamine staining (Fig. 5c,d). In step 11–12 spermatids, a slightly increased abundance of gold particles was evident, especially with the anti-protamine antibody, whereas no gold labeling was apparent in the negative controls.

Presence and expression level of TP and protamine of mature sperm

Profiles of BNPs extracted from *B. indica* spermatozoa were analyzed by AUT-PAGE (Fig. 6). Four major protein bands were found to occur, which had similar electrophoretic mobilities to those of the chicken erythrocyte histones H2A, H3, H2B, and H4 in sperm BNP extracts (Fig. 6a,

Fig. 5 Transmission electron micrographs of B. indica spermatids gold-labeled with the anti-TP2 or anti-protamine antibodies (n nucleus). Immunostaining with anti-TP2 antibody showed sparse gold labeling in the chromatin of spermatids at step 7 (a) and occurred throughout the chromatin at step 12 (b). No gold labelling was seen in the nuclear vacuoles (arrows in b) Immunostaining with anti-protamine antibody revealed the presence of gold particles in the chromatin of step 8 spermatids (c) and throughout the maturing spermatids (d). Bars 1 μm (a, c) 500 nm (b, d)





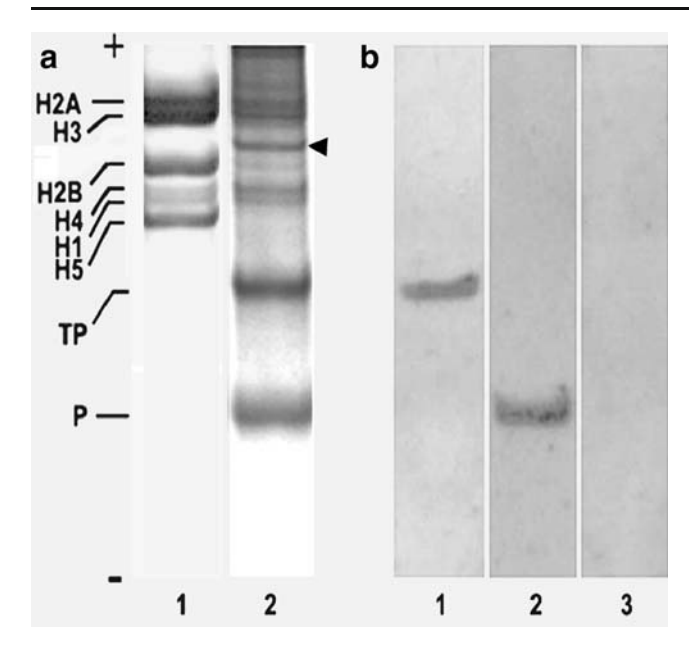


Fig. 6 a Comparison of BNPs from cauda epididymal spermatozoa of *B. indica* (*lane 2*) with BNPs from chick erythrocytes (*lane 1*) by 17% acid urea Triton X-100 polyacrylamide gel electrophoresis. Coomassie-blue-stained bands demonstrate core histones (*H2A*, *H3*, *H2B*, *H4*) together with TP and protamine (*P*) in *B. indica* sperm extracts. **b** Immunoblotting with anti-TP (*lane 1*) and anti-protamine (*lane 2*) of epididymal spermatozoa extracts (*lane 3* control–*arrowhead* presumed testis-specific H2B)

lanes 1, 2). Two other major basic proteins occurred, which were probably TP and protamine as judged by their positions on the gels. Results seen in gels of the cauda sperm extracts blotted with specific antibodies against TP and protamine supported the conclusion that TP and protamines occurred in the sperm extracts. The antibodies

Table 1 Occurrence (+) of histones, transition protein2 (*TP2*), and protamine and of the different sizes of chromatin fibers during spermiogenesis in *Bandicota indica* (*GP* Golgi phase, *ECP* early cap

specifically recognized a single protein band whose mobility was similar to that of TP or protamine (Fig. 6b, lanes 1, 2, respectively). BNP extracts exposed to secondary antibody, as a negative control, revealed only background staining (Fig. 6b, lane 3).

Discussion

Unlike in most murine rodents that have a falciform-shaped sperm head (see Retzius 1909; Friend 1936; Bishop and Austin 1960), the sperm head in male greater bandicoot rats is globular and more like that in other, distantly related, eutherian mammals, with the shape of the nucleus generally reflecting that of the overall head shape (Breed 1993, 1998, 2004; Worawittayawong et al. 2005). Preliminary observations suggested that, during chromatin condensation, the chromatin organization differed from that of the laboratory rat (Breed 1993, 1998). Thus, the question arises as to whether the pattern of chromatin condensation could result, at least in part, in the different final form of the sperm nucleus. In the present study of spermiogenesis in the greater bandicoot rat, we have found that a filamentous organization of the chromatin is evident during early spermiogenesis, similar to that of the laboratory rat (Balhorn et al. 1999; Wanichanon et al. 2001), but that the chromatin fibers then appear to assemble to form thicker chromatin cords. In addition, we have observed that nuclear vacuoles, with electron-dense particles, also occur.

In maturing mammalian spermatids, histones are generally replaced by TPs, which are, in turn, then replaced by protamines (Grimes et al. 1977; Meistrich 1989; Oliva and Dixon 1991; Biggiogera et al. 1992; Oko et al. 1996;

phase, *LCP* late cap phase, *EAP* early acrosome phase, *MAP* mid-acrosome phase, *LAP* late acrosome phase, *MP* maturation phase)

Presence of BNPs and sizes of chromatin fibers	Spermatid steps (1-12)											
	GP		ECP		LCP	EAP		MAP		LAP	MP	
	1	2	3	4	5	6	7	8	9	10	11	12
BNPs												
Histones	+	+	+	+	+	+	+	+	+	+	+	+
TP2							+	+	+	+	+	+
Protamine								+	+	+	+	+
Chromatin fibers (nm)												
10	+	+	+	+								
20	+	+	+	+	+	+						
30					+							
50						+	+	+				
70								+				
90									+			



Wouters-Tyrou et al. 1998). Nevertheless, in human spermatids, a small amount of histone is retained, perhaps localized to the telomere regions at the nuclear periphery (see, for example, Gatewood et al. 1990; Wykes and Krawetz 2003; Churikov et al. 2004), whereas in the laboratory mouse, sperm histones also occur around the peripheral nuclear region (Pittoggi et al. 1999). In the present study of the spermatids of the greater bandicoot rat, immunogold labeling suggests that, whereas only histones are present in the early spermatid nuclei, TPs and protamines are laid down at the time of the thickening of the chromatin fibers and the formation of cords. Information available from several species of mammals has revealed the toroidal chromatin structure of nucleoprotamine organization (Balhorn et al. 1999), but the structure of the DNA-TP complexes does not appear to have been determined. Our finding of chromatin fibers of ~50 nm in the mid-acrosomal phase spermatids suggests this may represent complexes of DNA and TPs (Akama et al. 1996; Singh and Rao 1988). These chromatin fibers then appear to associate with each other to form the thicker chromatin cords of ~90 to 100 nm, which are similar to nucleoprotamine complexes previously found in late spermatids of some other mammalian species (Sobhon et al. 1982; Balhorn et al. 1999) but quite unlike those in the spermatids of common laboratory rodents. The changes in the appearance of BNPs and the size of chromatin fibers in spermatids of the greater bandicoot rat during spermiogenesis is summarized in Table 1.

A further unusual characteristic suggested from the BNP profiles of the sperm extracts taken from the cauda epididymidis of the greater bandicoot rat is the apparent retention of TPs in the mature sperm nuclear extracts. TPs have been previously shown to play a role in chromatin condensation and perhaps in DNA repair during chromatin remodeling (Oko et al. 1996; Yu et al. 2000; Caron et al. 2001; Meistrich et al. 2003). These TPs are generally replaced by protamines (Zhao et al. 2001) and are thus eliminated prior to sperm maturation. However, the present study suggests that, in the sperm of the greater bandicoot rat, one of the TPs is retained even in the nuclei of the spermatozoa from the cauda epididymidis. Further work is now required to determine the distribution and relative abundance of the TPs in the mature sperm of this species. It also remains to be seen whether the remaining TPs and histones co-localize with protamines on the DNA strands to modulate DNA condensation or occur in the peripheral region of the nucleus leaving protamine as the major protein involved in DNA condensation.

Acknowledgements The authors thank Richard Oko for the transitional protein antibody, Sylviane Muller for the histone antibodies, and Rod Balhorn for the protamine antibody.

References

- Akama K, Sato H, Furihata-Yamauchi M, Komatsu Y, Tobita T, Nakano M (1996) Interaction of nucleosome core DNA with transition proteins 1 and 3 from boar late spermatid nuclei. J Biochem (Tokyo) 119:448–455
- Alfonso PJ, Kistler WS (1993) Immunohistochemical localisation of spermatid nuclear transition protein 2 in the testes of rats and mice. Biol Rep 48:522–539
- Allen MJ, Dong XF, O'Neill TE, Yau P, Kowalczykowski SC, Gatewood J, Balhorn R, Bradbury EM (1993) Atomic force microscope measurement of nucleosome cores assembled along defined DNA sequences. Biochemistry 32:8390–8396
- Balhorn R (1982) A model for the structure of chromatin in mammalian sperm. J Cell Biol 93:298–305
- Balhorn R (1989) Mammalian protamines: structure and molecular interactions. In: Adolph, KW (eds) Molecular biology of chromosome function. Springer, New York, pp 366–395
- Balhorn R, Weston S, Thomas C, Wyrobek AJ (1984) DNA packaging in mouse spermatids. Synthesis of protamine variants and four transition proteins. Exp Cell Res 150:298–308
- Balhorn R, Cosman M, Thornton K, Krishnan VV, Corzett M, Bench G, Kramer C, Lee JD, Hud NV, Allen MJ, Prieto M, Meyer-Iese W, Brown JT, Kirz J, Zhang X, Bradbury EM, Maki G, Braun RE, Breed W (1999) Protamine mediated condensation of DNA in mammalian sperm. In: Gagnon, C (eds) The male gamete: from basic science to clinical applications. Cache River, Vienna, pp 55–70
- Biggiogera M, Muller S, Courtens JL, Fakan S, Romanini MG (1992) Immunoelectron microscopical distribution of histones H2B and H3 and protamines in the course of mouse spermiogenesis. Microsc Res Tech 20:259–267
- Bishop MWH, Austin CR (1960) Mammalian spermatozoa. Endeavour 16:137–150
- Breed WG (1993) Novel organization of the spermatozoon in two species of murid rodents from southern Asia. J Reprod Fertil 99:149–158
- Breed WG (1998) Interspecific variation in structural organisation of the spermatozoon in the Asian bandicoot rats, *Bandicota* species (family Muridae). Acta Zool 79:277–285
- Breed WG (2004) The spermatozoon of Eurasian murine rodents: its morphological diversity and evolution. J Morphol 261:52–69
- Brewer L, Corzett M, Balhorn R (2002) Condensation of DNA by spermatid basic nuclear proteins. J Biol Chem 277:38895–38900 Caron N, Veilleux S, Boissonneault G (2001) Stimulation of DNA repair
- Caron N, Veilleux S, Boissonneault G (2001) Stimulation of DNA repartition by the spermatidal TP1 protein. Mol Reprod Dev 58:437–443
- Churikov D, Zalenskaya IA, Zelensky AO (2004) Male germlinespecific histones in mouse and man. Cytogenet Genome Res 105:203–214
- Corzett M, Mazrimas J, Balhorn R (2002) Protamine 1:protamine 2 stoichiometry in the sperm of eutherian mammals. Mol Reprod Dev 61:519–527
- Courtens JL, Loir M (1981) A cytochemical study of nuclear changes in boar, bull, goat, mouse, rat, and stallion spermatids. J Ultrastruct Res 74:327–340
- Courtens JL, Biggiogera M, Fakan S (1991) A cytochemical and immunocytochemical study of DNA distribution in spermatid nuclei of mouse, rabbit, and bull. Cell Tissue Res 265:517–525
- Dooher GB, Bennett D (1973) Fine structural observations on the development of the sperm head in the mouse. Am J Anat 136:339–361
- Friend GF (1936) The sperms of British Muridae. Q J Microsc Sci 78:419–443
- Gatewood JM, Cook GR, Balhorn R, Schmid CW, Bradbury EM (1990) Isolation of 4 core histones from human sperm chromatin

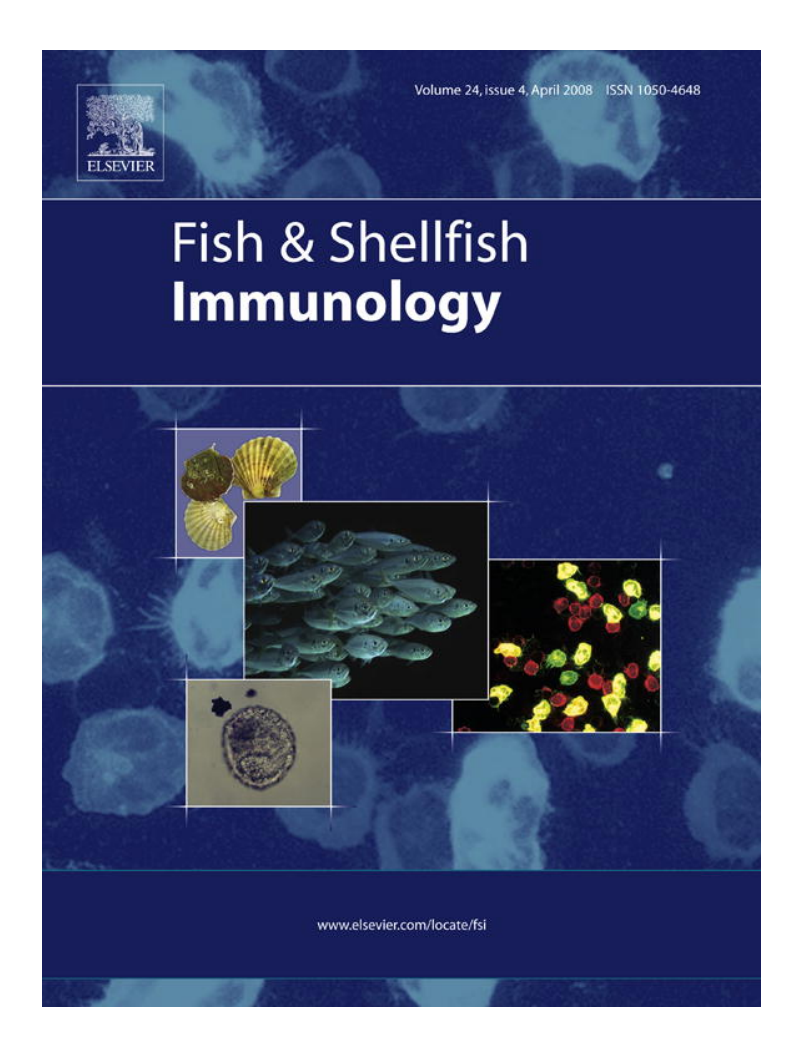


- represents a minor set of somatic histones. J Biol Chem 265:20662–20666
- Grimes SR, Meistrich ML, Platz RD, Hnilica LS (1977) Nuclear protein transitions in rat testis spermatids. Exp Cell Res 110:31– 39
- Kimmins S, Sassone-Corsi P (2005) Chromatin remodeling and epigenetic features of germ cells. Nature 434:583–589
- Lalli M, Clermont Y (1981) Structural changes of the head components of the rat spermatid during spermiogenesis. Am J Anat 160:419–434
- Loir M, Courtens JL (1979) Nuclear reorganization in ram spermatids. J Ultrastruct Res 67:309–324
- Manochantr S, Sretarugsa P, Chavadej J, Sobhon P (2005) Chromatin organization and basic nuclear proteins in the male germ cells of *Rana tigerina*. Mol Reprod Dev 70:184–197
- Meistrich ML (1989) Histone and basic nuclear protein transitions in mammalian spermatogenesis. In: Hnilica LS, Stein GS, Stein JL (eds) Histones and other basic nuclear proteins. CRC Press, Orlando, pp 165–182
- Meistrich ML, Mohapatra B, Shirley CR, Zhao M (2003) Roles of transition nuclear proteins in spermiogenesis. Chromosoma 111:483–488
- Oko RJ, Jando V, Wagner CL, Kistler WS, Hermo LS (1996) Chromatin reorganization in rat spermatids during the disappearance of testis-specific histone, H1t, and the appearance of transition proteins TP1 and TP2. Biol Reprod 54:1141–1157
- Oliva R, Dixon GH (1991) Vertebrate protamine genes and the histone-to-protamine replacement reaction. Prog Nucleic Acid Res Mol Biol 40:25–94
- Pittoggi C, Renzi L, Zaccagnini G, Cimini F, Degrassi F, Giordano R, Magnano AR, Lorenzini R, Lavia P, Spadafora C (1999) A fraction of mouse sperm chromatin is organized in nucleosomal hypersensitive domains enriched in retroposon DNA. J Cell Sci 112:3537–3548
- Platz RD, Grimes SR, Meistrich ML, Hnilica LS (1975) Changes in nuclear proteins of rat testis cells separated by velocity sedimentation. J Biol Chem 250:5791–5800
- Ploen L, Courtens J-L (1986) Comparative aspects of mammalian spermiogenesis. Scanning Electron Microsc 11:639–652
- Pradeepa MM, Rao MRS (2007) Chromatin remodeling during mammalian spermatogenesis: role of testis specific histone variants and transition proteins. In: Gupta SK, Koyoma K,

- Murray JF (eds) Gamete biology: emerging frontiers on fertility and contraceptive development. Nottingham University Press, Nottingham
- Queralt R, Adroer R, Oliva R, Winkfein RJ, Retief JD, Dixon GH (1995) Evolution of protamine P1 genes in mammals. J Mol Evol 40:601–607
- Retzius G (1909) Spermien der Nagetiere. Biol Untersuch N F 14:133-162
- Singh J, Rao MR (1988) Interaction of rat testis protein, TP, with nucleosome core particle. Biochem Int 17:701–710
- Sobhon P, Chutatape C, Chalermisarachai P, Vongpayabal P, Tanphaichitr N (1982) Transmission and scanning electron microscopic studies of the human sperm chromatin decondensed by micrococcal nuclease and salt. J Exp Zool 221:61–79
- Wanichanon C, Weerachatyanukul W, Suphamungmee W, Meepool A, Apisawetakan S, Linthong V, Sretarugsa P, Chavadej J, Sobhon P (2001) Chromatin condensation during spermiogenesis in rats. Sci Asia 27:211–220
- Worawittayawong P, Leigh CM, Cozens G, Peirce EJ, Setchell BP, Sretarugsa P, Dharmarajan A, Breed WG (2005) Unusual germ cell organization in the seminiferous epithelium of a murid rodent from southern Asia, the greater bandicoot rat, *Bandicota indica*. Int J Androl 28:180–188
- Wouters-Tyrou D, Martinage A, Chevaillier P, Sautiere P (1998) Nuclear basic proteins in spermiogenesis. Biochimie 80:117–128
- Wykes SM, Krawetz SA (2003) The structural organization of sperm chromatin. J Biol Chem 278:29471–29477
- Yu YE, Zhang Y, Unni E, Shirey CR, Deng JM, Russell LD, Weil MM, Behringer RR, Meistrich ML (2000) Abnormal spermatogenesis and reduced fertility in transition nuclear protein 1-deficient mice. Proc Natl Acad Sci USA 97:4683–4688
- Zhao M, Shirley CR, Yu YE, Mohapatra B, Zhang Y, Unni E, Deng JM, Arango NA, Terry NHA, Weil MM, Russel LD, Behringer RR, Meistrich ML (2001) Targeted disruption of the transition protein 2 gene affects sperm chromatin structure and reduces fertility in mice. Mol Cell Biol 21:7243–7255
- Zhao M, Shirley CR, Mounsey S, Meistrich ML (2004) Nucleoprotein transitions during spermiogenesis in mice with transition nuclear protein Tnp1 and TNP 2 mutations. Biol Rep 71:1016–1025
- Zweidler A (1978) Resolution of histones by polyacrylamide gel electrophoresis in presence of nonionic detergents. Methods Cell Biol 17:223–233



Provided for non-commercial research and education use. Not for reproduction, distribution or commercial use.



This article was published in an Elsevier journal. The attached copy is furnished to the author for non-commercial research and education use, including for instruction at the author's institution, sharing with colleagues and providing to institution administration.

Other uses, including reproduction and distribution, or selling or licensing copies, or posting to personal, institutional or third party websites are prohibited.

In most cases authors are permitted to post their version of the article (e.g. in Word or Tex form) to their personal website or institutional repository. Authors requiring further information regarding Elsevier's archiving and manuscript policies are encouraged to visit:

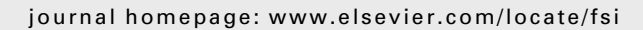
http://www.elsevier.com/copyright

Fish & Shellfish Immunology (2008) 24, 426-435



available at www.sciencedirect.com







Histological and three dimensional organizations of lymphoid tubules in normal lymphoid organ of *Penaeus monodon*

Pornsawan Duangsuwan a,b, Ittipon Phoungpetchara a,c, Yotsawan Tinikul a, Jaruwan Poljaroen a, Chaitip Wanichanon a, Prasert Sobhon a,*

Received 14 October 2007; revised 17 December 2007; accepted 29 December 2007 Available online 9 January 2008

KEYWORDS

Penaeus monodon; Lymphoid organ; Histology; Fibrous scaffold; Three dimension; Vimentin Abstract The normal lymphoid organ of Penaeus monodon (which tested negative for WSSV and YHV) was composed of two parts: lymphoid tubules and interstitial spaces, which were permeated with haemal sinuses filled with large numbers of haemocytes. There were three permanent types of cells present in the wall of lymphoid tubules: endothelial, stromal and capsular cells. Haemocytes penetrated the endothelium of the lymphoid tubule's wall to reside among the fixed cells. The outermost layer of the lymphoid tubule was covered by a network of fibers embedded in a PAS-positive extracellular matrix, which corresponded to a basket-like network that covered all the lymphoid tubules as visualized by a scanning electron microscope (SEM). Argyrophilic reticular fibers surrounded haemal sinuses and lymphoid tubules. Together they formed the scaffold that supported the lymphoid tubule. Using vascular cast and SEM, the three dimensional structure of the subgastric artery that supplies each lobe of the lymphoid organ was reconstructed. This artery branched into highly convoluted and blind-ending terminal capillaries, each forming the lumen of a lymphoid tubule around which haemocytes and other cells aggregated to form a cuff-like wall. Stromal cells which form part of the tubular scaffold were immunostained for vimentin. Examination of the whole-mounted lymphoid organ, immunostained for vimentin, by confocal microscopy exhibited the highly branching and convoluted lymphoid tubules matching the pattern of the vascular cast observed in SEM. © 2008 Elsevier Ltd. All rights reserved.

Introduction

The lymphoid or Oka organ was first described in *Penaeus orientalis* by Oka [1], and later in *Sicyonia ingentis* by

^a Department of Anatomy, Faculty of Science, Mahidol University, Rama VI Road, Bangkok 10400, Thailand

^b Department of Anatomy, Faculty of Science, Prince of Songkla University, Songkhla 90112, Thailand

^c Department of Anatomy, Faculty of Medical Sciences, Naresuan University, Phitsanulok 65000, Thailand

^{*} Corresponding author. Tel.: +662 201 5406; fax: +662 354 7168. E-mail address: scpso@mahidol.ac.th (P. Sobhon).

Martin et al. [2] who incorrectly described it as haematopoietic nodules. The lymphoid organ of penaeid shrimp consists of two lobes situated ventro-anterior to the hepatopancreas [3]. Each lobe receives the haemolymph from the anterior aorta via the subgastric artery [3,4], which is further branched several times in each lobe of the lymphoid organ. At the light microscope level, the lymphoid organ is composed of two parts: lymphoid tubules and the spaces in between which are occupied by haemal sinuses. Lymphoid tubules consist of the central lumen lined by flattened endothelial cells. Next to the endothelial lining are two types of stromal cells. Cells in the inner layer have a clear, unstained cytoplasm, whereas those in the outer layer have a more darkly stained cytoplasm with H and E staining [4]. It is believed that haemocytes penetrate the endothelial cells into the space between stromal cells, where they settle and later migrate into the haemal sinuses which form part of the open circulatory system [3]. Apart from cellular constituents, there is a connective tissue scaffold that provides support for the lymphoid tubules. In penaeid shrimp, there is no detailed description of the fibrous scaffold of the lymphoid organ. Furthermore, the three dimensional structure of lymphoid tubules and their relationship with the branching subgastric artery have never been demonstrated. In this study the normal lymphoid organ of Penaeus monodon, which tested negative for white spot syndrome virus (WSSV) and yellow head virus (YHV), was studied by light microscopy using special staining and transmission electron microscopy in order to demonstrate the histological organization, cellular components, and the connective tissue scaffold, and by a vascular cast technique and SEM to visualize the three dimensional structure of the tubules.

Materials and methods

Shrimps

Wild caught fully mature *P. monodon* were obtained from the Gulf of Thailand. The shrimps were confirmed to be WSSV-negative by PCR and YHV-negative by RT-PCR using the IQ 2000 detection kit (Farming IntelliGene Technology Corporation, Taipei, Taiwan).

Tissue preparation for light microscopic observation

Dissected lymphoid organs were fixed in Davidson's fixative, dehydrated through ascending concentrations of ethanol, cleared with dioxane, and embedded in paraffin wax. Four to six micron thick sections were cut and stained with hematoxylin—eosin (H and E), Periodic acid-Schiff (PAS), and Gomori's stains. All images were captured in a Nikon microscope fitted with a digital camera DXM 1200.

Periodic acid-Schiff stain (PAS)

This staining method was used to identify carbohydrate components especially the extracellular matrix (ECM) in tissue sections. Briefly, the sections were deparaffinized

and hydrated in distilled water. The sections were then oxidized by being immersed in 0.5% periodic acid solution for 5 min and washed thoroughly with three changes of distilled water. The sections were then placed in Schiff reagent for 15 min. The excess stain was removed by washing the sections thoroughly with two changes of 2% potassium metabisulfite before washing in running tap water for 10 min to develop full color. The sections were counterstained with hematoxylin, dehydrated with 95 and 100% ethanol, cleared with xylene, mounted with permount, and observed under a light microscope.

Gomori's stain

Gomori's stain was applied to detect reticular fibers in tissue sections because of their argyrophilic property. Briefly, the deparaffinized sections were treated with 0.5% potassium permanganate solution for 1 min and rinsed in tap water for 2 min. After that, the sections were differentiated in 2% potassium metabisulfite solution for 1 min and then washed in running tap water for 2 min. The sections were sensitized in 2% ferric ammonium sulfate for 1 min, washed thoroughly with tap water, and two changes of distilled water for 30 s each. The sections were then impregnated with 10% silver nitrate in distilled water for 1 min. Thereafter, the sections were rinsed in distilled water for 20 s, reduced for 3 min in the formalin solution and washed in tap water for 3 min. The sections were then toned in 0.2% gold chloride solution for 10 min and rinsed in distilled water. Subsequently, the sections were placed in 2% potassium metabisulfite for 1 min, in 2% sodium thiosulfate for 1 min, and washed in tap water for 2 min. Finally, the sections were dehydrated in 95 and 100% ethanol, cleared with xylene and mounted with permount before being observed under the light microscope.

Immunoperoxidase staining using antivimentin and anticytokeratin as cell markers

The deparaffinized sections of the lymphoid organ were prepared as mentioned above and haemolymph smears were prepared by taking haemolymph from the ventral sinus, fixing it with an equal volume of 4% paraformaldehyde for 1 h at 4 °C, and smearing onto glass slides, which were air-dried. Both the tissue sections and haemolymph smears were incubated in 0.3% hydrogen peroxide in methanol for 30 min to remove endogenous peroxidase activity. Thereafter, free aldehyde was quenched with 1% glycine in PBS for 5 min, followed by incubation in a blocking solution (4% BSA and 2% normal goat serum and 0.4% Triton X-100 in PBS) for 2 h. The sections were then incubated overnight at 4 °C in monoclonal antibodies against cytokeratin or vimentin (Sigma Chemical Co., St. Louis, MO, USA), as the primary antibodies, and goat anti-mouse IgG conjugated to HRP, as secondary antibody, for 1 h, respectively. Sections with the primary antibodies omitted or those treated with normal goat serum, served as controls. Subsequently, the sections were immersed in the substrate containing AEC-red (Zymed Laboratories, San Francisco, CA, USA) and counterstained with Mayer's hematoxylin. The sections were washed three times in PBS between each incubation step. All images were

P. Duangsuwan et al.

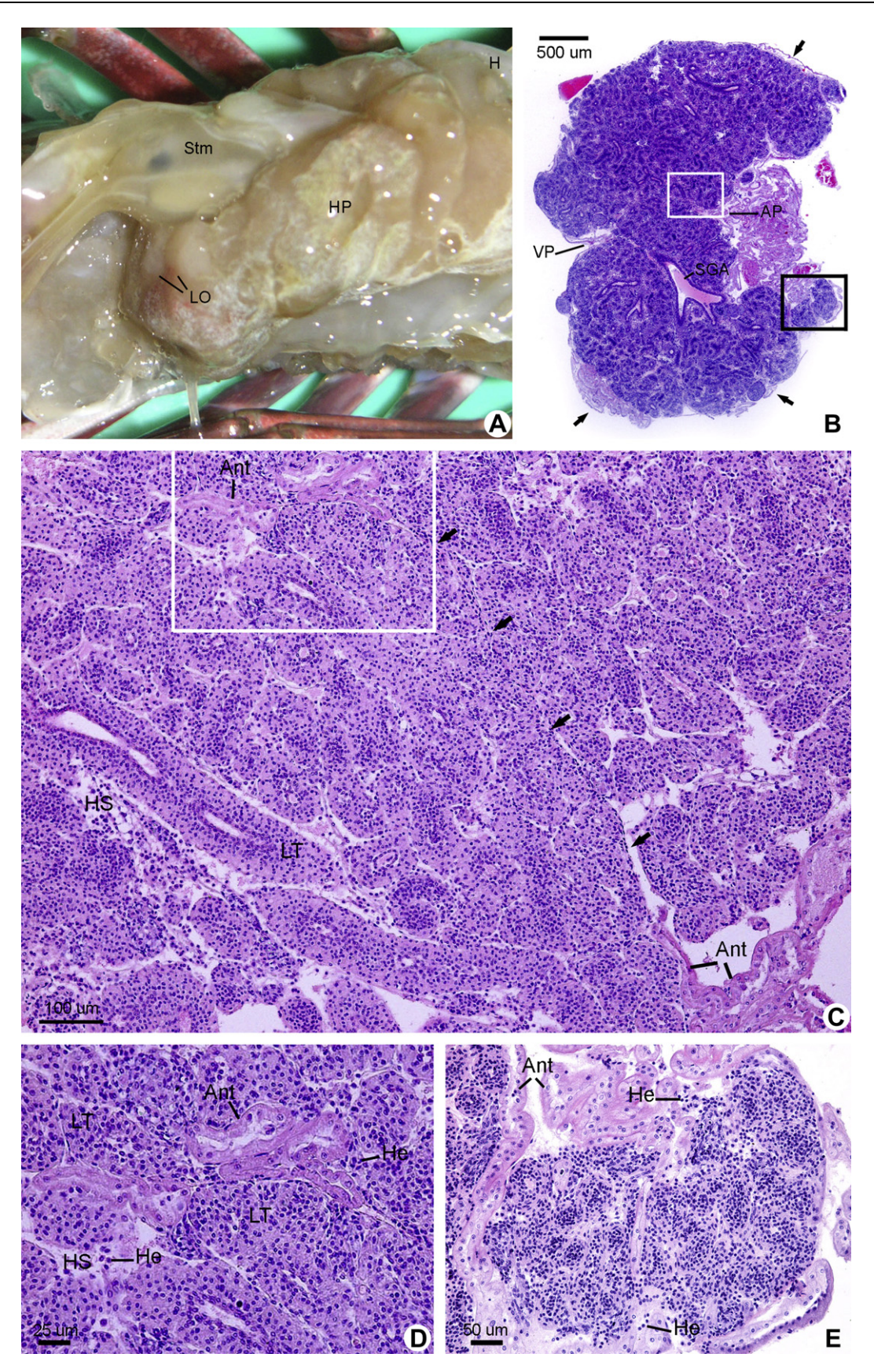


Figure 1 Position of lymphoid organ and light micrographs (LM) of paraffin sections stained with hematoxylin and eosin (H and E). (A) A photograph of the cephalothorax region of *Penaeus monodon* whose carapace was removed, showing the paired lymphoid organs (LO) lying ventral to the stomach (Stm) and dorso-anterior to the ventral hepatopancreas (HP). H: heart. (B) Low

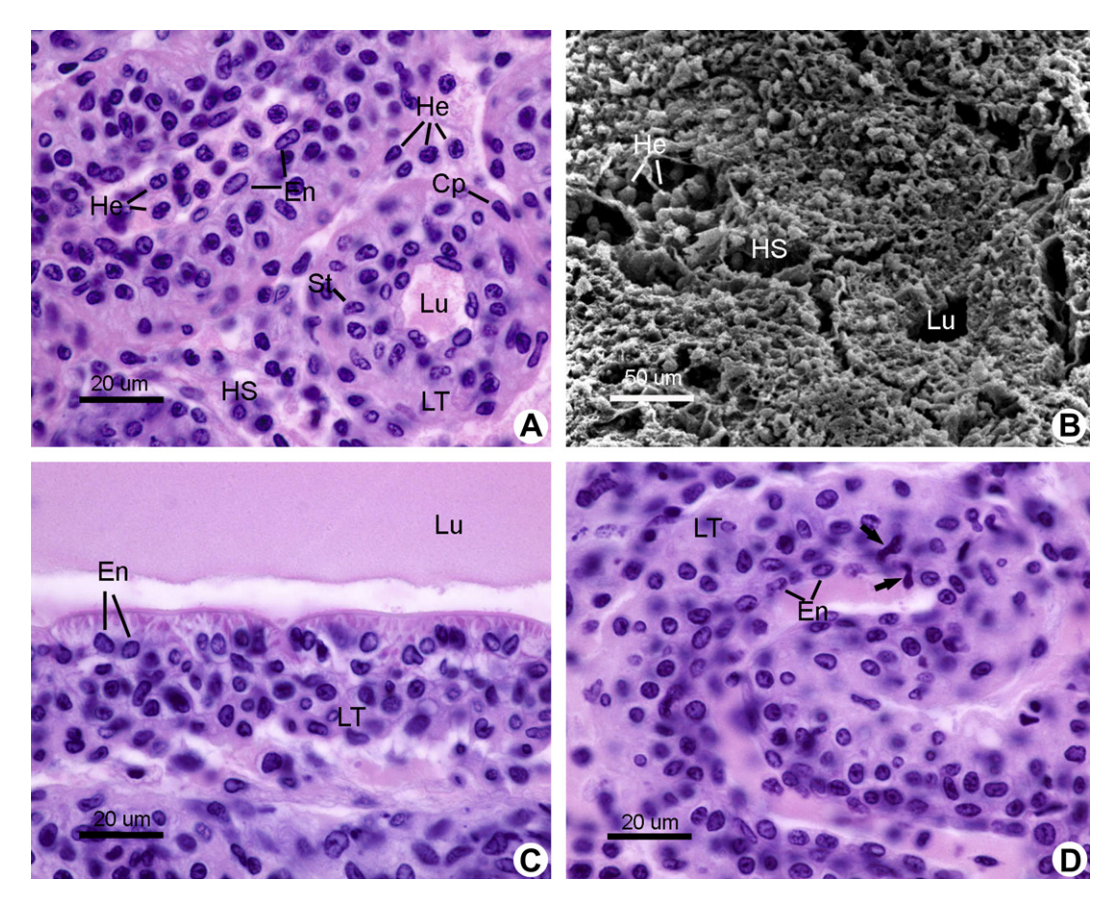


Figure 2 LM (H and E staining) and SEM micrographs of lymphoid tubules. (A, B) Comparable LM (A) and SEM (B) micrographs of lymphoid organs, showing lymphoid tubules (LT) and haemal sinuses (HS), which were packed with a large amount of haemocytes (He). The luminal surface of lymphoid tubule was lined by endothelial cells (En). Capsular cells (Cp) were located at the outermost layer of the lymphoid tubule. Stromal cells (St) were located between endothelial and capsular cells. (C) High magnification LM micrograph of a long section of the proximal part of the lymphoid tubule, showing high cuboidal endothelial cells (En) lining the lymphoid tubule (LT). Lu: lumen. (D) High magnification LM micrograph of a long section of the terminal blind ending of a lymphoid tubule (LT) where the endothelial cells (En) became simple squamous. Haemocytes (arrows) penetrating the endothelium into the wall of lymphoid tubules (LT) were observed.

captured in a Nikon microscope fitted with a digital camera DXM 1200.

Whole mount immunofluorescence observation

Dissected lymphoid organs were fixed with 4% paraformal-dehyde, dehydrated in ascending concentrations of ethanol (70 to 100%), permeabilized with Dent's solution (80% ethanol and 20% DMSO) and rehydrated in descending concentrations of ethanol (100 to 50%). Whole lymphoid organs were then incubated in mouse monoclonal anti-vimentin antibody (Sigma Chemical Co., St. Louis, MO, USA) at 4 °C for 3 days and Alexa 594-conjugated goat anti-mouse

IgG (Zymed Laboratories, San Francisco, CA, USA) overnight, respectively. The nuclei were stained with ToPro-3 (Zymed Laboratories, San Francisco, CA, USA). The specimens were then cleared in methyl salicylate before being observed under a confocal laser scanning microscope, Olympus FV1000.

Tissues preparation for electron microscopic observations

Dissected lymphoid organs were fixed in 4.2% glutaraldehyde and 1% paraformaldehyde in cacodylate buffer, post-fixed in 1% OsO_4 , and dehydrated through ascending concentrations of ethanol. For scanning electron microscopic

magnification LM micrograph, showing the general feature of the lymphoid organ surrounded by a capsule (arrows). Subgastric artery (SGA) entered at the vascular pole (VP) and branched 4–5 times to form vascular plexuses in the lymphoid organ. An antennal tubule complex was situated at the antennal pole (AP). (C—E) Medium and high magnification LM micrographs from the white-boxed area in B (C), white-boxed area in C (D), and black-boxed area in B (E), showing antennal tubules (Ant) which were the invaginating parts from the antennal complex that projected inwards and partitioned the lymphoid organ into lymphoid lobules (arrows in C). Antennal tubules (Ant) and haemocytes (He) in haemal sinuses were also observed (D, E). LT: lymphoid tubule, HS: haemal sinus.

430 P. Duangsuwan et al.

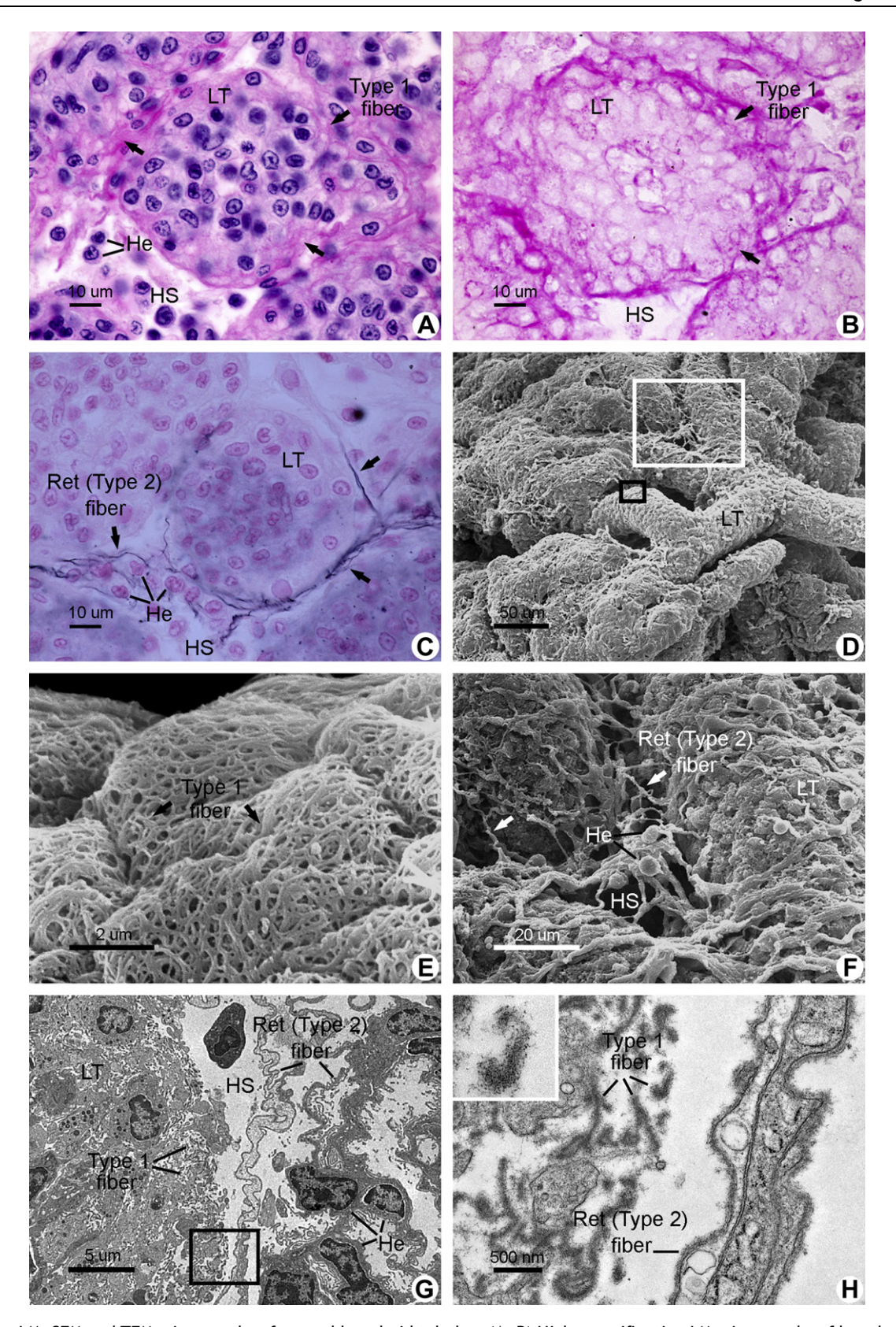


Figure 3 LM, SEM and TEM micrographs of normal lymphoid tubules. (A, B) High magnification LM micrographs of lymphoid tubule sections stained with PAS counterstained with Mayer's hematoxylin (in A) and uncounterstained (in B), showing intensely stained type 1 fibers and the extracellular matrix (ECM) in the capsular layer of lymphoid tubules (arrows), and there were also type 1 fibers running in the thinner ECM between stromal cells. There was no staining in haemal sinuses (HS). He: haemocyte. (C) High magnification LM micrograph of the lymphoid tubule section stained with Gomori's stain for reticular (type 2) fibers, showing thin black

observation, specimens were dried in a Hitachi HCP-2 critical point drying machine, mounted on aluminium planchettes and coated with platinum and palladium in an ion sputtering apparatus, Hitachi E-120, before being observed under a Hitachi scanning electron microscope S-2500, at an accelerating voltage of 15 kV. For transmission electron microscopic observation, specimens were embedded in Araldite-502 resin. Ultrathin sections were cut and stained with uranyl acetate and lead citrate before being observed under a Hitachi H600A and a Tecnai G² transmission electron microscope at 75 and 80 kV, respectively.

Vascular cast of lymphoid organ

A modified method of Chunhabundit and Somana [5] was used. Briefly, corrosion casts of the lymphoid organ vasculature were made by injecting the heart of the shrimps with Batson's No. 17 Anatomical Corrosion Kit (Polysciences Inc., Warrington, PA, USA). Soft tissues were removed by immersing the cast in 40% sodium hydroxide for 24–48 h, followed by slow rinsing in running tap water for 6–8 h, and washing in several changes of distilled water. Vascular casts were collected under a stereoscope, air-dried, mounted on aluminium planchettes, coated with platinum and palladium in an ion sputtering apparatus, Hitachi E-120, and then observed under a Hitachi scanning electron microscope S-2500 at an accelerating voltage of 15 kV.

Results

Gross anatomy of lymphoid organ

The lymphoid organs were paired and lay ventral to the stomach and dorso-anterior to the ventral hepatopancreas (Fig. 1A). Each lymphoid organ had an ovoid shape and was connected to the heart via the subgastric artery. In the fully mature shrimp (with the body length of 18–20 cm from head to telson, and body weight of 150–170 g), lymphoid organs were about 3–4 mm long, 2–3 mm wide, and 1–2 mm thick.

General histology of lymphoid organ

Each lymphoid organ was surrounded by a connective tissue capsule (Fig. 1B). The capsule invaginated inwards together with antennal tubules, and partitioned each lymphoid organ into lymphoid lobules (Fig. 1B, C). Antennal tubules were derived from the antennal tubule complex situated at the antennal pole of the lymphoid organ (Fig. 1B, C), and they were lined by simple cuboidal

epithelium (Fig. 1C, D). The subgastric artery originated from the heart, entered the lymphoid organ at the side opposite to the antennal pole, and branched a further 4-5 times to form vascular plexuses in the lymphoid organ (Fig. 1B, C). Each terminal capillary formed a lumen of a lymphoid tubule, whose interstitial spaces were permeated with haemal sinuses that were packed with large numbers of haemocytes (Fig. 2A, B). Along their entire length, lymphoid tubules generally had the same histological appearance. At the vascular pole, each lymphoid tubule was lined with cuboidal epithelium (Fig. 2C), and had a diameter of approximately 200-250 μm. At the distal end, the endothelial cells decreased in height until they became squamous (Fig. 2A, D), and the diameter of the tubule reached $50-60 \,\mu m$ near the blind ending (Fig. 2C). Encircling the endothelium were 2-6 stromal cell layers (Fig. 2A) with intervening stromal matrix. Cells in the inner layer were tightly packed, whereas fewer cells were observed in the outer layer. The outermost layer was composed of ovoidshaped capsular cells that ran circumferentially around the lymphoid tubule (Fig. 2A). Haemocytes appeared to penetrate the endothelium and move into the stromal cell layers in the wall of the lymphoid tubule (Fig. 2D).

Histology of the fibrous scaffold

Based on the histochemical staining and ultrastructural characteristics, the fibrous scaffold of the tubule was identified as fibers associated with the extracellular matrix (ECM) and reticular fibers. PAS stained the ECM and associated fibers (type 1) as pink structures, demonstrating the presence of carbohydrate components in both the fibers and ECM (Fig. 3A, B), while Gomori's stained reticular fibers which appeared as black lines representing the argyrophilic (type 2) fibers (Fig. 3C). In the normal lymphoid organ, the thick intensely PAS-positive ECM and associated type 1 fibers formed the capsular layer of each lymphoid tubule (Fig. 3A, B), and the lightly stained thinner ECM and associated type 1 fibers formed the scaffold between stromal cells (Fig. 3A, B). There was no staining of haemal sinuses. When observed by SEM, the type 1 fibers and ECM formed a basket-like network that covered all the lymphoid tubules (Fig. 3D, E). At the TEM level (Fig. 3G, H), the width of each type I fiber was about 100-150 nm. Unlike collagen fibers, no transverse striation was seen in these wavy type 1 fibers (inset in Fig. 3H). In contrast, black lines of argyrophilically stained reticular (type 2) fibers from Gomori's stain were observed around haemal sinuses and surrounding the outermost rim of lymphoid tubules (Fig. 3C). No Gomori's stain stained fibers were found within the wall of the lymphoid tubule (Fig. 3C). By SEM (Fig. 3D, F) and TEM (Fig. 3G, H),

lines around haemal sinuses and lymphoid tubules (arrows). (D) SEM micrograph of the outer surface of lymphoid tubules, showing the surface features of the lymphoid tubule (LT) and haemal sinus. (E) Higher magnification SEM micrograph of the black-boxed area in D, showing numerous basket-like networks of fine type 1 fibers (arrows) forming the capsular layer of lymphoid tubules. (F) Higher magnification SEM micrograph of the white-boxed area in D, showing reticular (type 2) fibers (arrows) surrounding the haemal sinus (HS) and lymphoid tubule (LT). (G) Low and (H) high TEM micrograph taken from the boxed area in G, showing wavy type 1 fibers embedded in the extracellular matrix (ECM) forming the capsular layer of lymphoid tubule. No cross-striation was observed in these fibers (inset in H) or reticular (type 2) fibers located around the lymphoid tubule and haemal sinuses (HS).